Institut für Theoretische Physik
Fakultät Mathematik und Naturwissenschaften
Technische Universität Dresden

High-precision QED calculations of the hyperfine structure in hydrogen and transition rates in multicharged ions

Dissertation
zur Erlangung des akademischen Grades
Doctor rerum naturalium

vorgelegt von

Andrey V. Volotka
geboren am 23. September 1979 in Murmansk, Rußland

Dresden 2006

Eingereicht am 14.06.2006

1. Gutachter: Prof. Dr. Rüdiger Schmidt

2. Gutachter: Priv. Doz. Dr. Günter Plunien

3. Gutachter: Prof. Dr. Vladimir M. Shabaev

Verteidigt am _____

Contents

Kurzfassung

Untersuchungen der Hyperfeinstrukturaufspaltung im Wasserstoff sind stark motiviert durch das erreichte Genauigkeitsniveau in gegenwärtigen atomphysikalischen Experimenten, welche mit höchster Präzision letztlich modellunabhängige Informationen über nukleare Strukturparameter liefern. Ausgehend vom gegenwärtigen Status betreffend der Deduktion von Korrekturen zur Hyperfeinstrukturaufspaltung des Grundzustands im Wasserstoff, werden hier verbesserte Berechnungen unter Berücksichtigung des aktuellsten Werts für den Ladungsradius des Protons bereitgestellt. Theoretische und empirische Werte für die Hyperfeinstruktur vergleichend wird der Beitrag aufgrund der Ausdehnung des Protons extrahiert und dafür eine relativistische Formel in Termen von Momenten der Kernladungsverteilung und der Magnetisierungsverteilung hergeleitet. Ein iteratives Schema zur Bestimmung des Zemach und des magnetischen Radius des Protons wird vorgestellt. Die hier deduzierten Werte für den Zemach sowie für den magnetische Radius des Protons werden mit denen aus experimentellen Elektronenstreudaten extrahierten Werten verglichen. Eine alternative Bestimmung des Zemach-Radius mittels einer reskalierten Differenz zwischen der Hyperfeinaufspaltung im Wasserstoff und Myonium wird ebenfalls diskutiert.

Das Studium von verbotenen Strahlungsübergängen in Mehr-Elektronenionen im Rahmen der QED bietet ein höchst sensitives Instrument um den Einfluß der relativistischen Elektronenkorrelation sowie QED-Korrekturen auf die Übergangsraten zu sondieren. Entsprechend widmet sich ein wesentlicher Teil diese Arbeit detailierten Berechnungen radiativer und interelektronischer Wechselwirkungseffekte auf die Übergangswahrscheinlichkeiten. Diesbezüglich werden renormierte Ausdrücke für die entsprechenden Korrekturen in Ein- und Zwei-Elektronenionen sowie in Ionen mit einem Elektron über abgeschlossenen Schalen im Rahmen der Zwei-Zeiten-Greens-Funktionsmethode hergeleitet. Numerische Resultate für die Korrelationskorrekturen zu magnetischen Übergangsraten in He-artigen Ionen werden präsentiert. Ebenfalls wird erstmals der frequenzabhängige Beitrag berechnet, dessen Berücksichtigung erst die Eichinvarianz der Ergebnisse gewährleistet. Die Ein-Loop-QED-Korrekturen zur magnetischen Dipolübergangsamplitude zwischen den Feinstrukturniveaus $2p_{3/2}$ und $2p_{1/2}$ werden exakt in allen Ordnungen αZ berechnet. Unter konstistenter Berücksichtigung relativistischer und QED-Korrekturen sowie der interelektronischen Wechselwirkung zu den magnetischen Dipolübergangsamplituden gelingt die Vorhersage der Lebensdauern der Zustände $(1s^2 2s^2 2p)\,^2P_{3/2}$ in B-artigen sowie $(1s^2 2s 2p)\,^3P_2$ in Be-artigen Ionen mit höchster Präzision. Die erzielten Ergebnisse dieser Berechnungen werden mit experimentellen Daten aus jüngsten Messungen an der Heidelberg EBIT verglichen.

Abschließend wird der sogenannte Hyperfein-Quenching-Effekt und dessen Einfluß auf die Lebensdauern der $2^3P_{0,2}$-Niveaus in He-artigen Ionen mit nichtverschwindendem Kernspin untersucht.

Abstract

Studies of the hyperfine splitting in hydrogen are strongly motivated by the level of accuracy achieved in recent atomic physics experiments, which yield finally model-independent informations about nuclear structure parameters with utmost precision. Considering the current status of the determination of corrections to the hyperfine splitting of the ground state in hydrogen, this thesis provides further improved calculations by taking into account the most recent value for the proton charge radius. Comparing theoretical and experimental data of the hyperfine splitting in hydrogen the proton-size contribution is extracted and a relativistic formula for this contribution is derived in terms of moments of the nuclear charge and magnetization distributions. An iterative scheme for the determination of the Zemach and magnetic radii of the proton is proposed. As a result, the Zemach and magnetic radii are determined and the values are compared with the corresponding ones deduced from data obtained in electron-proton scattering experiments. The extraction of the Zemach radius from a rescaled difference between the hyperfine splitting in hydrogen and in muonium is considered as well.

Investigations of forbidden radiative transitions in few-electron ions within ab initio QED provide a most sensitive tool for probing the influence of relativistic electron-correlation and QED corrections to the transition rates. Accordingly, a major part of this thesis is devoted to detailed studies of radiative and interelectronic-interaction effects to the transition probabilities. The renormalized expressions for the corresponding corrections in one- and two-electron ions as well as for ions with one electron over closed shells are derived employing the two-time Green's function method. Numerical results for the correlation corrections to magnetic transition rates in He-like ions are presented. For the first time also the frequency-dependent contribution is calculated, which has to be accounted for preserving gauge invariance. One-loop QED corrections to the magnetic-dipole transition amplitude between the fine-structure levels $2p_{3/2}$ and $2p_{1/2}$ are calculated to all orders in αZ. Taking into account consistently relativistic, interelectronic-interaction, and QED corrections to the magnetic-dipole transition amplitude allows for predictions of the lifetimes of the states $(1s^2 2s^2 2p)\,{}^2P_{3/2}$ in B-like ions and $(1s^2 2s 2p)\,{}^3P_2$ in Be-like ions with utmost precision. The results of corresponding calculations are compared with experimental data obtained in recent measurements at the Heidelberg EBIT.

Finally, for He-like ions with nonzero-spin nuclei the effect of hyperfine quenching on the lifetimes of the $2^3P_{0,2}$ states is investigated and again compared available experimental data.

1 Introduction

The structure and dynamic properties of atomic systems up to an extremely high precision are described ab initio by quantum electrodynamics (QED). In atomic physics it predominantly represents the relativistic quantum field theory of the fundamental electromagnetic interaction between electrons, positrons (in general charged particles and the corresponding antiparticles) and photons. Despite the mathematical complexity and difficulties associated with the occurrence of infrared and ultraviolet divergences in the perturbation expansion of the S-matrix the agreement between QED predictions and experiment is remarkably good.

1.1 Theory and experiment

The investigations of atomic systems go far beyond atomic physics. Our understanding of the different properties and processes in atoms provides access to an accurate determination of the fundamental physical parameters, such as the Rydberg constant R_∞, the fine structure constant α, the electron mass m_e and g factor, the nuclear radii and moments, etc. Comparison between theory and experiment serves not only for precision tests of QED. Since it describes the electromagnetic interaction from the fundamental principles, it is taken as generic example for the construction of quantum field theories of another interactions. Atomic systems provide various scenarios for high-precision tests of QED. For example, the g factor corresponds to the magnetic sector of QED, while highly-charged ions give access to investigations of QED in the strong field limit. Besides, the aspect of testing QED various fields of physics are involved, such as nuclear physics, laser spectroscopy, accelerator physics, etc., which may explain the intense and wide ranged research activities, e.g., at the present and at the new facilities at the GSI (Gesellschaft für Schwerionenforschung) in Darmstadt [1]. This provides unique possibilities to check general consistency of the different methods in theory and experiment.

Measurements with extremely high precision can be performed in light atomic systems, such as hydrogen, deuterium, helium, muonium, etc. The energy levels of bound electrons offer the traditional tool for the investigations. One of the most accurate experiment in physics has been performed by measuring the energy difference between the states $2s$ and $1s$ in hydrogen with the relative accuracy 1.9×10^{-14} [2]. The best value for the Rydberg constant has been determined using the set of spectroscopic data measured in hydrogen and deuterium (see CODATA [3]). The experimental value of the ground state Lamb shift can be also obtained from such experiments [4, 5]. The QED theory of Lamb shift in hydrogen has been considerably improved during the last years (see, e.g., Refs. [6, 7, 8] and references therein), and the uncertainty now comes mainly from nuclear contributions. Comparing experimental and theoretical values for the Lamb shift the mean-square charge radius of the proton has been extracted $\langle r^2 \rangle_\mathrm{E}^{1/2} = 0.8750(68)$ fm [3]. Another way to determine the proton charge radius is based on experimental data from elastic electron-proton scattering. Recent work [9] taking into account Coulomb and recoil corrections yielded $\langle r^2 \rangle_\mathrm{E}^{1/2} = 0.895(18)$ fm. A new determination of the proton charge radius via a Lamb shift experiment with muonic hydrogen, which is now in progress at the PSI (Paul Scherrer Institute) [10], could elucidate the situation. Muonic hydrogen is more sensitive to nuclear structure effects, since the massive muon is closer to the proton, in contrast to the electron.

Figure 1.1: Scheme representing the various theoretical corrections to the one-electron energy levels that have to be accounted for in atomic physics calculations.

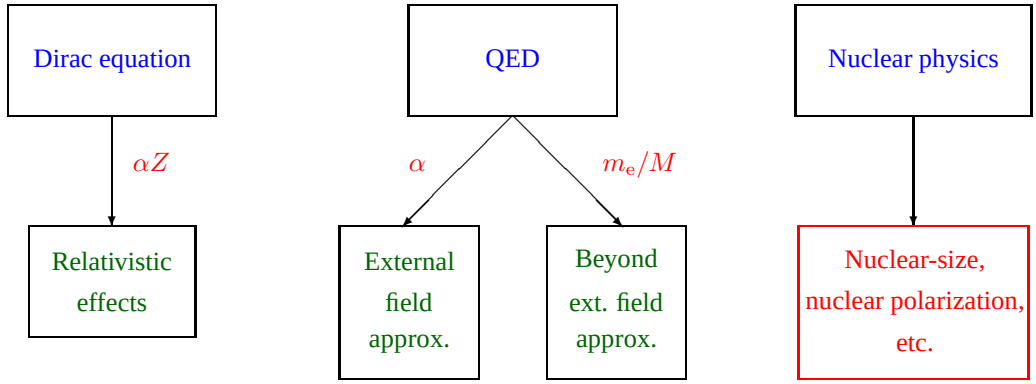

The various theoretical corrections to the one-electron energy levels occurring in investigations of atomic systems are indicated schematically in Fig. 1.1. The relativistic corrections originating from the Dirac equation can be represented as power series with respect to the coupling αZ. The QED terms in the framework of the external field approximation are expanded in powers of α, while the corrections due to the recoil of the nucleus are suppressed by a factor m_e/M, where M is the mass of the nucleus. The contributions mentioned can be precisely calculated order by order. However, this is not the case of the nuclear corrections, which can not be accurately evaluated from first principles due to the lack of knowledge of the nuclear properties. Therefore, one may proceed along two directions. One can either consider specific differences between atomic energy levels, where the nuclear corrections are essentially cancelled, or comparing the theoretical and experimental results in order to extract informations about the nucleus. Measurements of the fine-structure splitting of the states $2^3P_{0,1,2}$ in helium have recently achieved an accuracy of about 3×10^{-8} [11]. This level of accuracy is sufficient for a most precise determination of the fine structure constant α by making comparison with theory [12, 13]. From accurate measurements of the spectral lines for different isotopes the nuclear charge radii can be also deduced: ^{3}He [14], ^{6}He [15], ^{8}Li and ^{9}Li [16], ^{11}Li [17].

In the presence of external magnetic fields the energy levels split according to the projection of the total angular momentum relative to the direction of the field. Here we keep in mind that the Zeeman effect for atoms with zero nuclear spin is much smaller than the fine-structure splitting. The Zeeman structure is linear in the magnetic field strength with the proportionality factor which is called g factor. Experiments on the determination of the g factor can be performed with extremely high precision. Up to now the most accurate values for the g factor of a bound electron were measured for ions $^{12}C^{5+}$ [18, 19] and $^{16}O^{7+}$ [20], respectively. Comparing the experimental data and corresponding results from high-precision theoretical calculations (see, e.g., Refs. [23, 24, 25, 26, 27, 28]) one can determine fundamental constants and nuclear parameters. In particular, the currently accepted value of the electron mass was obtained from the analysis of g factor measurements (see CODATA [3]).

The hyperfine splitting is induced via the interaction of bound electrons with the magnetic dipole or electric quadrupole moments of the nucleus. One of the most precise measurement of the hyperfine splitting was performed for the ground state in hydrogen with an accuracy better than 10^{-12} [29] long ago, which has stimulated numerous theoretical investigations (see, e.g., Refs. [30, 31, 32, 33, 34, 35] and references therein). The hyperfine interaction operator is singular at the origin. For this reason, the hyperfine splitting is very sensitive to the charge and magnetization distributions of the nucleus. The lack of knowledge of the nuclear properties determines the uncertainty of the theoretical value of the hyperfine structure and sets the ultimate limit for any precision tests of

QED. In this context, it has been proposed to study the specific difference D_{n1} between the values of the hyperfine splitting of ns and $1s$ states [36, 37]. In this difference the nuclear structure corrections essentially cancel each other. During the last years theoretical calculations of this quantity have been substantially improved (see, e.g., Refs. [33, 35] and references therein). For hydrogen, deuterium, and helium-3 ion uncertainty of the theoretical predictions for the difference D_{21} became better than the error assigned to the experimental values. Another way to diminish nuclear structure effects is the investigations of pure leptonic systems, such as muonium and positronium. Accurate measurements of the hyperfine splitting in such systems [38, 39] provide a good test of the QED description and recoil corrections, see, e.g., Ref. [33]. On the other hand, having achieved such a considerable improvements of the accuracy of QED predictions and being aware of the strong dependence of hyperfine splitting on the nuclear structure effects allows to determine nuclear parameters from the comparison experimental and theoretical results with high accuracy. Within this thesis as one example of such investigations the Zemach and magnetic radii of the proton are determined.

In systems with low nuclear charge numbers Z as described above the electrons move in the relatively weak field of the nucleus. High-Z ions provide an appropriate scenario for probing the QED effects in the strong field limit. For example, the electric field strength at the surface of the uranium nucleus amounts $E \simeq 2 \times 10^{19}$ V/cm [40]. In the high-Z ions this strong field is not screened by numerous electrons, and on the other hand few-electron ions are relative simple systems for which the interelectronic-interaction effects can be calculated sufficiently precise. The calculation technique applied for high-Z ions is generically different, since now, the parameter αZ is not small. Accordingly, it can not be taken as an expansion parameter. Instead, calculations to all orders in αZ have to be performed, which require a great numerical precision due to appearing cancellations. The progress made in the development of techniques in bound-state QED by now allows for applications even in low-Z systems [8, 35]. During the last years the experimental techniques have also been substantially improved for high-Z ions.
A precision of about 10^{-2} was obtained in measurement of the ground state Lamb shift in the one-electron uranium ion [41]. The experimental uncertainty amounts to about 2% of the one-loop self-energy correction (see, e.g., Ref. [42]). An experiment for measuring the two-electron QED contribution to the ionization potential was proposed for He-like multicharged ions in Ref. [43]. For the ground state of $^{238}U^{90+}$ the most precise experiment has been recently performed in Ref. [44]. This way of measuring allows for testing the screened QED effects [42, 45]. Accurate measurements were recently performed with heavy Li-like ions. As the result, the energy difference between the states $1s^2 2s_{1/2}$ and $1s^2 2p_{1/2}$ was determined to be 216.134(96) eV in $^{197}Au^{76+}$ [46], 230.650(81) eV in $^{208}Pb^{79+}$ [46], 280.645(15) eV in $^{238}U^{89+}$ [47]. The experimental uncertainty of the energy difference between the $(1s^2 2s2p)\,^3P_1 - {}^1S_0$ levels in Be-like $^{238}U^{88+}$ was reported to be 4×10^{-5} [47], while the energy of the $(1s^2 2s2p)\,^3P_2 - {}^3P_1$ transition in $^{40}Ar^{14+}$ was determined with the relative accuracy of about 10^{-6} [48]. The energy difference between the levels $(1s^2 2s^2 2p)\,^2P_{3/2}$ and $(1s^2 2s^2 2p)\,^2P_{1/2}$ in B-like argon was measured with the relative accuracy of about 2×10^{-7} [48]. This accuracy even allows to probe QED radiative corrections of second order in α and the tiny effect of the relativistic nuclear recoil corrections. High-precision theoretical calculations (see, e.g., Refs. [45, 48, 49, 50, 51, 52, 53, 54]) agree well with aforesaid experimental results, although for Be-like and B-like ions the theory still needs to be improved.
High-precision experiments on measurements of the ground state hyperfine splitting in $^{207}Pb^{81+}$ [55], $^{185}Re^{74+}$ and $^{187}Re^{74+}$ [56], $^{203}Tl^{80+}$ and $^{205}Tl^{80+}$ [57] stimulate intensive theoretical investigations. The Bohr-Weisskopf effect, corresponding to the correction due to the nuclear magnetization distribution, restricted the test of QED predictions for the hyperfine splitting. In this context, it was proposed to consider a specific difference of the ground state hyperfine splitting in H-like and Li-like ions [58]. In this specific difference the nuclear corrections almost vanish completely. Besides, in the work [59] a method to deduce the Bohr-Weisskopf correction from experimental data for the hyperfine structure in corresponding muon ions was proposed.
The accuracy of the theoretical value of the g factor for high-Z ions is limited by nuclear structure corrections. In

Ref. [60] it was proposed to consider the difference between the g factors of H-like and Li-like ions. The most accurate calculations on the g factor in Li-like ions were performed in Refs. [61, 62, 63]. Besides, it is proposed to consider a specific difference of the g factors of H-like and B-like ions in the lead region [64]. This opens the prospective for a determination of the fine structure constant to an accuracy of about 10^{-9}, which is better than that of the currently accepted value.

Parity nonconservation (PNC) is caused by the weak interaction. Investigations of parity nonconservation effects in atomic systems play a prominent role in tests of the standard model and impose constraints on physics beyond it. Mixing of the states with different parity leads to an asymmetry in the circular polarization of the emitted photons [65]. Theoretical calculations of this effect were considerably improved for neutral atoms (see, e.g., Refs. [66, 67, 68, 69, 70]). The most precise determination of the weak charge from the atomic physics was provided by a comparison of experimental data [71] and theoretical results [69, 70] for the PNC-transition amplitudes in neutral ^{133}Cs. However, further improvements of the theoretical calculations are restricted by the accuracy in treatments of the electron-correlation effects. For this reason, investigations of He-like europium ^{152}Eu^{61+}, where a strong mixing of the levels 2^1S_0 and 2^3P_0 occurs, look very promising [72]. The theoretical evaluation of parity nonconservation effects require a very accurate knowledge of transition energies and levels widths.

Apart from the energy, the widths of electron levels represent most important spectroscopic properties of multicharged ions. The level width is determined by a sum of all possible transition rates to lower-lying states. For a long time, beam-foil spectroscopy has been the only technique available that permitted measurements of atomic lifetimes (see, e.g., Refs. [73, 74] and references therein). By means of this technique, one can prepare ions of any element passing the original beam through a thin foil at different energies. Displacing the foil from the line of sight of the spectrometer permits the recording of transition photons at given times after the excitation. And thus one can compile the distribution of the photons from the decay of excited states. However, this technique has serious disadvantages: the experimental results depend on less accessible parameters, such as the velocity of the ions after passing through the foil, background cascade decay processes from highly excited states, etc. Therefore, the relative uncertainty of this method usually cannot be reduced below the level of several percents. However, there exist interesting exceptions, the most striking example is the measurement of the decay rate of the state 2^3S_1 in He-like ^{93}Nb^{39+}, where an accuracy of about 0.35% [75] has been achieved.

Another techniques for the decay rate measurements utilize various types of ion traps: electrostatic, magnetic, and radio frequency fields. Within a trap the ions are kept at some low gas pressure, but to determine the lifetime under clean conditions the results are extrapolated to zero pressure. For a long time, experiments were conducted at a pressure within the range of $10^{-7} - 10^{-8}$ mbar, which kept the uncertainty of the extrapolation quite high. Recent developments in ionization techniques allow for a considerable reduction of the pressure inside of the trap by several orders in magnitude (up to $10^{-9} - 10^{-12}$ mbar). This opens new prospects for measurements of transition rates in multicharged ions. The Electron Beam Ion Trap (EBIT) is one of the most successful setup for measurements of decay rates, see, e.g., Refs. [76, 77]. A schematic setup of an EBIT combining the electron beam with a magnetic ion trap (with typically $3-8$ T field strength) is depicted in Fig. 1.2. The electron beam collimated along the magnetic field ionizes atoms in the trap via collisions and compensates simultaneously the space charge of the cloud of positive ions that is being built up in the trap. The drift tubes closest to the trap center accelerate the electrons and suppress axial ion losses. When the electron beam is switched off the excited states of the ions decay and one can measure the intensity of the radiation. Such techniques were successfully employed for multicharged ions, see, e.g., Refs. [76, 77, 78, 79, 80, 81, 82, 83, 84, 85]. The most accurate results were recently obtained at the Heidelberg EBIT: the lifetime of the state $(1s^22s^22p)\,^2P_{3/2}$ in ^{40}Ar^{13+} results 9.573(4)(5) ms [76, 77], and the lifetime of the state $(1s^22s^22p^63s^23p)\,^2P_{3/2}$ in ^{56}Fe^{13+} – 16.79(3) ms [85]. Thus best-to-date methods for the measuring of the decay rates allow to achieve an accuracy of the order of 0.1%. This opens new facilities for probing the influences of QED and relativistic-correlation effects on atomic transition probabilities. In addition to

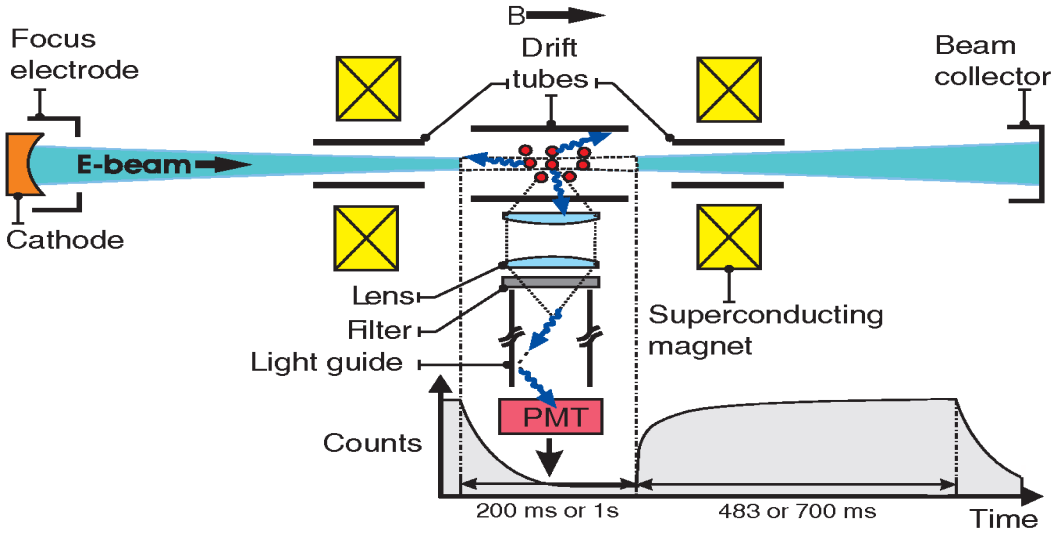

Figure 1.2: Experimental setup at the Heidelberg EBIT [76].

the detailed understanding of the atomic structure, investigations of transition rates in multicharged ions are of great interest in plasma diagnostics and astrophysics. The relative intensities of nonrelativistic forbidden transitions are often employed as a most sensitive tool for density diagnostics and coronal lines analysis.

A huge amount of works were devoted to the theoretical description of the atomic many-body problem. For the evaluation of correlation corrections to transition amplitudes various methods were employed: multiconfiguration Hartree-Fock (MCHF) [86], method of model potential [87], multiconfiguration Dirac-Fock (MCDF) [88, 89, 90, 91], many-body perturbation theory (MBPT) [92, 93, 94], etc. In work [90] for the first time the contribution from negative-continuum states is also incorporated. It turns out that this contribution crucially depends on the choice of the one-electron model potential, which is employed as the starting point of any MBPT or MCDF calculations. Despite a large number of theoretical works performed in the past the rigorous treatment of interelectronic-interaction corrections to the transition rates in the framework of QED has yet to be achieved. The radiative corrections to the decays $2p_{3/2}, 2p_{1/2}, 2s-1s$ in hydrogenic ions were recently evaluated to all orders in αZ in Ref. [95]. However, for the transition between fine-structure levels $2p_{3/2}$ and $2p_{1/2}$, which corresponds to the most precise measurement [76, 77], the QED corrections have not been calculated yet. In this thesis a complete QED calculation of interelectronic-interaction corrections to first order in $1/Z$ and the evaluation of QED corrections to the amplitude of the transition $2p_{3/2} - 2p_{1/2}$ are presented.

For ions with nonzero nuclear spin the additional reduction of lifetime can appear due to the hyperfine admixture of the levels with considerably larger transition probability to the ground state. This effect is known as hyperfine quenching. Investigation of the hyperfine quenching attracts essential interest due to its strong dependence on the energy of the fine-structure levels and nuclear moments. In particular, the measurements of the 2^3P_0 state lifetimes in Ag^{45+} [96, 97], Ni^{26+} [98], and Gd^{62+} [99] give precise values of the fine-structure splitting of the levels $2^3P_1 - 2^3P_0$. In present work the hyperfine quenching effect is considered for the $2^3P_{0,2}$ states in He-like ions.

1.2 Overview

Having motivated the main task of this thesis on the basis of recent experimental investigations of structure and dynamic processes in atomic systems aiming at utmost precision and given a brief overview of the present status of theoretical approaches to the atomic many-electron problem, the content will be as follows:

Chapter 2 is devoted to a determination of the Zemach and magnetic radii of the proton from a comparison between theoretical and experimental data of the hyperfine splitting in hydrogen and in muonium. The various theoretical contributions to the hyperfine splitting are considered. The formulas for the relativistic nuclear-size correction are derived in Appendix A. In order to obtain a refined value of the proton-size correction some of the contributions have to be recalculated. Employing the experimental value of the hyperfine structure in hydrogen we deduce the Zemach radius of the proton and compare it with previous results. The determination of the magnetic radius of the proton is performed employing an exponential parametrization for the electric and magnetic form factors. The results obtained are compared with corresponding data derived from elastic electron-proton scattering experiments. Moreover, we consider the extraction of the Zemach radius from a rescaled difference between the hyperfine splitting in hydrogen and muonium.

Chapter 3 presents the derivation of formal expressions for the radiative and interelectronic-interaction corrections to the transition amplitudes from the first principles of QED. Starting with detailed description of the basic theory of bound-state QED we employ the two-time Green's function method developed in Ref. [100]. It allows for the determination of the energy levels and transition probabilities from the poles of the two-time Green's functions. The formulas derived can be employed both for single and quasidegenerate or degenerate states. For the case of one-electron ions the derivation of formal expressions for the self-energy and vacuum-polarization correction to the transition amplitude is given next. For the case of two-electron ions and few-electron ions with one electron over the closed shells the application of the two-time Green's function approach to the interelectronic-interaction corrections is demonstrated.

Chapter 4 is devoted to the evaluation of the one-loop QED corrections to the transition rates. It mainly focuses on the one-electron transition $2p_{3/2} - 2p_{1/2}$. This calculation is motivated by the accurate measurement of the lifetime of the $(1s^2 2s^2 2p)\,^2P_{3/2}$ level in B-like Ar, recently performed at the Heidelberg EBIT [76, 77]. The calculation presented incorporates QED corrections to all orders in αZ. The vacuum-polarization contribution is evaluated in the Uehling approximation. For the self-energy correction the scheme allowing for a separate treatment of the one-potential term in the momentum space is employed. The approach developed here considerably improves the convergence of the partial-wave expansion. The derivation of formulas for the zero-potential vertex term, which is calculated in the momentum space, is given in Appendix B. Numerical results are presented for the experimentally most interesting region of nuclear charge numbers $Z = 16 - 22$.

In Chapter 5 we evaluate the following transition probabilities: $2^3S_1 - 1^1S_0$, $2^3P_2 - 1^1S_0$, and $3^3S_1 - 2^3S_1$ in He-like ions, $(1s^2 2s^2 2p)\,^2P_{3/2} - {}^2P_{1/2}$ in B-like ions and $(1s^2 2s 2p)\,^3P_1 - {}^3P_2$ in Be-like ions. Numerical solutions of the Dirac equation are generated. A most suitable finite-basis set is constructed in terms of B-splines utilizing the dual kinetic balance approach [101]. The latter also respects charge conjugation symmetry and considerably improves the convergence and the numerical accuracy. For He-like ions the systematic QED approach is employed for calculating the interelectronic-interaction corrections of first order in $1/Z$. For B-like and Be-like ions the interelectronic-interaction and radiative corrections to the transition amplitude are considered. The configuration-interaction method in the Dirac-Fock-Sturm basis (CIDFS) as described in details in Appendix C is employed in order to evaluate the interelectronic-interaction contribution for the transitions in B-like and Be-like ions. Corrections to the many-electron wave functions due to single-particle excitations from the negative-continuum energy states are taken into account. The frequency-dependent term is calculated within perturbation theory to first order in $1/Z$. The comparison of the obtained results with other theoretical and experimental data is

presented.
Chapter 6 is devoted to the effect of hyperfine quenching in He-like ions. Employing perturbation theory for quasidegenerate states we evaluate the proper wave functions including the hyperfine admixture. Considering the effective Hamiltonian [102], which treats some terms within jj-coupling scheme and others within LS-coupling, allows to take into account higher-order corrections. The results obtained are compared with other theoretical and experimental data.
Finally, Chapter 7 concludes this thesis with a summary.

1.3 Notations and conventions

Throughout the thesis relativistic units ($\hbar = c = m_{\rm e} = 1$) and the Heaviside charge unit, where $\alpha = e^2/(4\pi)$ and $e < 0$ are employed. However, whenever it seems convenient, the electron mass $m_{\rm e}$ is obviously restored in expressions. Besides, we employ following definitions: x^μ for contravariant four-vector, $x_\mu = g_{\mu\nu}x^\nu$ for covariant four-vector, $g_{\mu\nu}$ is the metric tensor

$$g_{\mu\nu} = g^{\mu\nu} = \begin{pmatrix} 1 & 0 & 0 & 0 \\ 0 & -1 & 0 & 0 \\ 0 & 0 & -1 & 0 \\ 0 & 0 & 0 & -1 \end{pmatrix} , \tag{1.1}$$

and $\gamma^\mu = (\beta, \beta\boldsymbol{\alpha})$ are the Dirac matrices in their standard representation

$$\alpha^0 = \begin{pmatrix} I & 0 \\ 0 & I \end{pmatrix} , \quad \boldsymbol{\alpha} = \begin{pmatrix} 0 & \boldsymbol{\sigma} \\ \boldsymbol{\sigma} & 0 \end{pmatrix} , \quad \beta = \begin{pmatrix} I & 0 \\ 0 & -I \end{pmatrix} \tag{1.2}$$

together with the 2×2 Pauli matrices

$$I = \begin{pmatrix} 1 & 0 \\ 0 & 1 \end{pmatrix} , \quad \sigma_1 = \begin{pmatrix} 0 & 1 \\ 1 & 0 \end{pmatrix} , \quad \sigma_2 = \begin{pmatrix} 0 & -i \\ i & 0 \end{pmatrix} , \quad \sigma_3 = \begin{pmatrix} 1 & 0 \\ 0 & -1 \end{pmatrix} . \tag{1.3}$$

The scalar product of four-vectors is defined by $kx = k^\mu x_\mu = k^0 x_0 - \mathbf{kx}$. By default, the summation over repeated indices is implied.

2 Proton structure

High-precision measurements and calculations of energy spectra of light atoms provide tests of QED with very high precision (see, e.g., CODATA [3] and references therein). In some cases, the current accuracy of QED calculations exceeds those of the known values of fundamental physical parameters. The hyperfine splitting in hydrogen represents exactly such a case. It thus provides a unique possibility for the deduction of proton structure (size) parameters via atomic physics measurements with higher accuracy, as it can be usually achieved in nuclear or high-energy physics experiments.

2.1 Hyperfine structure in hydrogen

The interaction between a bound electron and the magnetic field induced by a non-zero nuclear magnetic spin I leads to the hyperfine splitting of the atomic levels. In the point-dipole approximation the interaction Hamiltonian is given by the Fermi-Breit operator

$$H_\mu = \frac{|e|}{4\pi}\frac{(\boldsymbol{\alpha}\cdot[\boldsymbol{\mu}_I\times\mathbf{r}])}{r^3}\,, \tag{2.1}$$

where $\boldsymbol{\mu}_I$ is the nuclear magnetic moment operator. To evaluate the hyperfine splitting in a hydrogen-like ion in first order perturbation theory, one has to evaluate matrix elements of the Fermi-Breit operator with the unperturbed wave functions of the atomic system. In the case of an infinitely heavy point nucleus, this yields for an arbitrary state [103]

$$\begin{aligned}\Delta E &= \frac{|e|}{4\pi}\frac{\mu_I}{I}\frac{\kappa}{j(j+1)}\frac{(\alpha Z)^3[2\kappa(\gamma+n_r)-N]m_{\rm e}^2}{N^4\gamma(4\gamma^2-1)}\\ &\quad\times[F(F+1)-I(I+1)-j(j+1)]\,,\end{aligned} \tag{2.2}$$

where F is the total angular momentum of the ion, I and j are the nuclear and total electronic angular momenta, respectively, $n_r = n-|\kappa|$ is the radial quantum number, n is the principal quantum number, $\kappa = (-1)^{j+l+1/2}\times(j+\frac{1}{2})$ is the relativistic angular momentum quantum number, $l = j\pm 1/2$ determines the parity of the state, $\gamma = \sqrt{\kappa^2-(\alpha Z)^2}$, and $N = \sqrt{n_r^2+2n_r\gamma+\kappa^2}$.

Now let us turn to the hydrogen atom, where the measurement of the ground-state hyperfine splitting represents one of the most precise experiment with a relative accuracy better than 10^{-12} [29]

$$\Delta E^{\rm p}_{\rm exp} = 1420.405751767(1)\,{\rm MHz}\,. \tag{2.3}$$

The error associated with calculations of QED corrections to the hyperfine splitting is estimated to contribute on the level 10^{-9}. The major theoretical uncertainty arises from nuclear structure-dependent contributions. The most important one is the proton-size correction, which is determined exclusively by the spatial distributions of the charge and the magnetic moment of the proton. It contributes on the relative level of 10^{-5}. Assuming that all other theoretical corrections are accurately known, one can determine the proton-size contribution by comparing

Figure 2.1: Schematic decomposition of the hyperfine splitting in hydrogen.

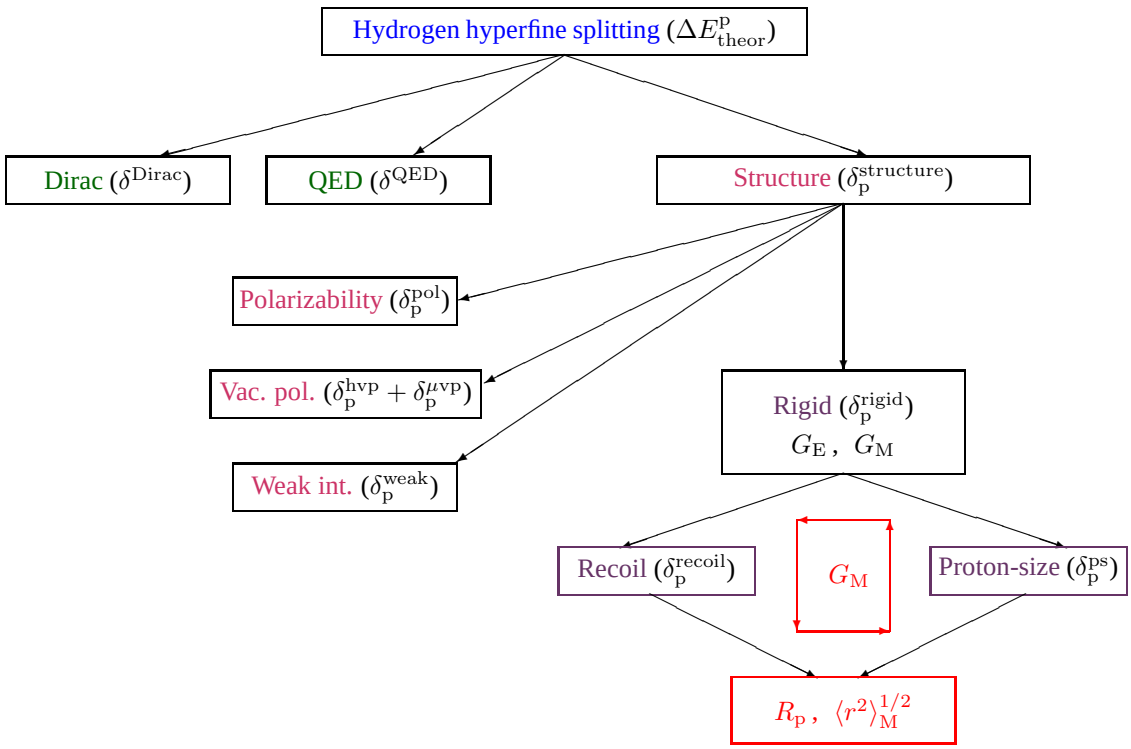

theoretical and experimental values for the hyperfine splitting in hydrogen. The major goal of this Chapter is to determine the Zemach and the magnetic radii of the proton via such a comparison.

The theoretical value for hyperfine splitting of the ground state in hydrogen ($Z = 1$) can be decomposed in the form

$$\Delta E^{\rm p}_{\rm theor} = E^{\rm p}_{\rm F}(1 + \delta^{\rm Dirac} + \delta^{\rm QED} + \delta^{\rm structure}_{\rm p})\,. \tag{2.4}$$

Fermi's expression for the magnetic-dipole interaction energy $E^{\rm p}_{\rm F}$ [104] appears as overall prefactor

$$E^{\rm p}_{\rm F} = \frac{8}{3}\alpha(\alpha Z)^3 \frac{m_{\rm e}^2 m_{\rm p}^2}{(m_{\rm e}+m_{\rm p})^3}\,\frac{\mu_{\rm p}}{\mu_{\rm N}}\,, \tag{2.5}$$

where $\mu_{\rm p}$ is the magnetic dipole moment of the proton, $\mu_{\rm N}$ is the nuclear magneton, and $m_{\rm p}$ denotes the proton mass. The subscript "p" defines the quantities depending on the proton parameters, such as mass or internal structure. The relativistic Dirac ($\delta^{\rm Dirac}$) and QED corrections ($\delta^{\rm QED}$) calculated in the external field approximation do not depend on the proton structure. Here and in what follows we keep explicitly the nuclear charge number Z to separate the relativistic and radiative corrections. The relativistic contribution $\delta^{\rm Dirac}$ can easily be obtained in terms of an αZ-expansion from the Dirac equation:

$$\delta^{\rm Dirac} = \frac{3}{2}(\alpha Z)^2 + \frac{17}{8}(\alpha Z)^4 + \dots\,. \tag{2.6}$$

For an overview on recent achievements in calculations of the radiative correction $\delta^{\rm QED}$ we refer to Refs. [30, 31, 32, 33, 105, 106], from where we can take the result

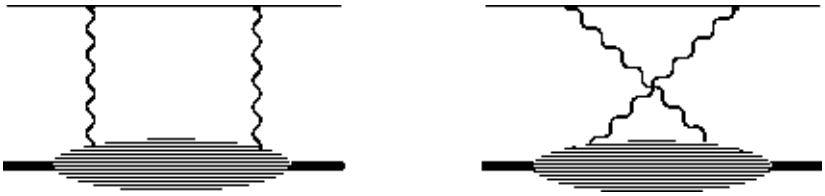

Figure 2.2: Feynman diagrams representing the proton-polarizability correction to the hyperfine splitting in hydrogen. The heavy and the thin lines represent the proton and the electron, respectively. The wavy lines describe the interaction between electron and proton via exchange of virtual photons. The shaded region indicates the internal dynamic of the proton.

$$\begin{aligned}\delta^{\rm QED} &= \kappa_{\rm e} + \frac{\alpha}{\pi}\left\{\alpha Z\pi\Big(\ln 2 - \frac{5}{2}\Big) + (\alpha Z)^2\left[\ln(\alpha Z)\Big(\frac{16}{3}\ln 2 - \frac{281}{180} - \frac{8}{3}\ln(\alpha Z)\Big) - \frac{8}{15}\ln 2\right.\right.\\ &\left.\left. + \frac{34}{225} + 17.122339\ldots\right] + (\alpha Z)^3\pi\left[\ln(\alpha Z)\Big(\frac{547}{48} - 5\ln 2\Big) + \frac{539}{288} - 4.55(35)\right]\right\}\\ &+ \frac{\alpha^2}{\pi^2}\left\{0.7718(4)\alpha Z\pi + (\alpha Z)^2\left[\ln(\alpha Z)\Big(1.278001088\ldots - \frac{4}{3}\ln(\alpha Z)\Big) + 10(2.5)\right]\right\} \quad (2.7)\end{aligned}$$

with the anomalous magnetic moment coefficient

$$\kappa_{\rm e} = \left[\frac{\alpha}{2\pi} - 0.328\,478\,965\ldots\left(\frac{\alpha}{\pi}\right)^2 + 1.181\,241\,456\ldots\left(\frac{\alpha}{\pi}\right)^3 + \cdots\right]. \quad (2.8)$$

The uncertainty of $\delta^{\rm QED}$ is mainly determined by uncalculated high-order terms $\alpha^3(\alpha Z)$ and by the uncertainties associated with some of the calculated terms indicated in Eq. (2.7). The proton structure-dependent correction $\delta_{\rm p}^{\rm structure}$ is usually expressed as the sum referring to various distinct physical processes and effects

$$\delta_{\rm p}^{\rm structure} = \delta_{\rm p}^{\rm pol} + \delta_{\rm p}^{\rm hvp} + \delta_{\rm p}^{\mu\rm vp} + \delta_{\rm p}^{\rm weak} + \delta_{\rm p}^{\rm rigid}. \quad (2.9)$$

This decomposition is illustrated in Fig. 2.1. The part $\delta_{\rm p}^{\rm pol}$ associated with polarizability effects due to intrinsic proton dynamics is mainly determined by the two-photon exchange diagrams depicted in Fig. 2.2. This correction was evaluated in work [34] employing semi-empirical structure functions of polarized protons.

The correction due to hadronic vacuum-polarization $\delta_{\rm p}^{\rm hvp}$ is determined by the Feynman diagrams depicted in Fig. 2.3. Currently the most accurate result for this term was obtained in Refs. [107, 108] utilizing dispersion relations together with experimental data on the annihilation cross section of e^+e^- into hadrons. The muonic vacuum-polarization contribution $\delta_{\rm p}^{\mu\rm vp}$ was evaluated in Ref. [109]. For the weak interaction term $\delta_{\rm p}^{\rm weak}$ we refer to the works [110, 111]. Values for all these corrections together with corresponding uncertainties are presented in Table 2.1. The Fermi energy shift $E_{\rm F}^{\rm p}$ is evaluated employing the values of the fundamental constants tabulated in Ref. [3].

The quantity $\delta_{\rm p}^{\rm rigid}$ parameterizing all remaining rigid properties of the proton can be deduce from a comparison between theoretical and experimental data of the hyperfine splitting

$$\delta_{\rm p}^{\rm rigid} = \Delta E_{\rm exp}^{\rm p}/E_{\rm F}^{\rm p} - 1 - \delta^{\rm Dirac} - \delta^{\rm QED} - \delta_{\rm p}^{\rm pol} - \delta_{\rm p}^{\mu\rm vp} - \delta_{\rm p}^{\rm hvp} - \delta_{\rm p}^{\rm weak}. \quad (2.10)$$

This equation yields the $\delta_{\rm p}^{\rm rigid} = -34.14(60)\times 10^{-6}$. It should be mentioned only that the leading chiral logarithms contributions to the structure-dependent correction have been also investigated within an effective field theory [115], which allows for an explanation of about 2/3 of the proton-structure correction.

In next Section we present our new results of the extraction of Zemach and magnetic radii from the rigid correction $\delta_{\rm p}^{\rm rigid}$.

Figure 2.3: Feynman diagrams representing the hadronic vacuum polarization correction to the hyperfine structure in hydrogen.

2.2 Zemach and magnetic radii of the proton

The rigid term $\delta_{\rm p}^{\rm rigid}$ is determined by the electric and magnetic form factors of the proton. This quantity may be decomposed into two parts: $\delta_{\rm p}^{\rm rigid} = \delta_{\rm p}^{\rm ps} + \delta_{\rm p}^{\rm recoil}$, where $\delta_{\rm p}^{\rm ps}$ represents the proton-size correction and $\delta_{\rm p}^{\rm recoil}$ is associated with recoil effects. The recoil part contains both contributions arising from a pointlike Dirac proton and additional recoil correction due to the internal proton structure, respectively. Following Ref. [112] we may not distinguish between them. The dominant contribution (relative order $(\alpha Z)m_{\rm e}/m_{\rm p}$) to the recoil correction is defined by the two-photon exchange diagrams depicted in Fig. 2.4. Following the systematic treatment presented in Ref. [112] and adopting the notations introduced in Ref. [113], it can be written as the sum of the following integrals:

$$\delta_{\rm p}^{\rm recoil}({\rm VO}) = -\frac{8\alpha m_{\rm e}m_{\rm p}}{\pi^2(m_{\rm p}^2-m_{\rm e}^2)}\int_0^\infty {\rm d}\xi{\rm d}p\,p^4\left\{\left[\frac{2m_{\rm e}^2}{(p^2+\xi^2)^2+4m_{\rm e}^2\xi^2}-\frac{2m_{\rm p}^2}{(p^2+\xi^2)^2+4m_{\rm p}^2\xi^2}\right]\right.$$
$$\left.\times\,\frac{G_{\rm E}(p^2+\xi^2)G_{\rm M}(p^2+\xi^2)}{(p^2+\xi^2)^2(1+\kappa_{\rm e})}-\left[\frac{2m_{\rm e}^2}{p^4+4m_{\rm e}^2\xi^2}-\frac{2m_{\rm p}^2}{p^4+4m_{\rm p}^2\xi^2}\right]\frac{G_{\rm E}(p^2)G_{\rm M}(p^2)}{p^4(1+\kappa_{\rm e})}\right\}, \qquad (2.11)$$

$$\delta_{\rm p}^{\rm recoil}({\rm VV}) = \frac{6\alpha m_{\rm e}m_{\rm p}}{\pi^2(m_{\rm p}^2-m_{\rm e}^2)}\int_0^\infty {\rm d}\xi{\rm d}p\,p^2\left[\frac{1}{(p^2+\xi^2)^2+4m_{\rm e}^2\xi^2}-\frac{1}{(p^2+\xi^2)^2+4m_{\rm p}^2\xi^2}\right]$$
$$\times\frac{[G_{\rm M}(p^2+\xi^2)]^2}{1+\kappa_{\rm e}}, \qquad (2.12)$$

$$\delta_{\rm p}^{\rm recoil}(\kappa_{\rm e}^2) = \frac{-2\alpha m_{\rm e}m_{\rm p}}{\pi^2(m_{\rm p}^2-m_{\rm e}^2)}\int_0^\infty {\rm d}\xi{\rm d}p\,p^2\frac{3\xi^2+2p^2}{p^2+\xi^2}\left[\frac{16m_{\rm p}^4}{(p^2+\xi^2)^2+4m_{\rm e}^2\xi^2}-\frac{16m_{\rm p}^4}{(p^2+\xi^2)^2+4m_{\rm p}^2\xi^2}\right]$$
$$\times\frac{[G_{\rm M}(p^2+\xi^2)-G_{\rm E}(p^2+\xi^2)]^2}{(p^2+\xi^2+4m_{\rm p}^2)^2(1+\kappa_{\rm e})}, \qquad (2.13)$$

$$\delta_{\rm p}^{\rm recoil}({\rm No.1}) = \frac{-2\alpha m_{\rm e}m_{\rm p}}{\pi^2(m_{\rm p}^2-m_{\rm e}^2)}\int_0^\infty {\rm d}\xi{\rm d}p\,p^2\frac{3\xi^2+2p^2}{p^2+\xi^2}\frac{16m_{\rm p}^4}{(p^2+\xi^2)^2+4m_{\rm p}^2\xi^2}$$
$$\times\frac{[G_{\rm M}(p^2+\xi^2)-G_{\rm E}(p^2+\xi^2)]^2}{(p^2+\xi^2+4m_{\rm p}^2)^2(1+\kappa_{\rm e})}, \qquad (2.14)$$

$$\delta_{\rm p}^{\rm recoil}({\rm No.2}) = \frac{4\alpha m_{\rm e}m_{\rm p}}{\pi^2(m_{\rm p}^2-m_{\rm e}^2)}\int_0^\infty {\rm d}\xi{\rm d}p\,p^2\frac{p^2}{p^2+\xi^2}\frac{4m_{\rm p}^2}{(p^2+\xi^2)^2+4m_{\rm p}^2\xi^2}$$
$$\times\frac{[G_{\rm M}(p^2+\xi^2)-G_{\rm E}(p^2+\xi^2)]G_{\rm M}(p^2+\xi^2)}{(p^2+\xi^2+4m_{\rm p}^2)(1+\kappa_{\rm e})}. \qquad (2.15)$$

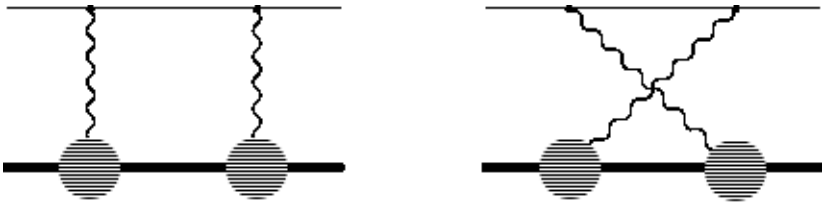

Figure 2.4: Feynman diagrams representing the two-photon exchange correction to the hyperfine splitting in hydrogen. The shaded circle defines the proton vertex operator.

Here the quantities $G_{\rm E/M}$ represent the electric and magnetic form factors, respectively. Since the atomic energy scale involved implies $q^0 \approx 0$, one can restrict to the static limit ($q^0 = 0$), and thus we define them to be dependent only on the spatial momentum transfer (squared), $\mathbf{q}^2 \equiv q^2 > 0$. For evaluating the higher-order recoil corrections it is sufficient to employ the point-dipole approximation. Accordingly, the contribution of the order $(\alpha Z)^2 m_{\rm e}/m_{\rm p}$ has been derived in Ref. [112] with the result 0.46 ppm, while the radiative-recoil correction of the order $\alpha(\alpha Z) m_{\rm e}/m_{\rm p}$ turns out to be $0.09(2)$ ppm [109].
The proton-size correction $\delta_{\rm p}^{\rm ps}$ in the nonrelativistic limit is given by the well-known Zemach formula [116]:

$$\delta_{\rm p}^{\rm Zemach} = -2\alpha Z \, \frac{m_{\rm e} m_{\rm p}}{m_{\rm e} + m_{\rm p}} \, R_{\rm p} \,, \tag{2.16}$$

where

$$R_{\rm p} = \int {\rm d}\mathbf{r} \, {\rm d}\mathbf{r}' \; \rho_{\rm E}(\mathbf{r}) \rho_{\rm M}(\mathbf{r}') |\mathbf{r} - \mathbf{r}'| = -\frac{4}{\pi} \int_0^\infty \frac{{\rm d}q}{q^2} \Big[\frac{\mu_{\rm N}}{\mu_{\rm p}} \, G_{\rm E}(q^2) \, G_{\rm M}(q^2) - 1 \Big] \tag{2.17}$$

defines the Zemach radius of the proton. This quantity represents the radius of interaction between the magnetic dipole distribution $\rho_{\rm M}(\mathbf{r})$ of the proton and the electron moving in the electric field of the distribution $\rho_{\rm E}(\mathbf{r})$. Here the nuclear charge and magnetization distributions $\rho_{\rm E}(\mathbf{r})$ and $\rho_{\rm M}(\mathbf{r})$, respectively, are normalized to unity. The charge and magnetic mean-square radii are defined by

$$\langle r^2 \rangle_{\rm E} = \int {\rm d}\mathbf{r} \, r^2 \rho_{\rm E}(\mathbf{r}) = -6 \frac{\rm d}{{\rm d}q^2} G_{\rm E}(q^2)|_{q^2=0} \tag{2.18}$$

and

$$\langle r^2 \rangle_{\rm M} = \int {\rm d}\mathbf{r} \, r^2 \rho_{\rm M}(\mathbf{r}) = -6 \frac{1}{\mu_{\rm p}} \frac{\rm d}{{\rm d}q^2} G_{\rm M}(q^2)|_{q^2=0} \,. \tag{2.19}$$

To determine the Zemach and magnetic radii of the proton from the hydrogen hyperfine splitting we propose the following. For a simpler understanding the procedure we again refer to Fig. 2.1. At first, we calculate the structure-dependent part of the recoil correction within a rough approach, taking the proton magnetic radius to be equal to the charge radius. Then we deduce the proton-size correction from a comparison between the experimental and theoretical values of the hyperfine splitting. Using the dipole parameterizations of the form factors we extract a preliminary value for the proton magnetic radius. Then, we recalculate the recoil-structure correction with the obtained value of the proton magnetic radius and take into account the radiative and binding contributions to the proton-size term. Finally, we again deduce the improved proton-size correction and determine the magnetic radius.
The dipole parameterization is a commonly used experimental fit for the proton form factors

$$G_{\rm D}(q^2) = \frac{1}{[1 + q^2 R_{\rm D}^2]^2} \,, \tag{2.20}$$

which descends from the exponential model of the charge/magnetization distribution. But recent investigations performed at the Jefferson Laboratory (JLab) [117, 118, 119] revealed, that for $q \geq 1$ GeV the behavior of the electric form factor deviates from the dipole parameterization. However, the Zemach correction is not sensitive to the form factors behavior for $q > 0.8$ GeV. As it was shown in Ref. [120], the contribution to the Zemach correction from the region $q > 0.8$ GeV remains almost the same for different experimental models of the proton electric and magnetic form factors. Therefore, in what follows, we stay with the dipole parameterizations for the form factors. In order to estimate the error associated with the slight model dependence, we consider also the parameterization

$$G_{\rm JLab}(q^2) = \left(1 - 0.13\frac{q^2}{\rm GeV^2}\right) G_{\rm D}(q^2)\,, \tag{2.21}$$

which is known as JLab model [117]. The parameters $R_{\rm D}$, one for the electric and another for the magnetic form factor, respectively, are fixed by the corresponding values for the root-mean-square radii.
In a first iteration one has to calculate the recoil-structure corrections $\delta_{\rm p}^{\rm recoil}({\rm VO})$, $\delta_{\rm p}^{\rm recoil}({\rm VV})$, $\delta_{\rm p}^{\rm recoil}(\kappa_{\rm e}^2)$, $\delta_{\rm p}^{\rm recoil}({\rm No.1})$, and $\delta_{\rm p}^{\rm recoil}({\rm No.2})$ given by Eqs. (2.11) – (2.15) with the best-to-date proton charge radius $\langle r^2\rangle_{\rm E}^{1/2} = 0.8750(68)$ fm [3] and with the same value for the magnetic proton radius. The total recoil correction turns out to be 5.84 ppm. Accordingly, the proton-size correction $\delta_{\rm p}^{\rm ps}$ is given by the expression

$$\delta_{\rm p}^{\rm ps} = \delta_{\rm p}^{\rm rigid} - \delta_{\rm p}^{\rm recoil}\,, \tag{2.22}$$

which yields the value $\delta_{\rm p}^{\rm ps} = -39.98(61)$ ppm. In a first step one can approximate the proton-size correction by the Zemach formula and can easily find the Zemach radius $R_{\rm p} = 1.058$ fm. To extract the magnetic radius of the proton from this result, one has to fit the parameter $R_{\rm D}$ associated with the magnetic form factor such as to reproduce the Zemach radius. As the result we find a preliminary value for the magnetic radius of the proton: $\langle r^2\rangle_{\rm M}^{1/2} = 0.800$ fm. The error associated with the model dependence is on the level of about 0.75%.
In a second step we account for corrections to the Zemach formula

$$\delta_{\rm p}^{\rm ps} = \delta_{\rm p}^{\rm Zemach} + \delta_{\rm p}^{\rm radiative} + \delta_{\rm p}^{\rm relativistic}\,, \tag{2.23}$$

where $\delta_{\rm p}^{\rm radiative}$ is the radiative structure-dependent correction obtained in Ref. [109] and $\delta_{\rm p}^{\rm relativistic}$ is the binding correction derived in Ref. [121]. The detailed description presented in Appendix A. The radiative correction has been derived assuming the exponential model with the same parameter $R_{\rm D}$ for both charge and magnetization distributions, i.e.

$$\delta_{\rm p}^{\rm radiative} = -\delta_{\rm p}^{\rm Zemach}\frac{\alpha}{3\pi}\Big[4\ln\left(m_{\rm e}R_{\rm D}\right) + \frac{4111}{420}\Big]\,. \tag{2.24}$$

The accuracy of this approximation is sufficient for our purpose here. Calculating $\delta_{\rm p}^{\rm radiative}$ for different $R_{\rm D}$, we obtain $\delta_{\rm p}^{\rm radiative} = 0.0153(2) \times \delta_{\rm p}^{\rm Zemach}$. The binding correction has been expressed in terms of electric and magnetic moments of the proton (see Appendix A):

$$\begin{aligned}
\delta_{\rm p}^{\rm relativistic} \;=\; & \delta_{\rm p}^{\rm Zemach}(\alpha Z)^2\Big[\frac{7}{4} - \gamma - \ln\left(2\alpha Z\right)\Big] - 2(\alpha Z)^3 m_{\rm e}\langle r\rangle_{\rm E}\left(\frac{\langle r\ln\left(m_{\rm e}r\right)\rangle_{\rm E}}{\langle r\rangle_{\rm E}} - \frac{839}{750}\right) \\
& -\frac{(\alpha Z)^3 m_{\rm e}R_0}{5}\left(\frac{3\langle r^4\rangle_{\rm M}}{2R_0^4} - \frac{19\langle r^6\rangle_{\rm M}}{42R_0^6} + \frac{19\langle r^8\rangle_{\rm M}}{360R_0^8} - \frac{2}{825}\frac{\langle r^{10}\rangle_{\rm M}}{R_0^{10}}\right) \\
& -(\alpha Z)^3 m_{\rm e}R_0\left(\frac{\langle r^2\rangle_{\rm M}}{R_0^2} - \frac{1}{10}\frac{\langle r^4\rangle_{\rm M}}{R_0^4}\right)\left(\ln\left(m_{\rm e}R_0\right) + \frac{1}{30}\right),
\end{aligned} \tag{2.25}$$

where γ is Euler's constant and $\langle r^n\rangle_{\rm E/M} = \int {\rm d}\mathbf{r}\; r^n \rho_{\rm E/M}(r)$. The radius parameter $R_0 = \sqrt{5/3}\langle r^2\rangle_{\rm E}^{1/2}$ corresponds to the radius of a homogeneously charged sphere taken as a model for the proton charge distribution.

Table 2.1: Numerical values for various corrections to the hyperfine splitting in hydrogen together with the assigned errors. The energies $\Delta E^{\rm p}_{\rm exp}$ and $E^{\rm p}_{\rm F}$ are given in units of MHz.

	Value	Error	Ref.
$\Delta E^{\rm p}_{\rm exp}$	1 420.405 751 767	0.000 000 001	[29]
$E^{\rm p}_{\rm F}$	1 418.840 08	0.000 02	[3]
$\Delta E^{\rm p}_{\rm exp}/E^{\rm p}_{\rm F}$	1.001 103 49	0.000 000 01	
$\delta^{\rm Dirac}$	0.000 079 88		
$\delta^{\rm QED}$	0.001 056 21	0.000 000 001	[30, 31, 32, 33, 105, 106]
$\delta^{\rm ps}_{\rm p}$	− 0.000 040 11	0.000 000 61	[114]
$\delta^{\rm recoil}_{\rm p}$	0.000 005 97	0.000 000 06	[109, 112, 113, 114]
$\delta^{\rm pol}_{\rm p}$	0.000 001 4	0.000 000 6	[34]
$\delta^{\rm hvp}_{\rm p}$	0.000 000 01		[107, 108]
$\delta^{\mu{\rm vp}}_{\rm p}$	0.000 000 07	0.000 000 02	[109]
$\delta^{\rm weak}_{\rm p}$	0.000 000 06		[110, 111]

Nevertheless, the error induced by using this model for the charge distribution in comparison to other models does not exceed 5%. Employing exponential parameterizations of the charge and magnetization distributions with electric and magnetic radii, $\langle r^2\rangle^{1/2}_{\rm E} = 0.8750(68)$ fm and $\langle r^2\rangle^{1/2}_{\rm M} = 0.800$ fm, respectively, we obtain $\delta^{\rm relativistic}_{\rm p} = 0.0002 \times \delta^{\rm Zemach}_{\rm p} + 1.4 \times 10^{-8}$. Thus the proton-size correction takes the form

$$\delta^{\rm ps}_{\rm p} = 1.0154(2) \times \delta^{\rm Zemach}_{\rm p} + 1.4 \times 10^{-8}\,. \tag{2.26}$$

In addition, we need to correct the dominant term of the recoil contribution with the magnetic radius $\langle r^2\rangle^{1/2}_{\rm M} = 0.800$ fm. As a result, the recoil correction turns out to be $5.94(6)$ ppm.
Deducing again the proton-size correction we finally deduce the Zemach radius of the proton:

$$R_{\rm p} = 1.045(16){\rm fm}\,. \tag{2.27}$$

This value differs from the one obtained in Ref. [122], $R_{\rm p} = 1.037(16)$ fm, mainly due our recalculated recoil corrections based on the improved and more accurate charge and magnetic moment distributions.

2.3 Results and discussion

The value for the Zemach radius obtained above enables us also to determine an improved magnetic radius of the proton:

$$\langle r^2\rangle^{1/2}_{\rm M} = 0.778(29){\rm fm}\,. \tag{2.28}$$

The corresponding uncertainty is mainly due to errors associated with the polarizability effect as well as the uncertainty of the charge radius of the proton. In Table 2.1 we present the final values for the contributions to the hyperfine splitting in hydrogen. The value for $\delta^{\rm ps}_{\rm p}$ has been obtained by means of the experimental energy splitting, according to Eqs. (2.10) and (2.22).
Recently Brodsky *et al.* [120] proposed an alternative method to extract the Zemach radius. They considered a rescaled difference between the hyperfine splitting in hydrogen and muonium

$$\frac{\Delta E^{\rm p}_{\rm exp}/E^{\rm p}_{\rm F}}{\Delta E^{\mu}_{\rm exp}/E^{\mu}_{\rm F}} = 1 + \delta^{\rm hfs}\,, \tag{2.29}$$

Table 2.2: Numerical values taken from the literature for various corrections to the hyperfine splitting in muonium together with the assigned errors. The energies $\Delta E^{\mu}_{\rm exp}$ and $E^{\mu}_{\rm F}$ are given in units of MHz.

	Value	Error	Ref.
$\Delta E^{\mu}_{\rm exp}$	4 463.302 765	0.000 053	[38]
$E^{\mu}_{\rm F}$	4 459.031 7	0.000 4	[3]
$\Delta E^{\mu}_{\rm exp}/E^{\mu}_{\rm F}$	1.000 957 84	0.000 000 09	
$\delta^{\rm Dirac}$	0.000 079 88		
$\delta^{\rm QED}$	0.001 056 21	0.000 000 001	[30, 31, 32, 33, 105, 106]
$\delta^{\rm recoil}_{\mu}$	− 0.000 178 33	0.000 000 02	[31, 112, 113, 123, 124, 125, 126]
$\delta^{\rm hvp}_{\mu}$	0.000 000 05		[107, 108]
$\delta^{\rm weak}_{\mu}$	− 0.000 000 01		[110, 111]

where "μ" indicates quantities which refer to the muon. $E^{\mu}_{\rm F}$ is the Fermi energy for muonium together with the experimental hyperfine structure value $\Delta E^{\mu}_{\rm exp} = 4\,463.302\,765(53)$ MHz [38]. Employing recent values of the fundamental constants [3] they have obtained $\delta^{\rm hfs} = 145.51$ ppm [120]. The ground state hyperfine splitting in muonium can be written as

$$\Delta E^{\mu}_{\rm theor} = E^{\mu}_{\rm F}(1 + \delta^{\rm Dirac} + \delta^{\rm QED} + \delta^{\rm recoil}_{\mu} + \delta^{\rm hvp}_{\mu} + \delta^{\rm weak}_{\mu})\,. \tag{2.30}$$

The corrections $\delta^{\rm Dirac}$ and $\delta^{\rm QED}$ are the same as in the case of hydrogen, $\delta^{\rm hvp}_{\mu}$ and $\delta^{\rm weak}_{\mu}$ are the hadronic vacuum-polarization and the weak interaction contributions, respectively, and $\delta^{\rm recoil}_{\mu}$ is the recoil term, which again consists of a relativistic and radiative part. With the aid of this formula together with Eqs. (2.4) and (2.29) one can immediately derive the proton-structure correction

$$\delta^{\rm structure}_{\rm p} = \delta^{\rm hfs} + \delta^{\rm recoil}_{\mu} + \delta^{\rm hvp}_{\mu} + \delta^{\rm weak}_{\mu} + \delta^{\rm hfs}(\delta^{\rm Dirac} + \delta^{\rm QED} + \delta^{\rm recoil}_{\mu} + \delta^{\rm hvp}_{\mu} + \delta^{\rm weak}_{\mu})\,. \tag{2.31}$$

Following Ref. [120], where the contributions $\delta^{\rm hvp}_{\mu}$ and $\delta^{\rm weak}_{\mu}$ have been neglected and only the relativistic part of the recoil correction [31, 112, 113, 123, 124, 125] has been taken into account, one obtains $\delta^{\rm structure}_{\rm p} = -31.8$ ppm. This yields the corresponding Zemach radius $R_{\rm p} = 1.019(16)$ fm [120], which differs significantly from our result, $R_{\rm p} = 1.045(16)$ fm. However, as we have found this difference disappears if one includes the omitted terms. This is mainly due to the radiative-recoil correction evaluated in Refs. [31, 123, 124, 125, 126]. With this term included, the total recoil correction is determined as $\delta^{\rm recoil}_{\mu} = -178.33(2)$ ppm. The hadronic vacuum-polarization contribution obtained in [107, 108] is $\delta^{\rm hvp}_{\mu} = 0.05$ ppm, while the value of the correction due to Z^0-boson exchange yields $\delta^{\rm weak}_{\mu} = -0.01$ ppm [110, 111]. Values for the corrections to the muonium hyperfine splitting are presented in Table 2.2. Substituting these contributions into expression (2.31), we find $\delta^{\rm structure}_{\rm p} = -32.64$ ppm. Utilizing the values presented in Tables 2.1 and 2.2, we obtain for the proton-size correction $\delta^{\rm ps}_{\rm p} = -40.15$ ppm. Then the Zemach radius can be easily determined with the result $R_{\rm p} = 1.047(16)$ fm, which is very close to the value obtained from the hydrogen hyperfine splitting alone, $R_{\rm p} = 1.045(16)$ fm.

Another way to determine the proton magnetic radius is based on experimental data from elastic electron-proton scattering. Accordingly, Friar and Sick have recently determined the Zemach radius of the proton to be $R_{\rm p} = 1.086(12)$ fm [127] and the proton charge radius $\langle r^2\rangle^{1/2}_{\rm E} = 0.895(18)$ fm [9]. Based on these values for $R_{\rm p}$ and $\langle r^2\rangle^{1/2}_{\rm E}$ and employing an exponential parameterization for both electric and magnetic form factors, we find the value of the proton magnetic radius $\langle r^2\rangle^{1/2}_{\rm M} = 0.824(27)$ fm. This value is in a good agreement with the recent experimental value of Sick – $0.855(35)$ fm presented in Ref. [128], and comes also close to the result of Hammer and Meißner 0.857 fm [128].

As one can see, only a disagreement with the value for the Zemach radius and, thus, with the magnetic radius, as it is obtained from the electron-proton scattering experiments, remains. We emphasize that a careful analysis of elastic form factor fits could well be warranted. Accordingly, the Zemach and magnetic radii obtained here could serve as reliable constraints for such fits evaluated solely from atomic spectroscopic data.

3 QED theory of the transition rates

This Chapter provides the basic formalism of the QED theory of transition probabilities taking into account QED and interelectronic-interaction corrections. Renormalized expressions for one- and two-electron ions as well as for ions with one electron over closed shells are derived within the two-time Green's function approach [100]. It allows for a nonperturbative treatment with respect to the effective coupling αZ. This is especially required, since in multicharged ions the parameter αZ is not small.

3.1 Bound-state QED

QED of bound electrons in atoms and ions is formulated within the interaction picture by starting with the single-particle Dirac equation [129]

$$h_{\rm D}\phi_n(\mathbf{x}) = [-i\boldsymbol{\alpha}\cdot\boldsymbol{\nabla} + V(\mathbf{x}) + \beta]\,\phi_n(\mathbf{x}) = \varepsilon_n\phi_n(\mathbf{x}) \tag{3.1}$$

with a static potential $V(\mathbf{x})$, which may contain both the potential of the nucleus and an effective single-particle potential which to some approximation accounts for the interelectronic interaction. The time-dependent single-particle solutions of the Dirac equation have the form

$$\phi_n(x) = \phi_n(\mathbf{x})e^{-i\varepsilon_n t}\,. \tag{3.2}$$

The Dirac field operator $\psi(x)$ describing the electrons and positrons is expanded in terms of the single-particle solutions (3.2) of the Dirac equation (3.1) according to

$$\psi(x) = \sum_{\varepsilon_n>0} a_n\phi_n(x) + \sum_{\varepsilon_m<0} b_m^\dagger\phi_m(x)\,, \tag{3.3}$$

where a_n denotes the electron annihilation operator for an electron in state n and $b_m^\dagger$ is the positron creation operator for a positron in state m. The canonical equal-time anticommutators for the field operators imply the anticommutation relations

$$\{a_n, a_m^\dagger\} = \delta_{nm}\,, \qquad \{a_n, a_m\} = \{a_n^\dagger, a_m^\dagger\} = 0\,, \tag{3.4}$$

$$\{b_n, b_m^\dagger\} = \delta_{nm}\,, \qquad \{b_n, b_m\} = \{b_n^\dagger, b_m^\dagger\} = 0\,, \tag{3.5}$$

$$\{a_n, b_m\} = \{a_n, b_m^\dagger\} = \{a_n^\dagger, b_m\} = \{a_n^\dagger, b_m^\dagger\} = 0\,. \tag{3.6}$$

The unperturbed state vectors are generated by the action of the creation operators on the Dirac vacuum state $|0\rangle$. For example, an N-electron one-determinant state is given by

$$|A\rangle = \frac{1}{\sqrt{N!}}\sum_P (-1)^P a_{Pa_1}^\dagger\cdots a_{Pa_N}^\dagger|0\rangle\,, \tag{3.7}$$

where the sum is carried out over all permutations, and P defines the parity of the permutation. The unperturbed Hamiltonian is given by the normal-ordered expression (N denotes normal ordering)

$$H_{\rm e} = \int {\rm d}\mathbf{x}\, N\psi^\dagger(x) h_{\rm D}\psi(x) = \sum_{\varepsilon_n>0} \varepsilon_n a_n^\dagger a_n - \sum_{\varepsilon_m<0} \varepsilon_m b_m^\dagger b_m \,. \tag{3.8}$$

The propagator of the electron-positron field is defined by the vacuum expectation value of the time-ordered product

$$S(x^0-y^0,\mathbf{x},\mathbf{y}) = -i\langle 0|T\psi(x)\overline{\psi}(y)|0\rangle = \frac{1}{2\pi}\int_{-\infty}^{\infty} {\rm d}\omega\, e^{-i\omega(x^0-y^0)} \sum_n \frac{\phi_n(\mathbf{x})\overline{\phi}_n(\mathbf{y})}{\omega-\varepsilon_n(1-i0)}\,, \tag{3.9}$$

where T denotes the time-ordering operator. Since the external potentials are static, in what follows we use the temporal Fourier-transformed propagation function in the eigenmode representation

$$S(\omega,\mathbf{x},\mathbf{y}) = \sum_n \frac{\phi_n(\mathbf{x})\overline{\phi}_n(\mathbf{y})}{\omega-\varepsilon_n(1-i0)}\,. \tag{3.10}$$

For the covariant quantization of the free electromagnetic field we employ the Gupta-Bleuler formalism presented in detail in a number classical textbooks, see, e.g. Ref. [130]. The free field equations in the Feynman gauge are

$$\Box A^\mu(x) = 0\,. \tag{3.11}$$

The corresponding plane wave solutions can be written as

$$A^\mu_{k,\lambda}(x) = A^\mu_{k,\lambda}(\mathbf{x}) e^{-ik^0x^0} = \frac{\epsilon^{(\lambda)\mu}\, e^{-ikx}}{\sqrt{2k^0(2\pi)^3}}\,, \tag{3.12}$$

where $k=(k^0=|\mathbf{k}|,\mathbf{k})$ is the wave vector, and $\epsilon^{(\lambda)\mu}$ determines the polarization of the photon. The electromagnetic field operator $A^\mu(x)$ can thus be expanded in terms of creation and annihilation operators

$$A^\mu(x) = \int \frac{{\rm d}\mathbf{k}}{\sqrt{2k^0(2\pi)^3}} \sum_\lambda \left[c(k,\lambda)A^\mu_{k,\lambda}(x) + c^\dagger(k,\lambda)A^{\mu*}_{k,\lambda}(x)\right]\,, \tag{3.13}$$

where $c(k,\lambda)$ and $c^\dagger(k,\lambda)$ annihilates and creates, respectively, a photon with the wave vector k and the polarization $\epsilon^{(\lambda)}$. They obey the following commutation relations:

$$[c(k,\lambda), c^\dagger(k',\lambda')] = -g^{\lambda\lambda'} 2k^0(2\pi)^3\delta^3(\mathbf{k}-\mathbf{k}')\,, \tag{3.14}$$

$$[c(k,\lambda), c(k',\lambda')] = [c^\dagger(k,\lambda), c^\dagger(k',\lambda')] = 0\,. \tag{3.15}$$

It can be shown, that the corresponding Fock space has an indefinite metric due to the presence of scalar and longitudinal photons. To eliminate these unphysical states one may employ the Gupta-Bleuler approach imposing the Lorentz condition on the matrix elements $\langle k,\lambda|\partial_\mu A^\mu(x)|k,\lambda\rangle = 0$ for the subspace of physical photon states $|k,\lambda\rangle$. This physical subspace of state vectors have positive norm and only the transverse photons contribute to observable quantities. The photon propagator is defined by the vacuum expectation value

$$D_{\mu\nu}(x^0-y^0,\mathbf{x}-\mathbf{y}) = i\langle 0|TA_\mu(x)A_\nu(y)|0\rangle\,. \tag{3.16}$$

The temporal Fourier-transformed photon propagation function has the form

$$D_{\mu\nu}(\varepsilon,\mathbf{x}-\mathbf{y}) = -4\pi g_{\mu\nu}\int \frac{{\rm d}\mathbf{k}}{(2\pi)^3}\,\frac{e^{i\mathbf{k}\cdot(\mathbf{x}-\mathbf{y})}}{\varepsilon^2-\mathbf{k}^2+i0} \tag{3.17}$$

in the Feynman gauge and

$$D_{00}(\varepsilon,\mathbf{x}-\mathbf{y}) = \frac{1}{|\mathbf{x}-\mathbf{y}|},\ D_{i0} = D_{0i} = 0,\ (i=1,2,3),$$
$$D_{ij}(\varepsilon,\mathbf{x}-\mathbf{y}) = 4\pi\int\frac{\mathrm{d}\mathbf{k}}{(2\pi)^3}\,\frac{e^{i\mathbf{k}\cdot(\mathbf{x}-\mathbf{y})}}{\varepsilon^2-\mathbf{k}^2+i0}\,\left(\delta_{ij}-\frac{k_i k_j}{\mathbf{k}^2}\right),\ (i,j=1,2,3) \tag{3.18}$$

in the Coulomb gauge.

For later purposes we introduce the operator $I(\varepsilon)$ representing the interelectronic interaction mediated via the exchange of virtual photons: $I(\varepsilon) = e^2\alpha^\mu\alpha^\nu D_{\mu\nu}(\varepsilon)$. Employing the Bohr radius a_0/Z as unit for lengths (and energies) implies a perturbation expansion of the interelectronic interaction in powers of $1/Z$.

The interaction between the electron-positron and electromagnetic fields is provided by the interaction Hamiltonian

$$H_{\rm I} = \int \mathrm{d}\mathbf{x}\, j^\mu(x)A_\mu(x) - \frac{\delta m}{2}\int \mathrm{d}\mathbf{x}\,[\overline{\psi}(x),\psi(x)]\,, \tag{3.19}$$

where $j^\mu(x) = (e/2)[\overline{\psi}(x)\gamma^\mu,\psi(x)]$ is the electron-positron current operator, δm is the mass renormalization counterterm.

For the rigorous derivation of formal expressions for the radiative and interelectronic-interaction corrections to the transition amplitudes from the first principles of QED it is most convenient to employ the two-time Green's function (TTGF) method. It was developed in works [131, 132, 133, 134, 135] and described in details in Ref. [100]. The TTGF formalism is based on the formulation of the perturbation theory for the Green's functions. We start our consideration with the definition of usual $2N$-time Green's functions, which will be needed hereinafter,

$$G(x'_1,\ldots,x'_N;x_1,\ldots,x_N) = \langle 0|T\psi(x'_1)\cdots\psi(x'_N)\overline{\psi}(x_N)\cdots\overline{\psi}(x_1)|0\rangle \tag{3.20}$$

and

$$G_{\gamma_f}(x'_1,\ldots,x'_N;x_1,\ldots,x_N) = \int \mathrm{d}^4y\,\langle 0|T\psi(x'_1)\cdots\psi(x'_N)A^{\mu*}_f(y)j_\mu(y)\overline{\psi}(x_N)\cdots\overline{\psi}(x_1)|0\rangle\,. \tag{3.21}$$

Here $j_\mu(y)$, $\psi(x)$ are operators in the Heisenberg representation, the subscript f by the photon wave function $A^{\mu*}_f(y)$ defines the quantum numbers (k_f,ϵ_f). To obtain the Feynman rules for these Green's functions one has to change from the Heisenberg to interaction representation and employ the Wick theorem (see details in Ref. [100]). However, the complete information about the energy levels and transition amplitudes is already contained in the two-time Green's functions defined with time arguments $x'^0_1 = x'^0_2 = \cdots = x'^0_N = x'^0$ and $x^0_1 = x^0_2 = \cdots = x^0_N = x^0$. Therefore, performing Fourier transformation over the time variables, we define the following two-time Green's functions

$$\mathcal{G}(E;\mathbf{x}'_1,\ldots,\mathbf{x}'_N;\mathbf{x}_1,\ldots,\mathbf{x}_N)\delta(E-E') = \frac{1}{2\pi i}\frac{1}{N!}\int_{-\infty}^{\infty}\mathrm{d}x^0\mathrm{d}x'^0 e^{(iE'x'^0-iEx^0)}$$
$$\times\langle 0|T\psi(x'^0,\mathbf{x}'_1)\cdots\psi(x'^0,\mathbf{x}'_N)\overline{\psi}(x^0,\mathbf{x}_N)\cdots\overline{\psi}(x^0,\mathbf{x}_1)|0\rangle \tag{3.22}$$

and

$$\mathcal{G}_{\gamma_f}(E',E;\mathbf{x}'_1,\ldots,\mathbf{x}'_N;\mathbf{x}_1,\ldots,\mathbf{x}_N)\delta(E'+k^0-E)$$
$$= \frac{1}{2\pi i}\frac{1}{2\pi}\frac{1}{N!}\int_{-\infty}^{\infty}\mathrm{d}x^0\mathrm{d}x'^0\int\mathrm{d}^4y\,e^{(iE'x'^0-iEx^0+ik^0y^0)}A^{\nu*}_f(\mathbf{y})$$
$$\times\langle 0|T\psi(x'^0,\mathbf{x}'_1)\cdots\psi(x'^0,\mathbf{x}'_N)j_\nu(y)\overline{\psi}(x^0,\mathbf{x}_N)\cdots\overline{\psi}(x^0,\mathbf{x}_1)|0\rangle\,. \tag{3.23}$$

Further, we briefly show how the information about the energy levels can be obtain from the poles of the Green's function $\mathcal{G}(E)$. The general case under consideration involves degenerate (or quasidegenerate) states. We assume

that in zeroth approximation the state A belongs to an s_A-dimensional subspace Ω_A of unperturbed states. The unperturbed energies we define as $E_1^{(0)},\dots,E_A^{(0)},\dots,E_{s_A}^{(0)}$, while the exact energies are defined as $E_1,\dots,E_A,\dots,E_{s_A}$. Let us introduce the projector onto the subspace Ω_A via

$$P_A^{(0)}=\sum_{k=1}^{s_A}u_k u_k^\dagger\,, \tag{3.24}$$

where u_k are the unperturbed one-determinant states of an N-electron system

$$u_k(\mathbf{x}_1,\dots,\mathbf{x}_N)=\frac{1}{\sqrt{N!}}\sum_P(-1)^P\phi_{Pa_1}(\mathbf{x}_1)\cdots\phi_{Pa_N}(\mathbf{x}_N)\,. \tag{3.25}$$

We project the Green's operator $\mathcal{G}(E)$ on the subspace Ω_A

$$g_{AA}(E)=P_A^{(0)}\mathcal{G}(E)\gamma_1^0\cdots\gamma_N^0P_A^{(0)}\,. \tag{3.26}$$

Here the integration over the electron coordinates is implied. From the spectral representation of the Green's function $g_{AA}(E)$ follows that in the complex plane E, at $E\sim E_A^{(0)}$, it possesses a Lorentz series of the form

$$g_{AA}(E)=\sum_{k=1}^{s_A}\frac{\varphi_k\varphi_k^\dagger}{E-E_k}\;+\;\text{terms regular at } E\sim E_A^{(0)}\,, \tag{3.27}$$

where $\{\varphi_k\}_{k=1}^{s_A}$ denotes a set of vectors in the subspace Ω_A (see Ref. [100]). We choose an integration contour Γ_A, which is oriented anticlockwise and encloses only the points $E_1^{(0)},\dots,E_{s_A}^{(0)}$. Let us introduce the operators K_A and P_A

$$K_A=\frac{1}{2\pi i}\oint_{\Gamma_A}\mathrm{d}E\,Eg_{AA}(E)=\sum_{k=1}^{s_A}E_k\varphi_k\varphi_k^\dagger\,, \tag{3.28}$$

$$P_A=\frac{1}{2\pi i}\oint_{\Gamma_A}\mathrm{d}E\,g_{AA}(E)=\sum_{k=1}^{s_A}\varphi_k\varphi_k^\dagger\,. \tag{3.29}$$

The vectors $\{\varphi_k\}_{k=1}^{s_A}$ form a nonorthogonal, linearly independent set. Due to the linear independence one can always find the vectors set $\{v_k\}_{k=1}^{s_A}$, which is orthogonal to $\{\varphi_k\}_{k=1}^{s_A}$. In this case, the biorthogonality condition holds

$$\varphi_k^\dagger v_{k'}=\delta_{kk'}\,. \tag{3.30}$$

The normalization condition for the vectors v_k has the form

$$v_k^\dagger P_A v_{k'}=\delta_{kk'}\,. \tag{3.31}$$

Finally, we have the generalized eigenvalue problem in the subspace Ω_A [100]

$$K_A v_k=E_k P_A v_k\,. \tag{3.32}$$

The operators K_A and P_A are constructed using the perturbation theory for $\mathcal{G}(E)$. In case of a single state, one can easily obtain the desired expression

$$E_A=\frac{\dfrac{1}{2\pi i}\displaystyle\oint_{\Gamma_A}\mathrm{d}EEg_{AA}(E)}{\dfrac{1}{2\pi i}\displaystyle\oint_{\Gamma_A}\mathrm{d}Eg_{AA}(E)}\,, \tag{3.33}$$

where $g_{AA}(E)=u_A^\dagger\mathcal{G}(E)\gamma_1^0\dots\gamma_N^0u_A$.

In the next Section we present the detailed description of the procedure of extracting the transition amplitudes from the poles of the Green's functions $\mathcal{G}(E)$ and $\mathcal{G}_{\gamma_f}(E',E)$.

3.2 Photon emission by an ion

According to the basic principles of quantum electrodynamics [136], the transition probability from the states A to B accompanied by photon emission with wave vector k_f and polarization ϵ_f is given by

$$\mathrm{d}W = 2\pi|\tau_{\gamma_f,B;A}|^2\delta(E_B + k_f^0 - E_A)\mathrm{d}\mathbf{k}_f\,, \tag{3.34}$$

where $\tau_{\gamma_f,B;A}$ is the transition amplitude which is connected with the S-matrix element by

$$S_{\gamma_f,B;A} = \langle k_f, \epsilon_f; B|\hat{S}|A\rangle = 2\pi i\tau_{\gamma_f,B;A}\delta(E_B + k_f^0 - E_A)\,, \tag{3.35}$$

E_A and E_B are the energies of the initial state A and the final state B, respectively.
Utilizing the standard reduction technique (see, e.g., Refs. [130, 137]), the S-matrix element can be given by the expression

$$S_{\gamma_f,B;A} = -iZ_3^{-\frac{1}{2}}\int \mathrm{d}^4y\frac{\epsilon_f^{\nu *}\, e^{ik_f\cdot y}}{\sqrt{2k_f^0(2\pi)^3}}\langle B|j_\nu(y)|A\rangle\,, \tag{3.36}$$

where Z_3 is a renormalization constant. Here for the electron-positron current operator $j_\nu(y)$ and vectors of the initial $|A\rangle$ and final $\langle B|$ states the Heisenberg picture is used. The equation (3.36) can be written as

$$S_{\gamma_f,B;A} = -2\pi i Z_3^{-\frac{1}{2}}\delta(E_B + k_f^0 - E_A)\int \mathrm{d}\mathbf{y}A_f^{\nu *}(\mathbf{y})\langle B|j_\nu(0,\mathbf{y})|A\rangle\,. \tag{3.37}$$

In a general case, we imply that to zeroth approximation the vector A belongs to the s_A-dimensional subspace Ω_A of degenerate (or quasidegenerate) states, and the state B belongs to the s_B-dimensional subspace Ω_B. $P_A^{(0)}$ and $P_B^{(0)}$ are the projectors onto the corresponding subspaces, $|k_A\rangle$ and $|k_B\rangle$ denote the states corresponded to the exact energies E_{k_a} and E_{k_b}.
Using the translation properties of the operators in the Heisenberg representation over the time variable, the Green's function $\mathcal{G}_{\gamma_f}(E', E)$, defined by the expression (3.23), can be written as

$$\begin{aligned}\mathcal{G}_{\gamma_f}(E', E; \mathbf{x}_1', ..., \mathbf{x}_N'; \mathbf{x}_1, ..., \mathbf{x}_N) &= \frac{1}{2\pi i}\frac{1}{N!}\int_{-\infty}^{\infty}\mathrm{d}t\,\mathrm{d}t'\int \mathrm{d}\mathbf{y}\, e^{(iE't' - iEt)}\sum_{n_1,n_2}A_f^{\nu *}(\mathbf{y})\\ &\times e^{(-iE_{n_1}t' + iE_{n_2}t)}\,\theta(t')\theta(-t)\langle 0|\psi(0,\mathbf{x}_1')\cdots\psi(0,\mathbf{x}_N')|n_1\rangle\\ &\times\langle n_1|j_\nu(0,\mathbf{y})|n_2\rangle\langle n_2|\overline{\psi}(0,\mathbf{x}_N)\cdots\overline{\psi}(0,\mathbf{x}_1)|0\rangle + \cdots\,.\end{aligned} \tag{3.38}$$

Here we have assumed that the all energies are counted off from the vacuum energy ($E_0 = 0$). For simplicity, we have not written out terms with another time ordering in Eq. (3.38). Taking into account the identities

$$\begin{aligned}\int_0^{\infty}\mathrm{d}t\, e^{i(E' - E_{n_1})t} &= \frac{i}{E' - E_{n_1} + i0}\,,\\ \int_{-\infty}^{0}\mathrm{d}t\, e^{i(-E + E_{n_2})t} &= \frac{i}{E - E_{n_2} + i0}\,,\end{aligned} \tag{3.39}$$

yields

$$\begin{aligned}\mathcal{G}_{\gamma_f}(E', E; \mathbf{x}_1', \ldots, \mathbf{x}_N'; \mathbf{x}_1, \ldots, \mathbf{x}_N) &= \frac{i}{2\pi}\frac{1}{N!}\sum_{n_1,n_2}\int \mathrm{d}\mathbf{y}A_f^{\nu *}(\mathbf{y})\frac{1}{E' - E_{n_1} + i0}\frac{1}{E - E_{n_2} + i0}\\ &\times\langle 0|\psi(0,\mathbf{x}_1')\cdots\psi(0,\mathbf{x}_N')|n_1\rangle\langle n_1|j_\nu(0,\mathbf{y})|n_2\rangle\\ &\times\langle n_2|\overline{\psi}(0,\mathbf{x}_N)\cdots\overline{\psi}(0,\mathbf{x}_1)|0\rangle + \cdots\,.\end{aligned} \tag{3.40}$$

From the spectral representation one can find that the Green's function $\mathcal{G}_{\gamma_f}(E',E)$ has isolated poles in the complex planes E' and E, at $E' \sim E_B^{(0)}$ and $E \sim E_A^{(0)}$, in the points $E' = E_{k_B}$ and $E' = E_{k_A}$, respectively. The detailed analysis is presented in Ref. [100]. Let us now introduce a Green's function $g_{\gamma_f,B;A}(E',E)$ by

$$g_{\gamma_f,B;A}(E',E) = P_B^{(0)} \mathcal{G}_{\gamma_f}(E',E)\gamma_1^0 \cdots \gamma_N^0 P_A^{(0)} \,. \tag{3.41}$$

According to Eq. (3.40) the Green's function $g_{\gamma_f,B;A}(E',E)$ can be written as

$$\begin{aligned} g_{\gamma_f,B;A}(E',E) = \frac{i}{2\pi} \sum_{k_A=1}^{s_A} \sum_{k_B=1}^{s_B} \frac{1}{E'-E_{k_B}} \frac{1}{E-E_{k_A}} \varphi_{k_B} \int \mathrm{d}\mathbf{y} A_f^{\nu *}(\mathbf{y}) \\ \times \langle k_B | j_\nu(0,\mathbf{y}) | k_A \rangle \varphi_{k_A}^\dagger + \text{terms regular at } E' \sim E_B^{(0)} \text{ or } E \sim E_A^{(0)} \,. \end{aligned} \tag{3.42}$$

Let the contours Γ_A and Γ_B surround the poles corresponding to the initial and final levels, respectively, and keep outside other singularities of $g_{\gamma_f,B;A}(E',E)$ including the cuts starting from the lower-lying bound states. Comparing Eq. (3.42) with Eq. (3.37) and taking into account biorthogonality condition Eq. (3.30), we obtain the desired formula [100, 132]

$$S_{\gamma_f,B;A} = Z_3^{-1/2} \delta(E_B + k_f^0 - E_A) \oint_{\Gamma_B} \mathrm{d}E' \oint_{\Gamma_A} \mathrm{d}E \, v_B^\dagger \, g_{\gamma_f,B;A}(E',E) v_A \,, \tag{3.43}$$

where A and B refer to one of the initial and final states under consideration, respectively. To find the transition amplitude $S_{\gamma_f,B;A}$ according to Eq. (3.43) one has to determine the perturbed vectors v_A and v_B as the solutions of the generalized eigenvalue problem (3.32).

Further we consider the single initial and final states. In this case, the vectors v_A and v_B simply appear as normalization factors. Thus, from Eq. (3.31) we find for the initial state

$$v_A^* P_A v_A = v_A^* \frac{1}{2\pi i} \oint_{\Gamma_A} \mathrm{d}E \, g_{AA}(E) v_A = 1 \,. \tag{3.44}$$

Choosing

$$v_A = \left[\frac{1}{2\pi i} \oint_{\Gamma_A} \mathrm{d}E \, g_{AA}(E) \right]^{-1/2}, \qquad v_B = \left[\frac{1}{2\pi i} \oint_{\Gamma_B} \mathrm{d}E \, g_{BB}(E) \right]^{-1/2}, \tag{3.45}$$

we obtain for the S-matrix element

$$\begin{aligned} S_{\gamma_f,B;A} &= Z_3^{-1/2} \delta(E_B + k_f^0 - E_A) \oint_{\Gamma_B} \mathrm{d}E' \oint_{\Gamma_A} \mathrm{d}E \, g_{\gamma_f,B;A}(E',E) \\ &\quad \times \left[\frac{1}{2\pi i} \oint_{\Gamma_B} \mathrm{d}E \, g_{BB}(E) \right]^{-1/2} \left[\frac{1}{2\pi i} \oint_{\Gamma_A} \mathrm{d}E \, g_{AA}(E) \right]^{-1/2} . \end{aligned} \tag{3.46}$$

Now we demonstrate the practicability of the formalism. In what follows, we derive formulas for the transition probability in a one-, two- and many-electron ions to first order in the perturbation expansion.

3.3 The transition probability in one-electron ions

3.3.1 Zeroth order approximation

To zeroth order the transition amplitude is described by the diagram shown in Fig. 3.1. Formula (3.46) yields

$$S_{\gamma_f,b;a}^{(0)} = \delta(E_b + k_f^0 - E_a) \oint_{\Gamma_b} \mathrm{d}E' \oint_{\Gamma_a} \mathrm{d}E \, g_{\gamma_f,b;a}^{(0)}(E',E) \,, \tag{3.47}$$

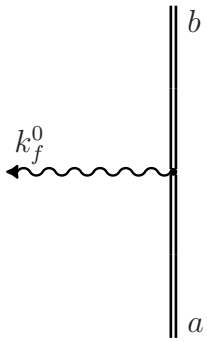

Figure 3.1: Feynman diagram representing the photon emission by a one-electron ion in zeroth-order approximation. The double line indicates the electron propagating in the external field of the nucleus. The single photon emission is depicted by the wavy line with arrow.

where the superscript "(0)" indicates the order in α. Initial and final one-electron states are denoted by a and b, respectively. According to the Feynman rules for the Green's function $G_{\gamma_f}(E', E)$ we have

$$G^{(0)}_{\gamma_f}((E', \mathbf{x}'); k^0; (E, \mathbf{x})) = \int \mathrm{d}\mathbf{y} \frac{i}{2\pi} S(E', \mathbf{x}', \mathbf{y})(-2\pi i e \gamma^\nu)\delta(E' + k^0 - E) \times A^*_{f,\nu}(\mathbf{y}) \frac{i}{2\pi} S(E, \mathbf{y}, \mathbf{x}) \tag{3.48}$$

together with

$$g_{\gamma_f, b;a}(E', E) = \frac{i}{2\pi} \frac{1}{E' - \varepsilon_b} \langle b | e\alpha^\nu A^*_{f,\nu} | a \rangle \frac{1}{E - \varepsilon_a} \,. \tag{3.49}$$

Eqs. (3.47) and (3.49) yield

$$S^{(0)}_{\gamma_f, b;a} = -2\pi i \, \delta(E_b + k^0_f - E_a) \langle b | e\alpha^\nu A^*_{f,\nu} | a \rangle \,, \tag{3.50}$$

or, in accordance with definition (3.35),

$$\tau^{(0)}_{\gamma_f, b;a} = -\langle b | e\alpha^\nu A^*_{f,\nu} | a \rangle \,. \tag{3.51}$$

Finally, integrating over the photon energy one finds immediately

$$\mathrm{d}W^{(0)}_{\gamma_f, b;a} = 2\pi (k^0_f)^2 |\langle b | e\alpha^\nu A^*_{f,\nu} | a \rangle|^2 \mathrm{d}\Omega_{\mathbf{k}_f} \,. \tag{3.52}$$

Note, that the matrices $\alpha^\nu = \gamma^0 \gamma^\nu$ have been introduced in the equations above.

3.3.2 QED corrections of first order in α

The QED corrections of the first order in the perturbation expansion are defined by the diagrams shown in Figs. 3.2 and 3.3. These corrections are suppressed by a factor α. Let us consider the derivation of the formulas for the self-energy (SE) correction (the diagrams depicted in Fig. 3.2). Applying formula (3.46) to the process and up to the order under consideration

$$S^{(1)}_{\gamma_f, b;a} = \delta(E_b + k^0_f - E_a) \left\{ \oint_{\Gamma_b} \mathrm{d}E' \oint_{\Gamma_a} \mathrm{d}E \, g^{(1)}_{\gamma_f, b;a}(E', E) - \frac{1}{2} \oint_{\Gamma_b} \mathrm{d}E' \oint_{\Gamma_a} \mathrm{d}E \right. \times g^{(0)}_{\gamma_f, b;a}(E', E) \left[\frac{1}{2\pi i} \oint_{\Gamma_b} \mathrm{d}E \, g^{(1)}_{bb}(E) + \frac{1}{2\pi i} \oint_{\Gamma_a} \mathrm{d}E \, g^{(1)}_{aa}(E) \right] \Bigg\} , \tag{3.53}$$

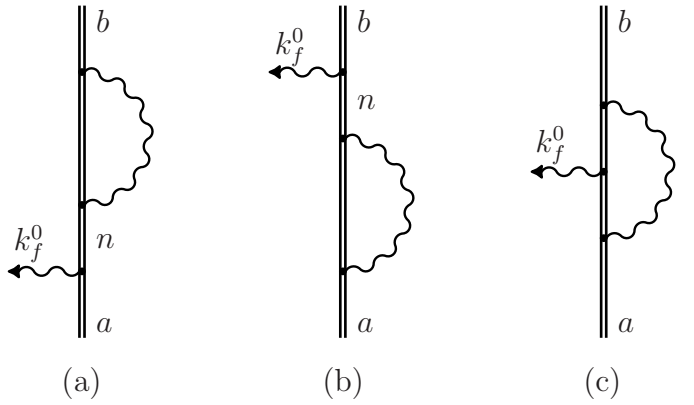

Figure 3.2: Feynman diagrams representing the one-loop self-energy correction to the transition amplitude. The photon propagator is represented by the wavy line.

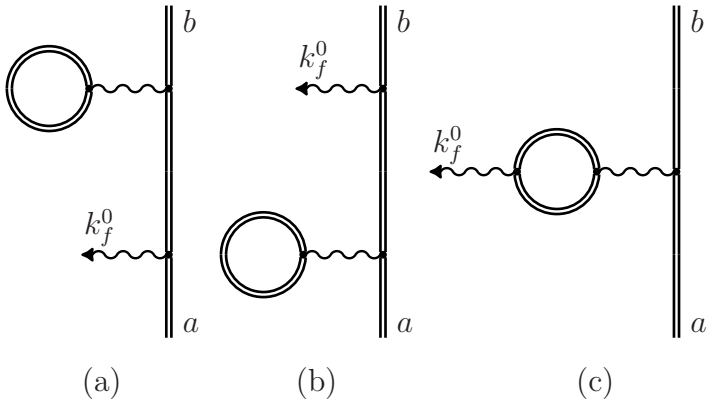

Figure 3.3: Feynman diagrams representing the one-loop vacuum-polarization correction to the transition amplitude.

where $g^{(1)}_{aa}(E)$ and $g^{(1)}_{bb}(E)$ are defined by the first-order self-energy corrections to the wave functions of the initial and final states, respectively. Here we have omitted a term of first order in α which comes from the factor $Z_3^{-1/2}$, since it has to be combined with the vacuum-polarization (VP) correction. We start with the diagram depicted in Fig. 3.2(a). According to the Feynman rules, we have

$$G^{\rm SEa}_{\gamma_f}((E',\mathbf{x}');k^0;(E,\mathbf{x})) = \delta(E'+k^0-E)\int {\rm d}\mathbf{y}{\rm d}\mathbf{y}'{\rm d}\mathbf{z}\,\frac{i}{2\pi}S(E',\mathbf{x}',\mathbf{y}) \times\frac{2\pi}{i}\gamma^0\Sigma(E',\mathbf{y}',\mathbf{y})\frac{i}{2\pi}S(E',\mathbf{y},\mathbf{z})A^*_{f,\nu}(\mathbf{z})(-2\pi ie\gamma^\nu)\frac{i}{2\pi}S(E,\mathbf{z},\mathbf{x})\,, \tag{3.54}$$

where

$$\Sigma(E',\mathbf{y}',\mathbf{y}) = e^2\frac{i}{2\pi}\int {\rm d}\omega\,\gamma^0\gamma^\rho S(E'-\omega,\mathbf{y}',\mathbf{y})\gamma^\sigma D_{\rho\sigma}(\omega,\mathbf{y}'-\mathbf{y}) \tag{3.55}$$

is the kernel of the self-energy operator. According to the definition of the Green's function $g_{\gamma_f,b;a}(E',E)$ (see Eq. (3.41)), we find

$$g^{\rm SEa}_{\gamma_f,b;a}(E',E) = \frac{i}{2\pi}\sum_n \frac{\langle b|\Sigma(E')|n\rangle\langle n|e\alpha^\nu A^*_{f,\nu}|a\rangle}{(E'-\varepsilon_b)(E'-\varepsilon_n)(E-\varepsilon_a)} \tag{3.56}$$

and

$$\oint_{\Gamma_b}{\rm d}E'\oint_{\Gamma_a}{\rm d}E\,g^{\rm SEa}_{\gamma_f,b;a}(E',E) = -2\pi i\left[\sum_n^{\varepsilon_n\neq\varepsilon_b}\frac{\langle b|\Sigma(\varepsilon_b)|n\rangle\langle n|e\alpha^\nu A^*_{f,\nu}|a\rangle}{\varepsilon_b-\varepsilon_n} +\langle b|\Sigma'(\varepsilon_b)|b\rangle\langle b|e\alpha^\nu A^*_{f,\nu}|a\rangle\right], \tag{3.57}$$

where $\Sigma'(\varepsilon_b)\equiv\partial\Sigma(\varepsilon)/\partial\varepsilon\Big|_{\varepsilon=\varepsilon_b}$. A similar calculation of the diagram depicted in Fig. 3.2(b) gives

$$\oint_{\Gamma_b}{\rm d}E'\oint_{\Gamma_a}{\rm d}E\,g^{\rm SEb}_{\gamma_f,b;a}(E',E) = -2\pi i\left[\sum_n^{\varepsilon_n\neq\varepsilon_a}\frac{\langle b|e\alpha^\nu A^*_{f,\nu}|n\rangle\langle n|\Sigma(\varepsilon_a)|a\rangle}{\varepsilon_a-\varepsilon_n} +\langle b|e\alpha^\nu A^*_{f,\nu}|a\rangle\langle a|\Sigma'(\varepsilon_a)|a\rangle\right]. \tag{3.58}$$

The second (reducible) terms in Eqs. (3.57) and (3.58) have to be combined with the second term in Eq. (3.53). Taking into account that (see Ref. [100])

$$\frac{1}{2\pi i}\oint_{\Gamma_a}{\rm d}E\,g^{(1)}_{aa}(E) = \langle a|\Sigma'(\varepsilon_a)|a\rangle\,, \tag{3.59}$$

$$\frac{1}{2\pi i}\oint_{\Gamma_b}{\rm d}E\,g^{(1)}_{bb}(E) = \langle b|\Sigma'(\varepsilon_b)|b\rangle\,, \tag{3.60}$$

one derives

$$-\frac{1}{2}\oint_{\Gamma_b}{\rm d}E'\oint_{\Gamma_a}{\rm d}E\,g^{(0)}_{\gamma_f,b;a}(E',E)\left[\frac{1}{2\pi i}\oint_{\Gamma_b}{\rm d}E\,g^{(1)}_{bb}(E)+\frac{1}{2\pi i}\oint_{\Gamma_a}{\rm d}E\,g^{(1)}_{aa}(E)\right] = \pi i\langle b|e\alpha^\nu A^*_{f,\nu}|a\rangle\left(\langle b|\Sigma'(\varepsilon_b)|b\rangle+\langle a|\Sigma'(\varepsilon_a)|a\rangle\right)\,. \tag{3.61}$$

For the diagram presented in Fig. 3.2(c) we find

$$\oint_{\Gamma_b}{\rm d}E'\oint_{\Gamma_a}{\rm d}E\,g^{\rm SEc}_{\gamma_f,b;a}(E',E) = -2\pi i\int{\rm d}\mathbf{z}\,eA^*_{f,\nu}(\mathbf{z})\Lambda^\nu(\varepsilon_b,\varepsilon_a,\mathbf{z})\,, \tag{3.62}$$

where the vertex function is given by

$$\Lambda^\nu(\varepsilon_b,\varepsilon_a,\mathbf{z}) = e^2\frac{i}{2\pi}\int_{-\infty}^{\infty}\mathrm{d}\omega\int\mathrm{d}\mathbf{x}\mathrm{d}\mathbf{y}\,\overline{\phi}_b(\mathbf{x})\gamma^\rho S(\varepsilon_b-\omega,\mathbf{x},\mathbf{z})\gamma^\nu \times S(\varepsilon_a-\omega,\mathbf{z},\mathbf{y})\gamma^\sigma D_{\rho\sigma}(\omega,\mathbf{x}-\mathbf{y})\phi_a(\mathbf{y})\,. \quad (3.63)$$

Summing all the first-order SE contributions derived above and adding the contribution of the mass counterterm yields [100]

$$\tau^{\rm SE}_{\gamma_f,b;a} = -\left[\sum_n^{\varepsilon_n\neq\varepsilon_b}\frac{\langle b|\Sigma_{\rm R}(\varepsilon_b)|n\rangle\langle n|e\alpha^\nu A^*_{f,\nu}|a\rangle}{\varepsilon_b-\varepsilon_n}+\sum_n^{\varepsilon_n\neq\varepsilon_a}\frac{\langle b|e\alpha^\nu A^*_{f,\nu}|n\rangle\langle n|\Sigma_{\rm R}(\varepsilon_a)|a\rangle}{\varepsilon_a-\varepsilon_n} + \int\mathrm{d}\mathbf{z}\,eA^*_{f,\nu}(\mathbf{z})\Lambda^\nu(\varepsilon_b,\varepsilon_a,\mathbf{z})+\frac{1}{2}\langle b|e\alpha^\nu A^*_{f,\nu}|a\rangle(\langle b|\Sigma'(\varepsilon_b)|b\rangle+\langle a|\Sigma'(\varepsilon_a)|a\rangle)\right], \quad (3.64)$$

where $\Sigma_{\rm R}(\varepsilon)=\Sigma(\varepsilon)-\gamma^0\delta m$.
A similar calculation of the vacuum-polarization diagrams depicted in Fig. 3.3 gives [100]

$$\tau^{\rm VP}_{\gamma_f,b;a} = -\left[\sum_n^{\varepsilon_n\neq\varepsilon_b}\frac{\langle b|U_{\rm VP}|n\rangle\langle n|e\alpha^\nu A^*_{f,\nu}|a\rangle}{\varepsilon_b-\varepsilon_n}+\sum_n^{\varepsilon_n\neq\varepsilon_a}\frac{\langle b|e\alpha^\nu A^*_{f,\nu}|n\rangle\langle n|U_{\rm VP}|a\rangle}{\varepsilon_a-\varepsilon_n} + \int\mathrm{d}\mathbf{z}\,eA^*_{f,\nu}(\mathbf{z})Q^\nu(k^0_f,\mathbf{z})+(Z_3^{-1/2}-1)\langle b|e\alpha^\nu A^*_{f,\nu}|a\rangle\right], \quad (3.65)$$

where the corresponding counterterm ($\sim Z_3^{-1/2}$) required for charge renormalization has been incorporated as well. The vacuum-polarization potential is defined according to

$$U_{\rm VP}(\mathbf{x})=\frac{\alpha}{2\pi i}\int\mathrm{d}\mathbf{y}\,\frac{1}{|\mathbf{x}-\mathbf{y}|}\int_{-\infty}^{\infty}\mathrm{d}\omega\,\mathrm{Tr}[S(\omega,\mathbf{y},\mathbf{y})\gamma^0]\,, \quad (3.66)$$

together with the VP-corrected photon emission vertex

$$Q^\nu(k^0,\mathbf{z}) = -e^2\int\mathrm{d}\mathbf{x}\mathrm{d}\mathbf{y}\,\overline{\phi}_b(\mathbf{x})\gamma^\rho\phi_a(\mathbf{x})D_{\rho\sigma}(k^0,\mathbf{x}-\mathbf{y}) \times\frac{i}{2\pi}\int_{-\infty}^{\infty}\mathrm{d}\omega\,\mathrm{Tr}[\gamma^\sigma S(\omega,\mathbf{y},\mathbf{z})\gamma^\nu S(\omega+k^0,\mathbf{z},\mathbf{y})]\,. \quad (3.67)$$

Some individual terms in Eqs. (3.64) and (3.65) contain ultraviolet divergences. These divergences arise solely from the zero- and one-potential terms in the expansion of the electron propagators in powers of the binding potential. Using the standard expressions for the divergent parts of the zero- and one-potential SE terms and the Ward identity ($Z_1=Z_2$), one can easily find that the ultraviolet divergences cancel each other in Eq. (3.64). As to Eq. (3.65), the divergent parts incorporate into the charge renormalization factor ($e=Z_3^{1/2}e_0$).

3.4 The transition probability in two-electron ions

Let us consider now the transition probability between the states A and B of a two-electron ion. To first order in the perturbation expansion, in addition to the one-electron SE and VP contributions we have to account for the interelectronic-interaction corrections corresponding to the diagrams depicted in Fig. 3.4. The derivation of the SE and VP contributions is easily reduced to the case of a one-electron ion by simple integration over the energy variable of a disconnected electron propagator. Therefore, below we discuss only the interelectronic-interaction terms. The interelectronic interaction is mediated by the exchange of virtual photon (inner photon propagator

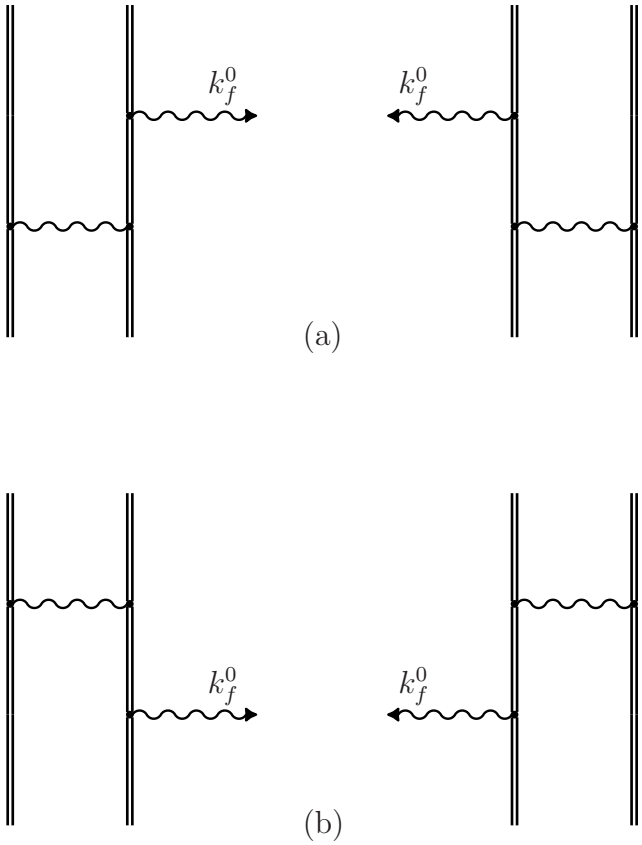

Figure 3.4: Feynman diagrams representing the interelectronic-interaction corrections of first order in α to the transition amplitude.

depicted in Fig. 3.4), which may be treated perturbatively with respect to an expansion in $1/Z$. The presentation of this Section follows the results of work [138].

The interelectronic-interaction corrections to the transition amplitude of first order in $1/Z$ are determined by Eq. (3.53). The Green's function $g^{(1)}_{\gamma_f,B;A}(E',E)$ now has to be constructed in accordance with the diagrams presented in Fig. 3.4, while $g^{(1)}_{AA}$ and $g^{(1)}_{BB}$ are defined by the one-photon exchange diagram. Let us consider first the contribution of the diagrams depicted in Fig. 3.4(a). We assume that in zeroth approximation the initial A and final B states are described by (two-by-two) one-determinant wave functions and determined by Eq. (3.7), where a_1, a_2 and b_1, b_2 are corresponding one-electron states. According to the definition of $g_{\gamma_f,B;A}(E',E)$ (see Eq. (3.41)) and the Feynman rules for the Green's function G_{γ_f}, we have

$$
\begin{aligned}
&g^{\rm INTa}_{\gamma_f,B;A}(E',E)\delta(E'+k^0-E)\\
&\quad=\sum_P(-1)^P\int_{-\infty}^{\infty}{\rm d}p_1^0{\rm d}p_2^0{\rm d}p_1'^0{\rm d}p_2'^0\delta(E-p_1^0-p_2^0)\delta(E'-p_1'^0-p_2'^0)\\
&\quad\times\left(\frac{i}{2\pi}\right)^3\int_{-\infty}^{\infty}{\rm d}q^0{\rm d}\omega\left[\frac{1}{p_1'^0-\varepsilon_{Pb_1}+i0}\sum_n\langle Pb_1|e\alpha_\mu A^{\mu*}_f|n\rangle\frac{1}{q^0-\varepsilon_n(1-i0)}\right.\\
&\quad\times\langle nPb_2|I(\omega)|a_1a_2\rangle\frac{1}{p_1^0-\varepsilon_{a_1}+i0}\frac{1}{p_2'^0-\varepsilon_{Pb_2}+i0}\frac{1}{p_2^0-\varepsilon_{a_2}+i0}\delta(p_1^0-\omega-q^0)\\
&\quad\times\delta(q^0-k^0-p_1'^0)\delta(p_2^0+\omega-p_2'^0)+\frac{1}{p_2'^0-\varepsilon_{Pb_2}+i0}\sum_n\langle Pb_2|e\alpha_\mu A^{\mu*}_f|n\rangle\\
&\quad\times\frac{1}{q^0-\varepsilon_n(1-i0)}\langle Pb_1n|I(\omega)|a_1a_2\rangle\frac{1}{p_2^0-\varepsilon_{a_2}+i0}\frac{1}{p_1'^0-\varepsilon_{Pb_1}+i0}\frac{1}{p_1^0-\varepsilon_{a_1}+i0}\\
&\quad\times\left.\delta(p_2^0-\omega-q^0)\delta(q^0-k^0-p_2'^0)\delta(p_1^0+\omega-p_1'^0)\right]. \qquad (3.68)
\end{aligned}
$$

Performing the integration with δ functions, we find

$$
\begin{aligned}
&g^{\rm INTa}_{\gamma_f,B;A}(E',E)\\
&\quad=\left(\frac{i}{2\pi}\right)^3\sum_P(-1)^P\sum_n\int_{-\infty}^{\infty}{\rm d}p_2^0{\rm d}p_2'^0\frac{1}{p_2'^0-\varepsilon_{Pb_2}+i0}\frac{1}{E'-p_2'^0-\varepsilon_{Pb_1}+i0}\\
&\quad\times\frac{1}{p_2^0-\varepsilon_{a_2}+i0}\frac{1}{E-p_2^0-\varepsilon_{a_1}+i0}\langle Pb_1|e\alpha_\mu A^{\mu*}_f|n\rangle\\
&\quad\times\frac{1}{E-p_2'^0-\varepsilon_n(1-i0)}\langle nPb_2|I(p_2'^0-p_2^0)|a_1a_2\rangle\\
&\quad+\left(\frac{i}{2\pi}\right)^3\sum_P(-1)^P\sum_n\int_{-\infty}^{\infty}{\rm d}p_1^0{\rm d}p_1'^0\frac{1}{p_1'^0-\varepsilon_{Pb_1}+i0}\frac{1}{E'-p_1'^0-\varepsilon_{Pb_2}+i0}\\
&\quad\times\frac{1}{p_1^0-\varepsilon_{a_1}+i0}\frac{1}{E-p_1^0-\varepsilon_{a_2}+i0}\langle Pb_2|e\alpha_\mu A^{\mu*}_f|n\rangle\\
&\quad\times\frac{1}{E-p_1'^0-\varepsilon_n(1-i0)}\langle Pb_1n|I(p_1'^0-p_1^0)|a_1a_2\rangle\,. \qquad (3.69)
\end{aligned}
$$

The expression (3.69) is conveniently divided into irreducible and reducible parts. The reducible part is the one with $\varepsilon_{Pb_2}+\varepsilon_n=E_A^{(0)}$ in first term and with $\varepsilon_{Pb_1}+\varepsilon_n=E_A^{(0)}$ in second term. Here $E_A^{(0)}$ and $E_B^{(0)}$ are the energies of the initial state A and the final state B in zeroth approximation, which are equal to the sum of the one-electron energies $E_A^{(0)}=\varepsilon_{a_1}+\varepsilon_{a_2}$ and $E_B^{(0)}=\varepsilon_{b_1}+\varepsilon_{b_2}$, respectively. The irreducible part is given by the reminder. Using

the identities

$$\frac{1}{p_1^0-\varepsilon_{a_1}+i0}\frac{1}{E-p_1^0-\varepsilon_{a_2}+i0}=\frac{1}{E-E_A^{(0)}}\left(\frac{1}{p_1^0-\varepsilon_{a_1}+i0}+\frac{1}{E-p_1^0-\varepsilon_{a_2}+i0}\right), \tag{3.70}$$

$$\frac{1}{p_1'^0-\varepsilon_{Pb_1}+i0}\frac{1}{E'-p_1'^0-\varepsilon_{Pb_2}+i0}=\frac{1}{E'-E_B^{(0)}}\left(\frac{1}{p_1'^0-\varepsilon_{Pb_1}+i0}+\frac{1}{E'-p_1'^0-\varepsilon_{Pb_2}+i0}\right), \tag{3.71}$$

and the definition (3.35), we obtain for the irreducible part

$$\begin{aligned}
\tau^{\mathrm{INTa,irred}}_{\gamma_f,B;A} &= \frac{1}{2\pi i}\oint_{\Gamma_B}\mathrm{d}E'\oint_{\Gamma_A}\mathrm{d}E\; g^{\mathrm{INTa,irred}}_{\gamma_f,B;A}(E',E)\\
&= \frac{1}{2\pi i}\oint_{\Gamma_B}\mathrm{d}E'\oint_{\Gamma_A}\mathrm{d}E\;\frac{1}{E'-E_B^{(0)}}\frac{1}{E-E_A^{(0)}}\Bigg[\sum_P(-1)^P\left(\frac{i}{2\pi}\right)^3\int_{-\infty}^{\infty}\mathrm{d}p_2^0\mathrm{d}p_2'^0\\
&\quad\times\left(\frac{1}{p_2'^0-\varepsilon_{Pb_2}+i0}+\frac{1}{E'-p_2'^0-\varepsilon_{Pb_1}+i0}\right)\left(\frac{1}{p_2^0-\varepsilon_{a_2}+i0}+\frac{1}{E-p_2^0-\varepsilon_{a_1}+i0}\right)\\
&\quad\times\sum_n^{\varepsilon_{Pb_2}+\varepsilon_n\neq E_A^{(0)}}\langle Pb_1|e\alpha_\mu A_f^{\mu*}|n\rangle\frac{1}{E-p_2'^0-\varepsilon_n(1-i0)}\langle nPb_2|I(p_2'^0-p_2^0)|a_1a_2\rangle\\
&\quad+\sum_P(-1)^P\left(\frac{i}{2\pi}\right)^3\int_{-\infty}^{\infty}\mathrm{d}p_1^0\mathrm{d}p_1'^0\left(\frac{1}{p_1'^0-\varepsilon_{Pb_1}+i0}+\frac{1}{E'-p_1'^0-\varepsilon_{Pb_2}+i0}\right)\\
&\quad\times\left(\frac{1}{p_1^0-\varepsilon_{a_1}+i0}+\frac{1}{E-p_1^0-\varepsilon_{a_2}+i0}\right)\sum_n^{\varepsilon_{Pb_1}+\varepsilon_n\neq E_A^{(0)}}\langle Pb_2|e\alpha_\mu A_f^{\mu*}|n\rangle\\
&\quad\times\frac{1}{E-p_1'^0-\varepsilon_n(1-i0)}\langle Pb_1n|I(p_1'^0-p_1^0)|a_1a_2\rangle\Bigg].
\end{aligned}\tag{3.72}$$

The expression in the curly brackets of Eq. (3.72) is a regular function of E or E' at $E\sim E_A^{(0)}$ and $E'\sim E_B^{(0)}$. Calculating the residues we obtain

$$\begin{aligned}
\tau^{\mathrm{INTa,irred}}_{\gamma_f,B;A} &= -\sum_P(-1)^P\Bigg[\sum_n^{\varepsilon_{Pb_2}+\varepsilon_n\neq E_A^{(0)}}\langle Pb_1|e\alpha_\mu A_f^{\mu*}|n\rangle\frac{\langle nPb_2|I(\varepsilon_{Pb_2}-\varepsilon_{a_2})|a_1a_2\rangle}{E_A^{(0)}-\varepsilon_{Pb_2}-\varepsilon_n}\\
&\quad+\sum_n^{\varepsilon_{Pb_1}+\varepsilon_n\neq E_A^{(0)}}\langle Pb_2|e\alpha_\mu A_f^{\mu*}|n\rangle\frac{\langle Pb_1n|I(\varepsilon_{Pb_1}-\varepsilon_{a_1})|a_1a_2\rangle}{E_A^{(0)}-\varepsilon_{Pb_1}-\varepsilon_n}\Bigg].
\end{aligned}\tag{3.73}$$

A similar calculation of the irreducible part of the diagrams shown in Fig. 3.4(b) yields

$$\begin{aligned}
\tau^{\mathrm{INTb,irred}}_{\gamma_f,B;A} &= -\sum_P(-1)^P\Bigg[\sum_n^{\varepsilon_{a_2}+\varepsilon_n\neq E_B^{(0)}}\frac{\langle Pb_1Pb_2|I(\varepsilon_{Pb_2}-\varepsilon_{a_2})|na_2\rangle}{E_B^{(0)}-\varepsilon_{a_2}-\varepsilon_n}\langle n|e\alpha_\mu A_f^{\mu*}|a_1\rangle\\
&\quad+\sum_n^{\varepsilon_{a_1}+\varepsilon_n\neq E_B^{(0)}}\frac{\langle Pb_1Pb_2|I(\varepsilon_{Pb_1}-\varepsilon_{a_1})|a_1n\rangle}{E_B^{(0)}-\varepsilon_{a_1}-\varepsilon_n}\langle n|e\alpha_\mu A_f^{\mu*}|a_2\rangle\Bigg].
\end{aligned}\tag{3.74}$$

In the reducible part of Eq. (3.69) we calculate the corresponding residues at $E'=E_B^{(0)}$ and $E=E_A^{(0)}$. As a result

we obtain

$$\tau^{\mathrm{INTa,red}}_{\gamma_f,B;A} = \sum_P (-1)^P \left[\frac{i}{2\pi} \sum_n^{\varepsilon_{Pb_2}+\varepsilon_n=E_A^{(0)}} \int_{-\infty}^{\infty} \mathrm{d}p_2^0 \, \langle Pb_1|e\alpha_\mu A_f^{\mu *}|n\rangle \right.$$
$$\times \frac{\langle nPb_2|I(\varepsilon_{Pb_2}-p_2^0)|a_1a_2\rangle}{(\varepsilon_{a_2}-p_2^0+i0)^2} + \frac{i}{2\pi} \sum_n^{\varepsilon_{Pb_1}+\varepsilon_n=E_A^{(0)}} \int_{-\infty}^{\infty} \mathrm{d}p_1^0 \, \langle Pb_2|e\alpha_\mu A_f^{\mu *}|n\rangle$$
$$\left. \times \frac{\langle Pb_1n|I(\varepsilon_{Pb_1}-p_1^0)|a_1a_2\rangle}{(\varepsilon_{a_1}-p_1^0+i0)^2} \right]. \tag{3.75}$$

In Eq. (3.75) we have to consider $(Pb_2, n) = (a_1, a_2)$ or (a_2, a_1) in first term and $(Pb_1, n) = (a_1, a_2)$ or (a_2, a_1) in second term. Therefore, the reducible part contributes only in the case when the states A and B have at least one common one-electron state. In what follows, we assume $a_1 = b_1$ and $a_2 \neq b_2$. In view of the aforesaid we obtain

$$\tau^{\mathrm{INTa,red}}_{\gamma_f,B;A} = \frac{i}{2\pi} \int_{-\infty}^{\infty} \mathrm{d}\omega \, \langle b_2|e\alpha_\mu A_f^{\mu *}|a_2\rangle$$
$$\times \left(\frac{\langle a_1a_2|I(\omega)|a_1a_2\rangle}{(\omega - i0)^2} - \frac{\langle a_2a_1|I(\omega)|a_1a_2\rangle}{(\omega - \Delta_A - i0)^2} \right), \tag{3.76}$$

where $\Delta_A \equiv \varepsilon_{a_2} - \varepsilon_{a_1}$. A similar calculation of the reducible part of the diagrams depicted in Fig. 3.4(b) gives

$$\tau^{\mathrm{INTb,red}}_{\gamma_f,B;A} = \frac{i}{2\pi} \int_{-\infty}^{\infty} \mathrm{d}\omega \, \langle b_2|e\alpha_\mu A_f^{\mu *}|a_2\rangle$$
$$\times \left(\frac{\langle b_1b_2|I(\omega)|b_1b_2\rangle}{(\omega - i0)^2} - \frac{\langle b_2b_1|I(\omega)|b_1b_2\rangle}{(\omega - \Delta_B - i0)^2} \right), \tag{3.77}$$

where $\Delta_B \equiv \varepsilon_{b_2} - \varepsilon_{b_1}$. The reducible contribution has to be considered together with second term of Eq. (3.53). Taking into account that for the initial state A (see Ref. [100])

$$\frac{1}{2\pi i} \oint_{\Gamma_A} \mathrm{d}E \, g^{(1)}_{AA}(E) = -\frac{i}{2\pi} \left[2 \int_{-\infty}^{\infty} \mathrm{d}p_1'^0 \frac{\langle a_1a_2|I(p_1'^0 - \varepsilon_{a_1})|a_1a_2\rangle}{(p'^0 - \varepsilon_{a_1} - i0)^2} \right.$$
$$- \int_{-\infty}^{\infty} \mathrm{d}p_1'^0 \frac{\langle a_2a_1|I(p_1'^0 - \varepsilon_{a_1})|a_1a_2\rangle}{(p_1'^0 - \varepsilon_{a_2} - i0)^2}$$
$$\left. - \int_{-\infty}^{\infty} \mathrm{d}p_1^0 \frac{\langle a_2a_1|I(p_1^0 - \varepsilon_{a_2})|a_1a_2\rangle}{(p_1^0 - \varepsilon_{a_1} - i0)^2} \right], \tag{3.78}$$

and a similar equation holds for the final state B, one derives

$$-\frac{1}{2} \oint_{\Gamma_B} \mathrm{d}E' \oint_{\Gamma_A} \mathrm{d}E \, g^{(0)}_{\gamma_f,B;A}(E', E) \left(\frac{1}{2\pi i} \oint_{\Gamma_A} \mathrm{d}E \, g^{(1)}_{AA}(E) + \frac{1}{2\pi i} \oint_{\Gamma_B} \mathrm{d}E \, g^{(1)}_{BB}(E) \right)$$
$$= \frac{1}{2} \langle b_2|e\alpha_\mu A_f^{\mu *}|a_2\rangle \int_{-\infty}^{\infty} \mathrm{d}\omega \left\{ 2\frac{\langle a_1a_2|I(\omega)|a_1a_2\rangle}{(\omega - i0)^2} + 2\frac{\langle b_1b_2|I(\omega)|b_1b_2\rangle}{(\omega - i0)^2} \right.$$
$$- \langle a_2a_1|I(\omega)|a_1a_2\rangle \left[\frac{1}{(\omega - \Delta_A - i0)^2} + \frac{1}{(\omega + \Delta_A - i0)^2} \right]$$
$$\left. - \langle b_2b_1|I(\omega)|b_1b_2\rangle \left[\frac{1}{(\omega - \Delta_B - i0)^2} + \frac{1}{(\omega + \Delta_B - i0)^2} \right] \right\}. \tag{3.79}$$

Summing up (3.76), (3.77), and (3.79) yields for the total reducible contribution

$$\begin{aligned}\tau^{\mathrm{INT,red}}_{\gamma_f,B;A} &= -\frac{1}{2}\langle b_2|e\alpha_\mu A^{\mu*}_f|a_2\rangle\frac{i}{2\pi}\int_{-\infty}^{\infty}\mathrm{d}\omega\Bigg\{\langle a_2a_1|I(\omega)|a_1a_2\rangle \\ &\times\left[\frac{1}{(\omega+\Delta_A+i0)^2}-\frac{1}{(\omega+\Delta_A-i0)^2}\right]+\langle b_2b_1|I(\omega)|b_1b_2\rangle \\ &\times\left[\frac{1}{(\omega+\Delta_B+i0)^2}-\frac{1}{(\omega+\Delta_B-i0)^2}\right]\Bigg\}. \end{aligned} \tag{3.80}$$

Here we have employed the symmetry property of the photon propagator: $I(\omega)=I(-\omega)$. Employing the identity

$$\frac{1}{(\omega+i0)^2}-\frac{1}{(\omega-i0)^2}=-\frac{2\pi}{i}\frac{\mathrm{d}}{\mathrm{d}\omega}\delta(\omega)\,, \tag{3.81}$$

and integrating by parts, the final result for the reducible part can be cast into the form [138]

$$\tau^{\mathrm{INT,red}}_{\gamma_f,B;A}=\frac{1}{2}\langle b_2|e\alpha_\mu A^{\mu*}_f|a_2\rangle\Big[\langle a_2a_1|I'(\Delta_A)|a_1a_2\rangle+\langle b_2b_1|I'(\Delta_B)|b_1b_2\rangle\Big]\,, \tag{3.82}$$

where $I'(\Delta)\equiv \mathrm{d}I(\omega)/\mathrm{d}\omega\Big|_{\omega=\Delta}$ and implying that $a_1=b_1$. The total expression for the interelectronic-interaction correction $\tau^{\mathrm{INT}}_{\gamma_f,B;A}$ to the transition amplitude is given by the sum of Eqs. (3.73), (3.74), and (3.82):

$$\tau^{\mathrm{INT}}_{\gamma_f,B;A}=\tau^{\mathrm{INTa,irred}}_{\gamma_f,B;A}+\tau^{\mathrm{INTb,irred}}_{\gamma_f,B;A}+\tau^{\mathrm{INT,red}}_{\gamma_f,B;A}\,. \tag{3.83}$$

3.5 The transition probability in ions with one electron over closed shells

The formalism provided in previous Sections can be immediately adopted for treating the case of an ion with one electron over closed shells. Let us consider the decays induced by the transition of the valence electron. The QED corrections of first order in the perturbation expansion are easily related to one-electron contributions. To keep the derivation of formal expressions for the interelectronic-interaction terms short, we specify the formalism regarding the core electrons as belonging to redefined vacuum (for details we refer to works [100, 139, 140]). The redefinition of the vacuum results in replacing in the electron propagator the $i0$-prescription by $-i0$ in the denominators of the states corresponding to the closed shells. This leads to merging the interelectronic-interaction corrections of first order in $1/Z$ with the one-loop QED terms. Thus, the corresponding formulas (3.64) and (3.65) can be used for the determination of the interelectronic-interaction contributions. However, the standard electron propagator $S(\varepsilon,\mathbf{x},\mathbf{y})$ entering in these equations, must be replaced by

$$\tilde{S}(\varepsilon,\mathbf{x},\mathbf{y})=S(\varepsilon,\mathbf{x},\mathbf{y})+2\pi i\sum_c\psi_c(\mathbf{x})\overline{\psi}_c(\mathbf{y})\delta(\varepsilon-\varepsilon_c)\,, \tag{3.84}$$

where the summation runs over all occupied one-electron states referring to the closed shells. Accordingly, the total expression is represented by the sum of the pure QED and interelectronic-interaction contributions, which correspond to the first and second terms in the right-hand side of Eq. (3.84). Substituting Eq. (3.84) into the

formulas (3.64) and (3.65) and extracting only the interelectronic-interaction terms we obtain [140]

$$\tau^{\rm INT}_{\gamma_f,b;a} = -\sum_c \Bigg\{ \sum_n^{\varepsilon_n\neq\varepsilon_b} \frac{\langle bc|I(0)|nc\rangle\langle n|e\alpha_\mu A^\mu_f|a\rangle}{\varepsilon_b-\varepsilon_n} + \sum_n^{\varepsilon_n\neq\varepsilon_a} \frac{\langle b|e\alpha_\mu A^\mu_f|n\rangle\langle cn|I(0)|ca\rangle}{\varepsilon_a-\varepsilon_n}$$
$$+\sum_n \frac{\langle bc|I(\varepsilon_a-\varepsilon_b)|an\rangle\langle n|e\alpha_\mu A^\mu_f|c\rangle}{\varepsilon_b+\varepsilon_c-\varepsilon_a-\varepsilon_n} + \sum_n \frac{\langle c|e\alpha_\mu A^\mu_f|n\rangle\langle nb|I(\varepsilon_a-\varepsilon_b)|ca\rangle}{\varepsilon_a+\varepsilon_c-\varepsilon_b-\varepsilon_n}$$
$$-\sum_n^{\varepsilon_n\neq\varepsilon_b} \frac{\langle bc|I(\varepsilon_b-\varepsilon_c)|cn\rangle\langle n|e\alpha_\mu A^\mu_f|a\rangle}{\varepsilon_b-\varepsilon_n} - \sum_n^{\varepsilon_n\neq\varepsilon_a} \frac{\langle b|e\alpha_\mu A^\mu_f|n\rangle\langle nc|I(\varepsilon_a-\varepsilon_c)|ca\rangle}{\varepsilon_a-\varepsilon_n}$$
$$-\sum_n \frac{\langle bc|I(\varepsilon_a-\varepsilon_c)|na\rangle\langle n|e\alpha_\mu A^\mu_f|c\rangle}{\varepsilon_b+\varepsilon_c-\varepsilon_a-\varepsilon_n} - \sum_n \frac{\langle c|e\alpha_\mu A^\mu_f|n\rangle\langle bn|I(\varepsilon_b-\varepsilon_c)|ca\rangle}{\varepsilon_a+\varepsilon_c-\varepsilon_b-\varepsilon_n}$$
$$-\frac{1}{2}\langle b|e\alpha_\mu A^\mu_f|a\rangle\left[\langle bc|I'(\varepsilon_b-\varepsilon_c)|cb\rangle + \langle ac|I'(\varepsilon_a-\varepsilon_c)|ca\rangle\right]\Bigg\}, \tag{3.85}$$

where the initial a and final b states determine the one-electron level of the valent electron. The pure one-loop QED corrections are given by Eqs. (3.64) and (3.65) with the standard electron propagation function $S(\varepsilon,\mathbf{x},\mathbf{y})$. In addition to the corrections to the transition amplitude, derived in these Sections, we must take into account the contribution originating from changing the photon energy in the zeroth-order transition probability Eq. (3.52). We have to add to the transition energy the QED and interelectronic-interaction corrections of the first order in the perturbation theory. It follows that the total correction of first order to the transition probability is given by

$$\begin{aligned} {\rm d}W^{(1)}_{\gamma_f,B;A} &= 2\pi(k^0_f)^2 2{\rm Re}\Big\{\tau^{(0)*}_{\gamma_f,B;A}\tau^{(1)}_{\gamma_f,B;A}\Big\}{\rm d}\Omega_{\mathbf{k}_f} \\ &\quad + \left[{\rm d}W^{(0)}_{\gamma_f,B;A}\Big|_{k^0_f=E_A-E_B} - {\rm d}W^{(0)}_{\gamma_f,B;A}\Big|_{k^0_f=E^{(0)}_A-E^{(0)}_B}\right]. \end{aligned} \tag{3.86}$$

Here $\tau^{(1)}_{\gamma_f,B;A} = \tau^{\rm SE}_{\gamma_f,B;A} + \tau^{\rm VP}_{\gamma_f,B;A} + \tau^{\rm INT}_{\gamma_f,B;A}$ is the sum of the QED and interelectronic-interaction corrections given by Eqs. (3.64), (3.65), (3.83), and (3.85). E_A, E_B and $E^{(0)}_A$, $E^{(0)}_B$ are the energies of the bound states A and B with and without the radiative and interelectronic-interaction contributions, respectively.

4 One-loop QED corrections to the magnetic-dipole transition amplitude

The most precise measurement of the decay rates has been performed for the magnetic-dipole transition $(1s^2 2s^2 2p)\,^2P_{3/2} - {}^2P_{1/2}$ in B-like $^{40}Ar^{13+}$ with the accuracy better than one part per thousand [76, 77]. This experimental precision demands the rigorous theoretical investigation of this transition rate. In this Chapter we present the exact calculation of the one-loop radiative corrections to the decay rate of the magnetic-dipole transition $2p_{3/2} - 2p_{1/2}$. The results reported here were obtained in the works [140, 141].

4.1 Magnetic-dipole transition rate

In practical calculations the photon wave function given by Eq. (3.12) is expanded in a multipole series (see, e.g., Ref. [142]). Then the summation over the photon polarization ϵ_f and the integration over the photon energy $\omega = k_f^0$ and angles $\Omega_{\mathbf{k}_f}$ can be carried out. As a result, the spontaneous L-pole transition probability is given by

$$W_L = \frac{2\pi}{2J_A+1} \sum_{M_A} \sum_{M_B} \sum_{M} |A^{(\lambda)}_{LM}|^2 \,, \tag{4.1}$$

where the initial electron state A is characterized by the total angular momentum J_A, its projection M_A, and the energy E_A, while the final state B has the corresponding quantum numbers J_B, M_B, and the energy E_B. $A^{(\lambda)}_{LM}$ is the L-pole transition amplitude corresponding to the emission of a magnetic ($\lambda = 0$) or electric ($\lambda = 1$) multipole photon, which is given by

$$A^{(\lambda)}_{LM} = i^{L+1} \sqrt{\frac{\omega}{\pi}}\, \sqrt{2L+1}\, \langle B|T^{(\lambda)}_{LM}|A\rangle \,. \tag{4.2}$$

Here $T^{(\lambda)}_{LM}$ denote the components of the multipole transition operator $\mathbf{T}^{(\lambda)}_L$, which transforms under rotations as a spherical tensor of rank L. Employing the Wigner-Eckart theorem [143] the L-pole transition probability can be expressed in terms of the reduced matrix element of $T^{(\lambda)}_{LM}$

$$W_L = 2\omega\, \frac{2L+1}{2J_A+1} \left| \langle B||\mathbf{T}^{(\lambda)}_L||A\rangle \right|^2 \,. \tag{4.3}$$

In case of a magnetic transition ($\lambda = 0$), $\mathbf{T}^{(0)}_L$ is proportional to the tensor product of the Dirac-matrix vector $\boldsymbol{\alpha}$ and the spherical tensor $C^L_M = \sqrt{4\pi/(2L+1)}\, Y_{LM}$ [143]

$$T^{(0)}_{LM} \;=\; ie\, j_L(\omega r)\, [\boldsymbol{\alpha} \times \mathbf{C}^L]^L_M \,, \tag{4.4}$$

where j_L is the spherical Bessel function and $\omega = E_A - E_B$.
In this Chapter we are interested in the magnetic-dipole (M1) transition between the fine-structure levels $2p_{1/2}$ and $2p_{3/2}$. Therefore, to simplify the notations, in what follows we take $\lambda = 0$, $L = 1$, $M = 0$ and omit the indices at

the corresponding quantities. The tensor product for the magnetic-dipole transition can be written in a way

$$\mathbf{T}_1^{(0)} = \frac{e}{\sqrt{2}}\, j_1(\omega r)\, \frac{[\mathbf{r}\times\boldsymbol{\alpha}]^1}{r}\,. \tag{4.5}$$

In further calculations we take into account only the first term in the power expansion of $j_1(\omega r)$, since for the case under consideration the transition wavelength is much larger than the typical ion size. Accordingly, the M1-transition operator $\mathbf{T}_1^{(0)}$ can be related to the magnetic moment operator $\boldsymbol{\mu} = e\,[\mathbf{r}\times\boldsymbol{\alpha}]/2$,

$$\mathbf{T} = \frac{e}{3\sqrt{2}}\,\omega\,[\mathbf{r}\times\boldsymbol{\alpha}] = \frac{\sqrt{2}}{3}\,\omega\,\boldsymbol{\mu}\,. \tag{4.6}$$

The nonrelativistic magnetic moment operator is given by

$$\boldsymbol{\mu}_{\rm nr} = -\mu_{\rm B}\,(\mathbf{L}+2\mathbf{S})\,, \tag{4.7}$$

where $\mathbf{L}$ and $\mathbf{S}$ are the orbital and spin angular momentum operators, respectively, and $\mu_{\rm B} = |e|\hbar/2mc$ denotes the Bohr magneton.

In the LS-coupling scheme, which is realized in the nonrelativistic case, the magnetic-dipole transition probability is nonzero only between fine-structure levels with $\Delta J = \pm 1$ [143]. The reduced matrix element of $\mathbf{T}_{\rm nr}$ within the LS-coupling is given by

$$\langle J_B||\mathbf{T}_{\rm nr}||J_A\rangle = -\frac{\sqrt{2}}{3}\,\omega\mu_{\rm B}\langle J_B||(\mathbf{J}+\mathbf{S})||J_A\rangle = -\frac{\sqrt{2}}{3}\omega\mu_{\rm B}\langle J_B||\mathbf{S}||J_A\rangle\,. \tag{4.8}$$

Utilizing the general formula for the reduced matrix element of the spin operator [143] yields the corresponding expression for the transition probability

$$W_{\rm nr} = \frac{4}{3}\omega^3\mu_{\rm B}^2\delta_{L_A,L_B}\delta_{S_A,S_B}S_A(S_A+1)(2S_A+1)(2J_B+1)\left\{\begin{array}{ccc} S_A & L_A & J_A \\ J_B & 1 & S_A\end{array}\right\}^2. \tag{4.9}$$

In particular, for the $(1s^22s^22p)\,^2P_{3/2} - {}^2P_{1/2}$ transition in B-like ions one can easily find

$$W_{\rm nr} = \frac{4}{9}\omega^3\mu_{\rm B}^2 = \frac{1}{3\lambda^3}\,2.6973500\times10^{13}\,[{\rm s}^{-1}]\,, \tag{4.10}$$

where λ is the transition wavelength, in Å. Thus, in the nonrelativistic limit the magnetic-dipole transition probability is completely determined by the quantum numbers of the initial and final electron states. From aforesaid follows that the interelectronic-interaction corrections are suppressed by the relativistic factor $(\alpha Z)^2$. To the lowest order the analytical expression for the relativistic correction to the transition amplitude is given in Ref. [87]. We calculate the relativistic contribution $\Delta W_{\rm D}$ using the numerical solution of the Dirac equation.

4.2 Calculation of the QED corrections

4.2.1 Lowest order

The QED correction of lowest order in αZ to the M1-transition amplitude can be derived by correcting the operator of the magnetic moment for the anomalous magnetic moment of a free electron (EAMM). In the nonrelativistic limit it yields

$$\boldsymbol{\mu}_{\rm nr} \to \boldsymbol{\mu}_a = -\mu_{\rm B}\,[\mathbf{L}+2(1+\kappa_{\rm e})\mathbf{S}] = \boldsymbol{\mu}_{\rm nr} + \delta\boldsymbol{\mu}_a\,, \tag{4.11}$$

where

$$\delta\boldsymbol{\mu}_a = -2\mu_{\rm B}\kappa_{\rm e}\mathbf{S}\,, \tag{4.12}$$

and $\kappa_{\rm e}$ is defined by Eq. (2.8). Therefore, the lowest-order QED correction to the M1-transition amplitude is given by

$$\Delta A_{\rm QED} = -\sqrt{\frac{2\omega^3}{3\pi}}\left(\langle B|(\boldsymbol{\mu}_{\rm nr}+\delta\boldsymbol{\mu}_a)|A\rangle - \langle B|\boldsymbol{\mu}_{\rm nr}|A\rangle\right)\,. \tag{4.13}$$

Taking into account that for the fine-structure level transition ($\Delta J = \pm 1$)

$$\langle B|\delta\boldsymbol{\mu}_a|A\rangle = 2\kappa_{\rm e}\langle B|\boldsymbol{\mu}_{\rm nr}|A\rangle\,, \tag{4.14}$$

we find

$$\Delta A_{\rm QED} = -2\kappa_{\rm e}\sqrt{\frac{2\omega^3}{3\pi}}\langle B|\boldsymbol{\mu}_{\rm nr}|A\rangle = 2\kappa_{\rm e}A_{\rm nr}\,. \tag{4.15}$$

The higher-order QED corrections, which are not taken into account by this formula, are suppressed by a factor $(\alpha Z)^2$.

4.2.2 Vacuum-polarization correction

Further we consider the one-loop QED contributions to the transition amplitude to all orders in αZ. The self-energy and vacuum-polarization (VP) corrections, which one has to account for, are diagrammatically depicted in Figs. 3.2 and 3.3, respectively. Let us start with the VP contribution. The VP correction is divided into the electric-loop term depicted in Fig. 3.3(a),(b), which accounts for the VP correction to the nuclear Coulomb potential, and the magnetic-loop term corresponding to the VP-corrected photon emission presented in Fig. 3.3(c). The electric-loop term leading to a modified binding potential gives rise to wave function corrections $|\delta a_{\rm VP}\rangle$ and $|\delta b_{\rm VP}\rangle$. The corresponding contribution is given by (see Eq. (3.65))

$$\Delta A^{\rm el} = -\sqrt{\frac{2\omega^3}{3\pi}}\left(\langle b|\mu_z|\delta a_{\rm VP}\rangle + \langle \delta b_{\rm VP}|\mu_z|a\rangle\right)\,, \tag{4.16}$$

where the perturbed functions have the form

$$|\delta a_{\rm VP}\rangle = \sum_n^{\varepsilon_n\neq\varepsilon_a}\frac{|n\rangle\langle n|U_{\rm VP}|a\rangle}{\varepsilon_a-\varepsilon_n}, \qquad |\delta b_{\rm VP}\rangle = \sum_n^{\varepsilon_n\neq\varepsilon_b}\frac{|n\rangle\langle n|U_{\rm VP}|b\rangle}{\varepsilon_b-\varepsilon_n}\,, \tag{4.17}$$

where $U_{\rm VP}$ implies the renormalized VP potential. The proper renormalized expression for the magnetic-loop term, where the M1-operator enters into the loop, is defined by

$$\Delta A^{\rm ml} = \sqrt{\frac{2\omega^3}{3\pi}}\Bigg\{2i\alpha\int {\rm d}\mathbf{x}{\rm d}\mathbf{y}{\rm d}\mathbf{z}\,\overline{\phi}_b(\mathbf{x})\gamma^\rho\phi_a(\mathbf{x})D_{\rho\sigma}(k^0,\mathbf{x}-\mathbf{y})$$
$$\times\int_{-\infty}^{\infty}{\rm d}\omega\,{\rm Tr}[\gamma^\sigma S(\omega,\mathbf{y},\mathbf{z})\gamma^0\mu_z(\mathbf{z})S(\omega+k^0,\mathbf{z},\mathbf{y})] - (Z_3^{-1/2}-1)\langle b|\mu_z|a\rangle\Bigg\}\,, \tag{4.18}$$

where we explicitly introduce the counterterm $\sim Z_3^{-1/2}$. Further we apply the potential expansion for the loop. Such an expansion is diagrammatically depicted in Fig. 4.1, where the first term in the expansion refers to the Uehling contribution and the remainder is Wichmann-Kroll correction. The Uehling part contains the leading term of the expansion in powers of αZ. Formally, the VP loop in the Uehling contribution corresponds to a replacement of the interaction with a potential A_μ [144, 145]

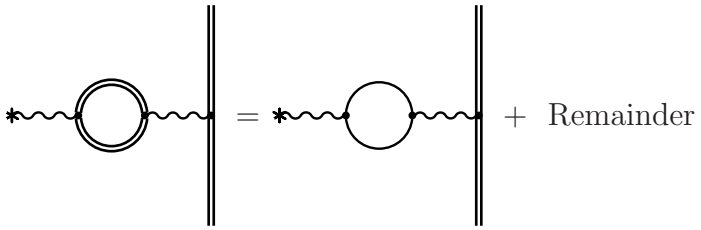

Figure 4.1: The potential expansion of the vacuum-polarization diagram. The single line indicates the free-electron propagator and the wavy line ending with the asterisk denotes either the interaction with the field of the nucleus or emitted photon. The first term represents the contribution in the Uehling approximation, while the Remainder contains the higher-orders terms.

$$A_\mu \to -D_{\mu\alpha}\Pi^{\alpha\beta}(k^2)A_\beta\,, \tag{4.19}$$

where $k = (k^0, \mathbf{k})$. The polarization tensor $\Pi^{\alpha\beta}(k^2)$ has the structure $\Pi^{\alpha\beta}(k^2) = (k^\alpha k^\beta - g^{\alpha\beta}k^2)\Pi(k^2)$. This, in turn, follows because gauge invariance demands

$$k_\alpha \Pi^{\alpha\beta}(k^2) = 0\,. \tag{4.20}$$

To the leading order in α we have after renormalization [144, 145]

$$\Pi_{\rm R}(k^2) = \frac{2\alpha}{3\pi}\int_1^\infty {\rm d}t\,\sqrt{t^2-1}\left(\frac{1}{t^2}+\frac{1}{2t^4}\right)\frac{k^2}{4t^2-k^2}\,. \tag{4.21}$$

For the magnetic-loop term, where the potential $A_\mu(k)$ representing the external photon line (see diagram depicted in Fig. 3.3(c)), one can drop the Uehling contribution [145]. This is because of the momentum of a real photon has to be on "mass-shell" $k^2 = 0$, while $\Pi_{\rm R}(k^2)$ is proportional to k^2 and thus $\Pi_{\rm R}(0)$ vanishes. For the electric-loop term, where the potential induced by the density of the spherically symmetric nucleus charge distribution $\rho(r)$ $\left[\int {\rm d}\mathbf{r}\,\rho(r) = 1\right]$, the result is not zero. And the VP potential in the Uehling approximation can be evaluated according to [40]

$$U_{\rm VP}^{\rm Uehl}(r) = -\frac{2\alpha^2 Z}{3\pi}\int_1^\infty {\rm d}t\,\sqrt{t^2-1}\left(\frac{1}{t^2}+\frac{1}{2t^4}\right)\int {\rm d}^3r'\,e^{-2|\mathbf{r}-\mathbf{r}'|t}\,\frac{\rho(r')}{|\mathbf{r}-\mathbf{r}'|}\,. \tag{4.22}$$

Employing this expression and Eqs. (4.16) and (4.17) we have calculated the VP contribution in the Uehling approximation. The Wichmann-Kroll correction to the energy levels to all orders in αZ was calculated in works [146, 147, 148]. Based on the results of these works, one can find that the Wichmann-Kroll term essentially smaller that the Uehling contribution for the middle Z region. For this reason, it can be neglected.

4.2.3 Self-energy correction

Now let us turn to the evaluation of the SE correction. We divide the correction (3.64) into three parts: irreducible, reducible, and vertex. The irreducible part is represented by the expression

$$\Delta A^{\rm irr} = -\sqrt{\frac{2\,\omega^3}{3\pi}}\left(\langle b|\mu_z|\delta a_{\rm SE}\rangle + \langle \delta b_{\rm SE}|\mu_z|a\rangle\right)\,, \tag{4.23}$$

where the perturbed wave functions are given by

$$|\delta a_{\rm SE}\rangle = \sum_n^{\varepsilon_n\neq\varepsilon_a}\frac{|n\rangle\langle n|\Sigma_{\rm R}(\varepsilon_b)|a\rangle}{\varepsilon_a-\varepsilon_n}, \qquad |\delta b_{\rm SE}\rangle = \sum_n^{\varepsilon_n\neq\varepsilon_b}\frac{|n\rangle\langle n|\Sigma_{\rm R}(\varepsilon_a)|b\rangle}{\varepsilon_b-\varepsilon_n}\,. \tag{4.24}$$

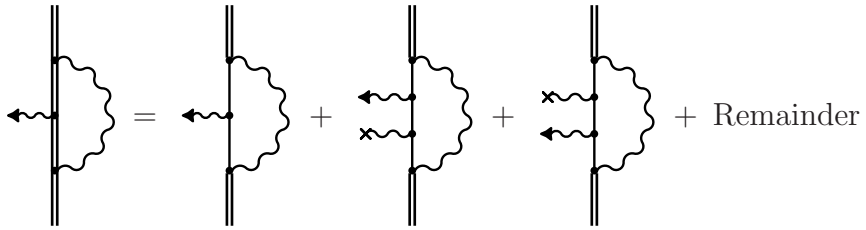

Figure 4.2: The potential expansion of the vertex diagram. The wavy line ending with the cross denotes the interaction with the field of the nucleus. All higher-order contributions are contained in the Remainder.

The irreducible term is renormalized in the same manner as the ordinary SE correction to the energy. This renormalization is well-known and discussed in details in Refs. [149, 150, 151]. The ultraviolet divergence contained in the vertex

$$\begin{aligned}\Delta A^{\rm ver} &= -\sqrt{\frac{2\,\omega^3}{3\pi}}2i\alpha\int_{-\infty}^{\infty}{\rm d}\omega\int{\rm d}\mathbf{x}{\rm d}\mathbf{y}{\rm d}\mathbf{z}\,\overline{\phi}_b(\mathbf{x})\gamma^\rho S(\varepsilon_b-\omega,\mathbf{x},\mathbf{z})\gamma^0\mu_z(\mathbf{z})\\ &\quad\times S(\varepsilon_a-\omega,\mathbf{z},\mathbf{y})\gamma^\sigma D_{\rho\sigma}(\omega,\mathbf{x}-\mathbf{y})\phi_a(\mathbf{y})\end{aligned}\tag{4.25}$$

and reducible

$$\Delta A^{\rm red}=-\sqrt{\frac{\omega^3}{6\pi}}\langle b|\mu_z|a\rangle(\langle b|\Sigma'(\varepsilon_b)|b\rangle+\langle a|\Sigma'(\varepsilon_a)|a\rangle)\tag{4.26}$$

contributions can be isolated by performing a potential expansion of the bound-electron propagator with respect to the interaction with the field of the nucleus. For our purposes, it is convenient to decompose the total contribution into zero-, one-, and many-potential terms according to the number of interactions with the external field

$$\Delta A^{\rm ver}=\Delta A^{\rm ver(0)}+\Delta A^{\rm ver(1)}+\Delta A^{\rm ver(2+)}\tag{4.27}$$

and

$$\Delta A^{\rm red}=\Delta A^{\rm red(0)}+\Delta A^{\rm red(1)}+\Delta A^{\rm red(2+)}\,.\tag{4.28}$$

This expansion for the vertex diagram is schematically presented in Fig. 4.2. In order to achieve cancellation of the divergences in the vertex and reducible terms, one has to consider them simultaneously. Combining the corresponding parts, we define

$$\Delta A^{{\rm vr}(i)}=\Delta A^{{\rm ver}(i)}+\Delta A^{{\rm red}(i)}\,,\qquad(i=0,1,2+)\,.\tag{4.29}$$

It can be shown, that the ultraviolet-divergent terms, which are present in $\Delta A^{\rm ver(0)}$ and $\Delta A^{\rm red(0)}$, cancel each other in $\Delta A^{\rm vr(0)}$. The remaining one- and many-potential terms of the vertex and reducible corrections are ultraviolet finite.

The zero- and one-potential contributions are evaluated in momentum space, while the many-potential term is calculated in the coordinate space employing the partial-wave description. The scheme for the separate treatment of the one-potential term has also been successfully applied in previous g factor calculations presented in Refs. [22, 23, 26, 27]. It improves considerably the convergence of the partial-wave expansion in the low and middle Z region. The expressions for the reducible correction are similar to those derived for the g factor (see Ref. [27])

$$\begin{aligned}\Delta A^{\rm red(0)} &= -\sqrt{\frac{\omega^3}{6\pi}}\langle b|\mu_z|a\rangle\int\frac{{\rm d}\mathbf{p}}{(2\pi)^3}\left[\overline{\phi}_a(\mathbf{p})\frac{\partial}{\partial\varepsilon_a}\Sigma^{(0)}_{\rm R}(\varepsilon_a,\mathbf{p})\phi_a(\mathbf{p})\right.\\ &\quad\left.+\phi_b(\mathbf{p})\frac{\partial}{\partial\varepsilon_b}\Sigma^{(0)}_{\rm R}(\varepsilon_b,\mathbf{p})\phi_b(\mathbf{p})\right]\end{aligned}\tag{4.30}$$

and

$$\Delta A^{\mathrm{red}(1)} = -\sqrt{\frac{\omega^3}{6\pi}}\langle b|\mu_z|a\rangle \int \frac{\mathrm{d}\mathbf{p}\mathrm{d}\mathbf{p}'}{(2\pi)^6} V(\mathbf{q}) \left[\overline{\phi}_a(\mathbf{p})\frac{\partial}{\partial\varepsilon_a}\Gamma^0_{\mathrm{R}}(\varepsilon_a,\mathbf{p};\varepsilon_a,\mathbf{p}')\phi_a(\mathbf{p}') + \overline{\phi}_b(\mathbf{p})\frac{\partial}{\partial\varepsilon_b}\Gamma^0_{\mathrm{R}}(\varepsilon_b,\mathbf{p};\varepsilon_b,\mathbf{p}')\phi_b(\mathbf{p}')\right], \tag{4.31}$$

where $V(\mathbf{q})$ is the Fourier transform of the binding potential. Here the renormalized zero-potential self-energy function $\Sigma^{(0)}_{\mathrm{R}}(p)$ is defined by the expression

$$\Sigma^{(0)}_{\mathrm{R}}(p) = \frac{\alpha}{4\pi}\gamma^0\left[2 + \frac{4\rho}{1-\rho}\ln\rho - \not{p}\frac{2-\rho}{1-\rho}\left(1+\frac{\rho}{1-\rho}\ln\rho\right)\right], \tag{4.32}$$

where $\rho = 1-p^2$. The renormalized vertex function $\Gamma^\mu_{\mathrm{R}}(p;p')$ can be evaluated to be (see Ref. [151])

$$\Gamma^\mu_{\mathrm{R}}(p;p') = \frac{\alpha}{4\pi}\left[A\gamma^\mu + \not{p}(B_1 p^\mu + B_2 p'^\mu) + \not{p}'(C_1 p^\mu + C_2 p'^\mu) + D\,\not{p}\gamma^\mu\not{p}' + H_1 p^\mu + H_2 p'^\mu\right], \tag{4.33}$$

$$A = C_{24} - 2 + p^2 C_{11} + p'^2 C_{12} + 4pp'(C_0 + C_{11} + C_{12}) - 2C_0 + C_{11} + C_{12}\,, \tag{4.34}$$

$$B_1 = -4(C_{11} + C_{21})\,, \tag{4.35}$$

$$B_2 = -4(C_0 + C_{11} + C_{12} + C_{23})\,, \tag{4.36}$$

$$C_1 = -4(C_0 + C_{11} + C_{12} + C_{23})\,, \tag{4.37}$$

$$C_2 = -4(C_{12} + C_{22})\,, \tag{4.38}$$

$$D = 2(C_0 + C_{11} + C_{12})\,, \tag{4.39}$$

$$H_1 = 4(C_0 + 2C_{11})\,, \tag{4.40}$$

$$H_2 = 4(C_0 + 2C_{12})\,, \tag{4.41}$$

where

$$C_0 = \int_0^1 \frac{\mathrm{d}y}{(yp + (1-y)p')^2}(-\ln X)\,, \tag{4.42}$$

$$\begin{pmatrix} C_{11} \\ C_{12} \end{pmatrix} = \int_0^1 \frac{\mathrm{d}y}{(yp + (1-y)p')^2}\begin{pmatrix} y \\ 1-y \end{pmatrix}(1 - Y\ln X)\,, \tag{4.43}$$

$$\begin{pmatrix} C_{21} \\ C_{22} \\ C_{23} \end{pmatrix} = \int_0^1 \frac{\mathrm{d}y}{(yp + (1-y)p')^2}\begin{pmatrix} y^2 \\ (1-y)^2 \\ y(1-y) \end{pmatrix}\left(\frac{1}{2} + Y - Y^2\ln X\right), \tag{4.44}$$

$$C_{24} = -\int_0^1 \mathrm{d}y\, \ln(y^2(p-p')^2 - y(p-p')^2 + 1)\,, \tag{4.45}$$

and

$$X = 1 + \frac{1}{Y}\,, \tag{4.46}$$

$$Y = \frac{1 - yp^2 - (1-y)p'^2}{(yp + (1-y)p')^2}\,. \tag{4.47}$$

Here $p = (\varepsilon, \mathbf{p})$, $p' = (\varepsilon', \mathbf{p}')$, and $\not{p} = p_\mu \gamma^\mu$.
The renormalized zero-potential vertex contribution $\Delta A^{\mathrm{ver}(0)}$ can be written as

$$\Delta A^{\mathrm{ver}(0)} = -\sqrt{\frac{\omega^3}{6\pi}}\, ie \int \frac{\mathrm{d}\mathbf{p}\,\mathrm{d}\mathbf{p}'}{(2\pi)^3}\, \overline{\phi}_b(\mathbf{p}) \left[\mathbf{\Gamma}_{\mathrm{R}}(\varepsilon_b, \mathbf{p}; \varepsilon_a, \mathbf{p}') \times \boldsymbol{\nabla}_{\mathbf{p}'} \delta^3(\mathbf{p} - \mathbf{p}')\right]_z \phi_a(\mathbf{p}')\,, \tag{4.48}$$

and the one-potential vertex term has the form

$$\begin{aligned}\Delta A^{\mathrm{ver}(1)} &= -\sqrt{\frac{\omega^3}{6\pi}}\, ie \int \frac{\mathrm{d}\mathbf{p}\,\mathrm{d}\mathbf{q}\,\mathrm{d}\mathbf{p}'}{(2\pi)^6} \Big\{ \overline{\phi}_b(\mathbf{p}) V(\mathbf{q}) \\ &\times \left[\mathbf{\Lambda}(\varepsilon_b, \mathbf{p}; \varepsilon_b, \mathbf{q}; \varepsilon_a, \mathbf{p}') \times \boldsymbol{\nabla}_{\mathbf{r}} \delta^3(\mathbf{p} - \mathbf{p}' - \mathbf{q})\right]_z \phi_a(\mathbf{p}') + \overline{\phi}_a(\mathbf{p}) V(\mathbf{q}) \\ &\times \left[\mathbf{\Lambda}(\varepsilon_a, \mathbf{p}; \varepsilon_a, \mathbf{q}; \varepsilon_b, \mathbf{p}') \times \boldsymbol{\nabla}_{\mathbf{r}} \delta^3(\mathbf{p} - \mathbf{p}' - \mathbf{q})\right]_z \phi_b(\mathbf{p}') \Big\}\,. \end{aligned} \tag{4.49}$$

Here the function $\mathbf{\Lambda}(p; q; p')$ is given by

$$\begin{aligned}\mathbf{\Lambda}(p; q; p') &= -4\pi i\alpha \int \frac{\mathrm{d}^4 k}{(2\pi)^4} \gamma_\mu \frac{\not{p} - \not{k} + m}{(p-k)^2 - m^2} \gamma^0 \\ &\times \frac{\not{p} - \not{k} - \not{q} + m}{(p-k-q)^2 - m^2} \boldsymbol{\gamma} \frac{\not{p}' - \not{k} + m}{(p'-k)^2 - m^2} \gamma^\mu\,. \end{aligned} \tag{4.50}$$

Therefore, one can see that the vertex contributions have some principal differences. In contrast to the vertex formulas for the g factor, the functions $\mathbf{\Gamma}_{\mathrm{R}}(p; p')$ in Eq. (4.48) and $\mathbf{\Lambda}(p, r, p')$ in Eq. (4.49) depend on two different energies ε_a and ε_b. Taking these differences into account, we derive the corresponding formulas for the $\Delta A^{\mathrm{ver}(0)}$ term in the Appendix B. The derivation of the formulas for the one-potential vertex contribution is somewhat more complicated. However, taking the energy to be the same in both electron propagators (e.g., ε_a or ε_b), the expressions for $\Delta A^{\mathrm{ver}(1)}$ can be obtained in the same manner as for the g factor [27]. The remaining many-potential term can be evaluated by the point-by-point subtraction of the corresponding zero- and one-potential contributions in the coordinate space. Consistently, we subtract the one-potential vertex contribution with the same energy variable in the electron propagators as it is taken in the $\Delta A^{\mathrm{ver}(1)}$ term calculated in the momentum space.

4.2.4 Numerical results

For the numerical evaluation we employ the finite-basis-set method for the Dirac equation, which is described in next Chapter. The summation of the partial-wave expansion was performed up to $|\kappa_{\max}| = 10$, while the remaining tail ($|\kappa| > 10$) was approximated by a least-square inverse-polynomial fitting.
One-loop QED corrections beyond the electron anomalous magnetic moment approximation are conveniently expressed in terms of the correction δ, which is defined through

$$\Delta A_{\mathrm{QED}} = A_{\mathrm{nr}}\,(2\kappa_{\mathrm{e}} + \frac{\alpha}{\pi}\delta)\,. \tag{4.51}$$

Here the first term represents the EAMM contribution. In Table 4.1 we present our results for the one-electron SE correction to the amplitude of the $2p_{3/2} - 2p_{1/2}$ M1-transition. The VP term calculated within the Uehling

Table 4.1: Individual contributions to the one-electron self-energy correction expressed in terms of the various δ corrections, defined by Eq. (4.51). Numbers in parenthesis represent error in the last digit.

Z	δ^{irr}	$\delta^{\mathrm{vr}(0)}$	$\delta^{\mathrm{vr}(1+)}$	δ
16	0.0177	−0.0124	−0.0065(1)	−0.0012(1)
17	0.0195	−0.0136	−0.0075(1)	−0.0016(1)
18	0.0213	−0.0148	−0.0084(1)	−0.0019(1)
19	0.0232	−0.0160	−0.0094(1)	−0.0022(1)
20	0.0252	−0.0172	−0.0105(1)	−0.0025(1)
21	0.0272	−0.0185	−0.0116(1)	−0.0029(1)
22	0.0292	−0.0197	−0.0128(1)	−0.0033(1)

Table 4.2: The vacuum-polarization contribution in the Uehling approximation, expressed in terms of the δ correction defined by Eq. (4.51).

Z	δ^{Uehl}
16	-1.2×10^{-7}
17	-1.8×10^{-7}
18	-2.5×10^{-7}
20	-4.7×10^{-7}
22	-8.4×10^{-7}

approximation has been found to be negligible, see Table 4.2. The various contributions corresponding to the SE corrections to the transition amplitude are given. The one- and many-potential terms are represented as the sum $\delta^{\mathrm{vr}(1+)} = \delta^{\mathrm{vr}(1)} + \delta^{\mathrm{vr}(2+)}$. As one can see from Table 4.1, the occurring cancellation reduces the total value for the correction δ by an order of magnitude compared to the individual terms. Most serious computational difficulties arise from the extrapolation of the partial-wave expansion of the many-potential term. In order to estimate the error, we perform a second evaluation of $\delta^{\mathrm{vr}(1+)}$ without separating out the one-potential term. The difference between the results of both calculations is taken as the uncertainty.

5 Transition rates in He-, B-, and Be-like ions

In this Chapter high-precision QED evaluations of the decay rates in He-, B-, and Be-like multicharged ions are presented. This calculation is motivated by the increasing accuracy of the experimental results and the request for improving the theoretical accuracy of the predictions. Simultaneously, this provides good prospects for probing the relativistic-correlation and QED corrections to atomic transition amplitudes. The formal expressions for various contributions under consideration are derived in Chapter 3. The numerical results provided in this Chapter are relevant for the analysis of data obtained in recent measurements at the Heidelberg EBIT [76, 77].

5.1 Numerical solution of the Dirac equation

In order to obtain the wave functions we consider the one-particle Dirac equation (3.1) with the spherically symmetric Coulomb potential of an extended nucleus $V(\mathbf{r}) = V(r)$,

$$V(r) = -4\pi\alpha Z \left[\frac{1}{r}\int_0^r \mathrm{d}r'\, r'^2\rho(r') + \int_r^\infty \mathrm{d}r'\, r'\rho(r')\right], \tag{5.1}$$

where $\rho(r)$ is the nuclear density of the charge distribution, which is normalized on the unity. For some models of the distribution the potential has the simple analytical form:

$$V(r) = -\frac{\alpha Z}{r} \tag{5.2}$$

for a point-like nucleus,

$$V(r) = \begin{cases} -\dfrac{\alpha Z}{r}, & r \geq R_0 \\ -\dfrac{\alpha Z}{R_0}, & 0 \leq r \leq R_0 \end{cases} \tag{5.3}$$

for the spherical shell model corresponding to the distribution $\rho(r) = \delta(R_0 - r)/(4\pi R_0^2)$, and

$$V(r) = \begin{cases} -\dfrac{\alpha Z}{r}, & r \geq R_0 \\ -\dfrac{\alpha Z}{R_0}\left(\dfrac{3}{2} - \dfrac{1}{2}\dfrac{r^2}{R_0^2}\right), & 0 \leq r \leq R_0 \end{cases} \tag{5.4}$$

for the homogeneous sphere nucleus corresponding to the distribution $\rho(r) = 3\theta(R_0 - r)/(4\pi R_0^3)$. In our calculations we use the values of the mean-square radii published in Ref. [152]. The solutions of the Dirac equation with the spherically symmetric potential can be written as

$$\phi(\mathbf{r}) = \frac{1}{r}\begin{pmatrix} G_{n\kappa}(r)\Omega_{\kappa m}(\mathbf{n}) \\ iF_{n\kappa}(r)\Omega_{-\kappa m}(\mathbf{n}) \end{pmatrix}, \tag{5.5}$$

where $G_{n\kappa}(r)$ and $F_{n\kappa}(r)$ are the upper and lower radial components of the wave function, respectively. Substitution leads to the coupled radial equations

$$H_\kappa \Phi(r) = E\Phi(r)\,, \tag{5.6}$$

where

$$H_\kappa = \begin{pmatrix} V(\mathbf{r})+1 & -\dfrac{\mathrm{d}}{\mathrm{d}r}+\dfrac{\kappa}{r} \\ \dfrac{\mathrm{d}}{\mathrm{d}r}+\dfrac{\kappa}{r} & V(\mathbf{r})-1 \end{pmatrix} \tag{5.7}$$

and

$$\Phi(r) = \begin{pmatrix} G(r) \\ F(r) \end{pmatrix}. \tag{5.8}$$

In all calculations based on perturbation theory one has to represent the electron propagator, which appears as the sum over the entire Dirac spectrum. The methods used are: analytical or numerical representations for the Coulomb-Green function [153, 154, 155, 156, 157], the space discretization [22, 158, 159], and the finite-basis sets [101, 160, 161]. In this work we employ finite-basis set approach utilizing the B-splines constructed basis set. For the construction we employed the dual kinetic balance approach [101]. The latter treats large and small components on equal level respects charge conjugation symmetry. As a consequence no unphysical spurious states appear and moreover, it improves the convergence properties and accuracy considerably. We solve the Dirac equation in a cavity with the radius R. We define the grid $\{t_i\}_{i=1}^n$ in the interval $[0, R]$. The B splines of the first order $B_{i,1}(r)$ are defined as

$$B_{i,1}(r) = \begin{cases} 1 & t_i \le r < t_{i+1} \\ 0 & \text{otherwise} \end{cases}. \tag{5.9}$$

The B splines of the order k $B_{i,k}(r)$ are defined by the recurrence relations

$$B_{i,k}(r) = \frac{r-t_i}{t_{i+k-1}-t_i} B_{i,k-1}(r) + \frac{t_{i+k}-r}{t_{i+k}-t_{i+1}} B_{i+1,k-1}(r)\,. \tag{5.10}$$

It follows that $B_{i,k}(r)$ is a piecewise polynomial of the degree $(k-1)$ that is zero except within the interval $r \in [t_i, t_{i+k})$. Expanding the radial functions $\Phi(r)$ in terms of the B-splines basis yields

$$\Phi(r) = \sum_{i=1}^{2n} c_i u_i(r) \tag{5.11}$$

with corresponding two-component vectors $u_i(r)$ generated via

$$u_i(r) = \begin{pmatrix} B_i(r) \\ \dfrac{1}{2}\left(\dfrac{\mathrm{d}}{\mathrm{d}r}+\dfrac{\kappa}{r}\right) B_i(r) \end{pmatrix}, \qquad i \le n\,, \tag{5.12}$$

$$u_i(r) = \begin{pmatrix} \dfrac{1}{2}\left(\dfrac{\mathrm{d}}{\mathrm{d}r}-\dfrac{\kappa}{r}\right) B_{i-n}(r) \\ B_{i-n}(r) \end{pmatrix}, \qquad i > n\,. \tag{5.13}$$

The equations for the expansion coefficients c_i can be derived from variational principle ($\delta S = 0$)

$$\mathrm{d}S/\mathrm{d}c_i = 0, \qquad i = 1, \ldots, 2n\,, \tag{5.14}$$

Table 5.1: The decay rates of the magnetic-dipole transition $2^3S_1 - 1^1S_0$ in units s^{-1}. The negative-continuum contribution $\Delta W_{\rm neg}$ and the frequency-dependent correction $\Delta W_{\rm freq}$ are expressed in % with respect to the main term W. $W_{\rm total}$ denotes the value for the total decay rate. The values presented in the upper part of the Table were calculated in the Feynman gauge, whereas the results presented in the lower part were obtained using the Coulomb gauge.

Z	W	$\Delta W_{\rm neg}$	$\Delta W_{\rm freq}$	$W_{\rm total}$
30	8.9994×10^8	-0.043%	-0.029%	8.9929×10^8
50	1.7303×10^{11}	-0.08%	-0.042%	1.7282×10^{11}
70	5.9872×10^{12}	-0.132%	-0.045%	5.9766×10^{12}
90	9.4551×10^{13}	-0.205%	-0.036%	9.4323×10^{13}
30	9.0012×10^8	-0.05%	-0.042%	8.9929×10^8
50	1.7308×10^{11}	-0.09%	-0.062%	1.7282×10^{11}
70	5.9896×10^{12}	-0.145%	-0.073%	5.9766×10^{12}
90	9.4596×10^{13}	-0.218%	-0.07%	9.4323×10^{13}

with

$$S = \langle\Phi|H_\kappa|\Phi\rangle - E\langle\Phi|\Phi\rangle\,. \tag{5.15}$$

Employing the action principle we obtain a generalized eigenvalue problem:

$$A_{ik}c_k = \varepsilon B_{ik}c_k\,, \tag{5.16}$$

where the summation over repeated indices is implicit, $A_{ik} = (\langle u_i|H_\kappa|u_k\rangle + \langle u_k|H_\kappa|u_i\rangle)/2$ and $B_{ik} = \langle u_i|u_k\rangle$ are the matrices $2n \times 2n$.

5.2 He-like ions

In this Section we present the results for the following transitions: $2^3S_1 - 1^1S_0$, $2^3P_2 - 1^1S_0$, and $3^3S_1 - 2^3S_1$ in He-like ions, which were obtained in work [138]. For these transitions we evaluate the first-order interelectronic-interaction corrections in the framework of QED. For this purpose we use the corresponding expressions, derived in Chapter 3. The transition energies for the one-photon decays $2^3S_1 - 1^1S_0$ and $2^3P_2 - 1^1S_0$ were taken from Ref. [92], and for $3^3S_1 - 2^3S_1$ – from work [93]. In the calculations we employ the homogeneously charged sphere model for generating electron wave functions and bound-electron propagator.

In Tables 5.1, 5.2, and 5.3, we compile our numerical results for the decay rates of the magnetic transitions $2^3S_1 - 1^1S_0$, $2^3P_2 - 1^1S_0$, and $3^3S_1 - 2^3S_1$, respectively. The values presented in the upper and lower parts of these Tables have been obtained by specifying the photon propagator in the Feynman and Coulomb gauges, respectively. To analyze the obtained results we extract from the total value $W_{\rm total}$ the frequency-dependent part $\Delta W_{\rm freq}$ and the negative-continuum contribution $\Delta W_{\rm neg}$. The first term is determined as the difference between the exact value and the one, calculated under the assumption of zero the energy in the photon propagator, i.e. in the static limit $I(\varepsilon) \approx I(0)$. Within the Coulomb gauge $\Delta W_{\rm freq}$ is identified as a correction to the Breit approximation, which has not been considered for the transition amplitudes before. The second contribution $\Delta W_{\rm neg}$ originates from the summation over the negative-continuum states in the electron propagator. The transition probability, obtained without taking into account these both corrections, is denoted as W. It can be seen from Tables 5.1, 5.2, and 5.3, that the total values of the transition probabilities calculated in different gauges coincide with each other.

Table 5.2: The decay rates of the magnetic-quadrupole transition $2^3P_2 - 1^1S_0$ in units s^{-1}. The negative-continuum contribution $\Delta W_{\rm neg}$ and the frequency-dependent correction $\Delta W_{\rm freq}$ are expressed in % with respect to the main term W. $W_{\rm total}$ denotes the value for the total decay rate. The values presented in the upper part of the Table were calculated in the Feynman gauge, whereas the results presented in the lower part were obtained using the Coulomb gauge.

Z	W	$\Delta W_{\rm neg}$	$\Delta W_{\rm freq}$	$W_{\rm total}$
30	2.1047×10^{10}	-0.0001%	0.021%	2.1052×10^{10}
50	1.3654×10^{12}	-0.001%	0.038%	1.3660×10^{12}
70	2.1480×10^{13}	-0.005%	0.063%	2.1493×10^{13}
90	1.7231×10^{14}	-0.017%	0.097%	1.7245×10^{14}
30	2.1051×10^{10}	-0.0001%	0.001%	2.1052×10^{10}
50	1.3659×10^{12}	-0.001%	0.005%	1.3660×10^{12}
70	2.1491×10^{13}	-0.005%	0.014%	2.1493×10^{13}
90	1.7242×10^{14}	-0.017%	0.033%	1.7245×10^{14}

Table 5.3: The decay rates of the magnetic-dipole transition $3^3S_1 - 2^3S_1$ in units s^{-1}. The negative-continuum contribution $\Delta W_{\rm neg}$ and the frequency-dependent correction $\Delta W_{\rm freq}$ are expressed in % with respect to the main term W. $W_{\rm total}$ denotes the value for the total decay rate. The values presented in the upper part of the Table were calculated in the Feynman gauge, whereas the results presented in the lower part were obtained using the Coulomb gauge.

Z	W	$\Delta W_{\rm neg}$	$\Delta W_{\rm freq}$	$W_{\rm total}$
30	6.1245×10^{5}	3.867%	0.022%	6.3626×10^{5}
50	1.3019×10^{8}	2.204%	0.034%	1.3311×10^{8}
70	4.9886×10^{9}	1.488%	0.046%	5.0651×10^{9}
90	9.0496×10^{10}	1.055%	0.059%	9.1503×10^{10}
30	6.1273×10^{5}	3.837%	0.004%	6.3626×10^{5}
50	1.3029×10^{8}	2.158%	0.006%	1.3311×10^{8}
70	4.9936×10^{9}	1.428%	0.005%	5.0651×10^{9}
90	9.0610×10^{10}	0.984%	0.002%	9.1503×10^{10}

Table 5.4: The decay rate (s^{-1}) of the transition $2^3S_1 - 1^1S_0$ calculated in this work is compared to the previous calculations and experiment. The experimental values and their error bars are given in second and fourth columns, respectively. In the last column the sum of our results and radiative corrections obtained in work [95] are presented. In round brackets the uncertainty of present calculations are indicated. Relative differences are calculated using experimental results as a reference.

Z	Exp. [s^{-1}]	Ref.	Prec.	MBPT [92]	MCDF [90]	LPA [162]	Present	Present+Rad.
23	5.917×10^7	[163]	4.1%	-0.07%	-0.4%		0.1%	0.03(60)%
26	2.083×10^8	[163]	12.5%	-0.4%	-0.7%		-0.3%	-0.4(5)%
35	4.462×10^9	[164]	3.2%	-2.3%	-2.5%		-2.1%	-2.3(4)%
36	5.848×10^9	[165]	1.3%	-0.4%	-0.6%		-0.3%	-0.5(4)%
41	2.200×10^{10}	[75]	0.4%	0.8%	0.6%		0.9%	0.7(4)%
47	8.969×10^{10}	[96]	1.8%	1.3%	1.2%		1.4%	1.1(2)%
54	3.915×10^{11}	[166]	3.0%	-1.8%		-1.7%	-1.6%	-2.1(2)%

For the decays with $\Delta S \neq 0$ (see Tables 5.1 and 5.2) the frequency-dependent correction is of the same or even larger magnitude than the negative-continuum contribution. However, this does not hold for the $3^3S_1 - 2^3S_1$ transition, where the correction $\Delta W_{\rm freq}$ is small compared to the $\Delta W_{\rm neg}$ term. The behavior of the negative-continuum correction as a function of the nuclear charge number Z agrees well with the scaling ratio of the negative- to positive-energy contributions found in [93] for all the transitions under consideration.

In Tables 5.4 and 5.5 we compare our results with those of the previous calculations [90, 92, 93, 162]. Both methods, MCDF [90] and MBPT [92, 93], respectively, include partially the contributions of order $1/Z^2$ and higher-orders terms in the Breit approximation. In work [162] the correlation correction of first order in $1/Z$ was calculated within the rigorous QED framework employing the line profile approach (LPA). In Table 5.4 experimental data for the most precisely measured transition $2^3S_1 - 1^1S_0$ are presented. In the last column of this Table our results are combined with the radiative corrections, except those, which are already included in the transition energy. These corrections to $2s_{1/2} - 1s_{1/2}$ decay of hydrogenlike ions were obtained in Ref. [95] for $Z \geq 50$. We have extrapolated these data for $Z < 50$ and interpolated for $Z = 54$. The uncertainty due to the extrapolation, the $1/Z^2$ and higher-orders terms are indicated in round brackets. The radiative contribution at $Z = 41$ removes the discrepancy between theory and experiment, as it was suggested in Ref. [90]. In Table 5.5 the comparison with the results calculated in Refs. [93, 162] is presented for the transitions $2^3P_2 - 1^1S_0$ and $3^3S_1 - 2^3S_1$. For these decays we have estimated the uncertainty due to the radiative corrections assuming that they are of the same order of magnitude as in the case of $2s_{1/2} - 1s_{1/2}$ decay. It can be seen that for all the transitions under consideration the frequency-dependent contribution is smaller than the current experimental accuracy.

5.3 B- and Be-like ions

In this Section we present the values obtained in works [140, 141] for the lifetime of the states $(1s^2 2s^2 2p)\,^2P_{3/2}$ in B-like ions and $(1s^2 2s 2p)\,^3P_2$ in Be-like ions. Due to the smallness of the electric-quadrupole transition the lifetimes are essentially determined by the M1-transition. In case of B-like ions, the experimental values of the transition energies were taken from Ref. [167] for S^{11+}, Cl^{12+}, K^{14+}, Ti^{17+} and from Ref. [48] for Ar^{13+}. For Be-like ions, the transition energies were taken from Ref. [168] for S^{12+}, Cl^{13+}, K^{15+}, Ti^{18+} and from Ref. [48] for Ar^{14+}. The individual contributions to the M1-transition probabilities and the corresponding lifetimes for B-like and Be-like ions are presented in Tables 5.6 and 5.7, respectively. The nonrelativistic transition probability $W_{\rm nr}$

Table 5.5: The decay rates (s^{-1}) of the transitions $2^3P_2 - 1^1S_0$ and $3^3S_1 - 2^3S_1$ obtained in this work are compared with the results obtained by MBPT [93] and LPA [162]. In round brackets the uncertainty of present calculations are indicated.

	$2^3P_2 - 1^1S_0$			$3^3S_1 - 2^3S_1$	
Z	This work	MBPT [93]	LPA [162]	This work	MBPT [93]
30	$2.105(4) \times 10^{10}$	2.104×10^{10}	2.105×10^{10}	$6.363(48) \times 10^{5}$	6.35×10^{5}
50	$1.366(5) \times 10^{12}$	1.365×10^{12}	1.366×10^{12}	$1.331(8) \times 10^{8}$	1.33×10^{8}
70	$2.149(21) \times 10^{13}$	2.146×10^{13}	2.148×10^{13}	$5.065(54) \times 10^{9}$	5.06×10^{9}
90	$1.724(22) \times 10^{14}$	1.718×10^{14}	1.721×10^{14}	$9.15(12) \times 10^{10}$	9.15×10^{10}

Table 5.6: The decay rates W [s^{-1}] of the magnetic-dipole transition $(1s^22s^22p)\ ^2P_{1/2} - \ ^2P_{3/2}$ and the lifetimes τ [ms] of the $(1s^22s^22p)\ ^2P_{3/2}$ state in B-like ions. Numbers in parentheses give the estimated error.

	S^{11+}	Cl^{12+}	Ar^{13+}	K^{14+}	Ti^{17+}
Energy [cm^{-1}]	13135(1)	17408(20)	22656.22(1)	29006(25)	56243(4)
$W_{\rm nr}$	20.37538	47.43068	104.56308	219.4222	1599.635
$\Delta W_{\rm D}$	-0.03542	-0.09302	-0.23145	-0.5436	-5.355
$\Delta W_{\rm CI}$	0.00637	0.01586	0.03723	0.0802	0.597
$\Delta W_{\rm neg}$	-0.00159	-0.00396	-0.00929	-0.0206	-0.176
$\Delta W_{\rm QED}$	0.09444	0.21972	0.48419	1.0156	7.393
$\Delta W_{\rm freq}$	0.00007	0.00019	0.00049	0.0012	0.013
$W_{\rm total}$	20.439(5)	47.57(16)	104.844(3)	220.0(6)	1602.1(5)
$\tau_{\rm total}$	48.93(1)	21.02(7)	9.5380(3)	4.546(12)	0.6242(2)

Table 5.7: The decay rates W [s^{-1}] of the magnetic-dipole transition $(1s^22s2p)\ ^3P_1 - \ ^3P_2$ and the lifetimes τ [ms] of the $(1s^22s2p)\ ^3P_2$ state in Be-like ions. Numbers in parentheses give the estimated error.

	S^{12+}	Cl^{13+}	Ar^{14+}	K^{15+}	Ti^{18+}
Energy [cm^{-1}]	9712(14)	12913(16)	16819.36(1)	21571(20)	42638(4)
$W_{\rm nr}$	12.35488	29.03947	64.17056	135.36899	1045.4311
$\Delta W_{\rm D}$	-0.02017	-0.05389	-0.13242	-0.31247	-3.2611
$\Delta W_{\rm CI}$	-0.01302	-0.04909	-0.16457	-0.50484	-10.0481
$\Delta W_{\rm neg}$	-0.00053	-0.00133	-0.00313	-0.00704	-0.0649
$\Delta W_{\rm QED}$	0.05723	0.13440	0.29674	0.62535	4.8078
$W_{\rm total}$	12.38(5)	29.07(11)	64.167(2)	135.2(4)	1036.9(4)
$\tau_{\rm total}$	80.79(33)	34.40(13)	15.5843(5)	7.398(22)	0.9645(4)

is determined by Eq. (4.9), while $\Delta W_{\rm D}$ denotes the relativistic correction. The interelectronic-interaction term $\Delta W_{\rm CI}$ is calculated to all orders in $1/Z$ employing the configuration-interaction method in the basis of Dirac-Fock-Sturm orbitals (CIDFS). The negative-continuum contribution $\Delta W_{\rm neg}$ is obtained in the same basis. Some details of this calculation are presented in Appendix C. The frequency-dependent term $\Delta W_{\rm freq}$ is calculated in case of B-like ions to first order in the perturbation expansion, according to the formulas derived in Chapter 3. The Coulomb gauge for the photon propagator is used. What the QED correction $\Delta W_{\rm QED}$ is concerned, we take the values obtained in previous Chapter. It should be mentioned, that for the ions under consideration the fine splitting is of the same order of magnitude as the correlation correction. Therefore, in a systematic treatment by the perturbation theory one has to treat the fine-structure levels as being quasidegenerate.

As one can see from Tables 5.6 and 5.7 the interelectronic-interaction correction $\Delta W_{\rm CI}$ turns out to be relatively small due to the factor $(\alpha Z)^2$, as already mentioned in Chapter 4. Except for Ar^{13+} and Ar^{14+} ions, the uncertainties of the total transition probabilities are mainly determined by the experimental uncertainties of the corresponding transition energies. For argon ions, the theoretical uncertainty originates mainly from the uncalculated recoil correction.

In Table 5.8 our results for the lifetime of the $(1s^22s^22p)\,^2P_{3/2}$ state are compared with those of other calculations and with corresponding experimental data. It should be noted, that the QED correction in the EAMM approximation was taken into account only in Refs. [86, 169]. For reason of comparison, we present our results without inclusion of the radiative correction ($\tau^0_{\rm pres}$) as well. Besides, different values of the transition energies ω, indicated in Table 5.8, were used in the different calculations. Since the M1-transition probability, according to the Eq. (4.6), scales as ω^3, a small deviation in ω can change the decay rate significantly. For this reason, we recalculated the numbers presented in works [86, 88] for the $(1s^22s^22p)\,^2P_{3/2}$ state in B-like ions for the transition energies ω, which we have employed in our calculations. Table 5.9 compiles these values with (τ [86]) and without (τ^0 [88]) the QED correction together with the corresponding values ($\tau_{\rm pres}$ and $\tau^0_{\rm pres}$) obtained in this work. As one can see from this Table, there is an excellent agreement between our "non-QED" results ($\tau^0_{\rm pres}$) and those from Ref. [88] (τ^0). There is also a good agreement between our total results ($\tau_{\rm pres}$) and the values from Ref. [86] (τ), where the QED correction was calculated to the lowest order in αZ. The comparison of our theoretical results with the experimental data shows a good overall agreement as well. However, in the case of Ar^{13+} a discrepancy between our value of the lifetime $9.5380(3)$ ms of the $^2P_{3/2}$ state and the most accurate experimental value $9.573(4)(5)$ ms [76, 77] can be stated.

Table 5.10 shows a fair agreement of our results for the lifetime of the $(1s^22s2p)\,^3P_2$ state in Be-like ions with corresponding results obtained by other authors and with available experimental data. We emphasize that the QED correction has not been considered in the previous theoretical calculations cited in Table 5.10.

In conclusion, we have performed one of the most accurate existing calculation of the magnetic-dipole transition probabilities between the fine-structure levels $(1s^22s^22p)\,^2P_{1/2} - {}^2P_{3/2}$ in B-like ions and $(1s^22s2p)\,^3P_1 - {}^3P_2$ in Be-like ions. The relativistic, interelectronic-interaction, and radiative corrections to the transition probabilities have been incorporated. Except for a recent high-precision lifetime measurement on Ar^{13+} [76, 77] with a level of accuracy level of about 0.1%, most of the experimental results have still large error bars greater than 1.5% and, within these error bars, most of them are in a fair agreement with our theoretical predictions. In case of Ar^{13+}, the disagreement of our prediction with the high-precision experimental value amounts to 0.37% of the total transition probability, less than the value of the corresponding QED correction. At present we have no explanation for this discrepancy.

Table 5.8: The lifetimes of the $(1s^2 2s^2 2p)\ ^2P_{3/2}$ level in B-like ions calculated in this work with ($\tau_{\rm pres}$) and without ($\tau^0_{\rm pres}$) the QED correction are compared with previous calculations ($\tau_{\rm theor}$) and experiment ($\tau_{\rm exp}$). The values of the lifetime are given in ms. The values of the transition energy given in square brackets [Energy] are presented in units cm^{-1}. Numbers in parentheses indicate the estimated error.

Ions	$\tau^0_{\rm pres}$	$\tau_{\rm pres}$[Energy]	$\tau_{\rm theor}$[Energy]	Method & Ref.	$\tau_{\rm exp}$ & Ref.
S^{11+}	49.15	48.93(1) [13135]	47.35 [13300]	MCDF [88]	
			49.07 [13115]	MCBP [86]	
			49.33 [13144]	MCDF [89]	
			49.07 [13136]	SS [170]	
			49.26 [13122]	MRCI [171]	
			49.60	RQDO [172]	
Cl^{12+}	21.12	21.02(7) [17408]	20.55 [17565]	MCDF [88]	21.2(6)[84]
			21.02 [17400]	MCBP [86]	21.1(5)[84]
			21.19 [17421]	MCDF [89]	
			21.08 [17410]	SS [170]	
			21.19 [17386]	MRCI [171]	
			21.13	RQDO [172]	
Ar^{13+}	9.5822	9.5380(3) [22656]	9.407 [22795]	MCDF [88]	8.7(5)[80]
			9.515 [22660]	MCBP [86]	9.12(18)[79]
			9.618 [22666]	MCDF [89]	9.70(15)[82]
			9.569 [22653]	SS [170]	9.573(4)(5)[76, 77]
			9.588 [22657]	RQDO [172]	
			9.606 [22636]	MCDF [91]	
			9.615 [22619]	MRCI [171]	
			9.534 [22658]	[169]	
K^{14+}	4.567	4.546(12) [29006]	4.509 [29129]	MCDF [88]	4.47(10)[83]
			4.521 [29044]	MCBP [86]	
			4.583 [29019]	MCDF [89]	
			4.558 [29004]	SS [170]	
			4.587 [28960]	MRCI [171]	
			4.577	RQDO [172]	
Ti^{17+}	0.6271	0.6242(2) [56243]	0.6254 [56275]	MCDF [88]	0.627(10)[81]
			0.6150 [56465]	MCBP [86]	
			0.6290 [56258]	MCDF [89]	
			0.6254 [56240]	SS [170]	
			0.6289 [56166]	MRCI [171]	
			0.6270	RQDO [172]	

MCDF – multiconfiguration Dirac-Fock method
MCBP – multiconfiguration Breit-Pauli method
SS – "SUPERSTRUCTURE" program
MRCI – multireference relativistic configuration-interaction method
RQDO – relativistic quantum defect orbital method

Table 5.9: The lifetimes of the $(1s^2 2s^2 2p)\ ^2P_{3/2}$ level in B-like ions calculated in this work with ($\tau_{\rm pres}$) and without ($\tau^0_{\rm pres}$) the QED correction are compared with previous theoretical results (Refs. [86, 88]), recalculated to the transition energy (Energy in units cm^{-1}) employed in this paper. The lifetime values are given in ms.

Ions	Energy	$\tau^0_{\rm pres}$	τ^0 Ref. [88]	$\tau_{\rm pres}$	τ Ref. [86]
S^{11+}	13135	49.15	49.16	48.93	48.85
Cl^{12+}	17408	21.12	21.11	21.02	20.99
Ar^{13+}	22656	9.5822	9.581	9.5380	9.520
K^{14+}	29006	4.567	4.567	4.546	4.539
Ti^{17+}	56243	0.6271	0.6265	0.6242	0.6223

Table 5.10: The lifetimes of the $(1s^2 2s 2p)\ ^3P_2$ level in Be-like ions calculated in this work with ($\tau_{\rm pres}$) and without ($\tau^0_{\rm pres}$) the QED correction are compared with previous calculations ($\tau_{\rm theor}$) and experiment ($\tau_{\rm exp}$). The lifetime values are given in ms. The values of the transition energy [Energy] are presented in units cm^{-1}. Numbers in parentheses indicate the estimated error.

Ions	$\tau^0_{\rm pres}$	$\tau_{\rm pres}$ [Energy]	$\tau_{\rm theor}$ [Energy]	Method & Ref.	$\tau_{\rm exp}$ & Ref.
S^{12+}	81.16	80.79(33) [9712]	83.3 [9743]	SHF [173]	
			80.65 [9720]	MBPT [94]	
Cl^{13+}	34.56	34.40(13) [12913]	35.7 [12893]	SHF [173]	
			34.60 [12903]	MBPT [94]	
Ar^{14+}	15.6567	15.5843(5) [16819]	16.31 [16818]	MCHF [174]	15.0(7)[78]
			16.1 [16824]	SHF [173]	13.4(7)[79]
			15.63 [16834]	MBPT [94]	15.0(8)[82]
			15.76 [16782]	MCDF [91]	
K^{15+}	7.432	7.398(22) [21571]	7.63 [21575]	SHF [173]	7.6(5)[83]
			7.353 [21633]	MBPT [94]	
Ti^{18+}	0.9689	0.9645(4) [42638]	0.990 [42653]	SHF [173]	
			0.9615 [42651]	MBPT [94]	

SHF – scaled Hartree-Fock method
MBPT – many-body perturbation theory
MCHF – multiconfiguration Hartree-Fock method

6 Hyperfine quenching in He-like ions

6.1 Quenching effect

The effect of hyperfine quenching in He-like ions serves as one of the interesting tools for investigations in the atomic physics. The main feature of the effect can be illustrated in the following way. If the nucleus has zero spin, there are two decay modes for the 2^3P_2 level: a magnetic-quadrupole (M2) transition into the ground state 1^1S_0 and an electric- dipole (E1) transition to the 2^3S_1 state, while the 2^3P_0 level decays primarily to the 2^3S_1 state by an E1-transition. For the ions with non-zero nuclear spins the hyperfine interaction leads to a small mixing of the $2^3P_{0,2}$ states with the $2^{3,1}P_1$ states. This admixture now opens an additional E1(HFQ) decay channel to the ground state. As a result the lifetimes of the $2^3P_{0,2}$ states decrease considerably, an effect which is known as hyperfine quenching. Fig. 6.1 shows the energy levels under consideration and the corresponding decay modes for the ion $^{51}V^{21+}$.

For the 2^3P_2 and 2^3P_0 states this effect was first calculated in Refs. [163] and [175], respectively. In these calculations the interelectronic-interaction corrections of order $1/Z$ and the leading relativistic corrections of the order $(\alpha Z)^2$ to the transition amplitudes were taken into account. The hyperfine interaction was approximated by contact-interaction term. Later, the MCDF method was used for the calculation of the lifetime of the 2^3P_0 state [176]. Within the range of $Z = 2 - 100$ the lifetimes of the $2^3P_{0,2}$ states were calculated in Ref. [177], using the configuration-interaction (CI) method.

However, the measurement of the lifetime of the 2^3P_2 state in He-like $^{51}V^{21+}$, which was recently performed in Ref. [178], gave the result $\tau_{\rm exp} = 314(30)$ ps, which disagrees with the prediction $\tau_{\rm theor} = 242.0$ ps [177]. For this reason, we perform an independent calculation of the decay rates of the transitions $2^3P_0 - 1^1S_0$ and $2^3P_2 - 1^1S_0$ in He-like ions for $Z = 15 - 30$. The material presented in this Chapter was based on the work [179].

6.2 Hyperfine mixing and interelectronic-interaction corrections

Hyperfine quenching may be described well within the framework of ordinary quantum mechanical perturbation theory for quasidegenerate states. The interelectronic interaction is treated within the Breit approximation.

To take into account the additional decay mode, induced by the hyperfine interaction, we consider the mixing of the 2^3P_2 and 2^3P_0 states with the only nearby $(1s2p_{\frac{1}{2}})^*_1$ and $(1s2p_{\frac{3}{2}})^*_1$ states. Asterisks designate the two-electron states in the intermediate coupling scheme, which are linearly linked with jj-coupling states

$$\begin{pmatrix} |(1s2p_{\frac{1}{2}})^*_1\rangle \\ |(1s2p_{\frac{3}{2}})^*_1\rangle \end{pmatrix} = \begin{pmatrix} a & -b \\ b & a \end{pmatrix} \begin{pmatrix} |(1s2p_{\frac{1}{2}})_1\rangle \\ |(1s2p_{\frac{3}{2}})_1\rangle \end{pmatrix} , \tag{6.1}$$

where the positive real coefficients a and b obey the condition $a^2 + b^2 = 1$. The jj-coupling states are eigenstates of the relativistic Hamiltonian H_0, which describes two noninteracting electrons moving in the field of the nucleus,

$$H_0 = h_{\rm D}(1) + h_{\rm D}(2) , \tag{6.2}$$

Figure 6.1: Electronic energy-level diagram for the levels of $^{51}V^{21+}$ showing the decay modes.

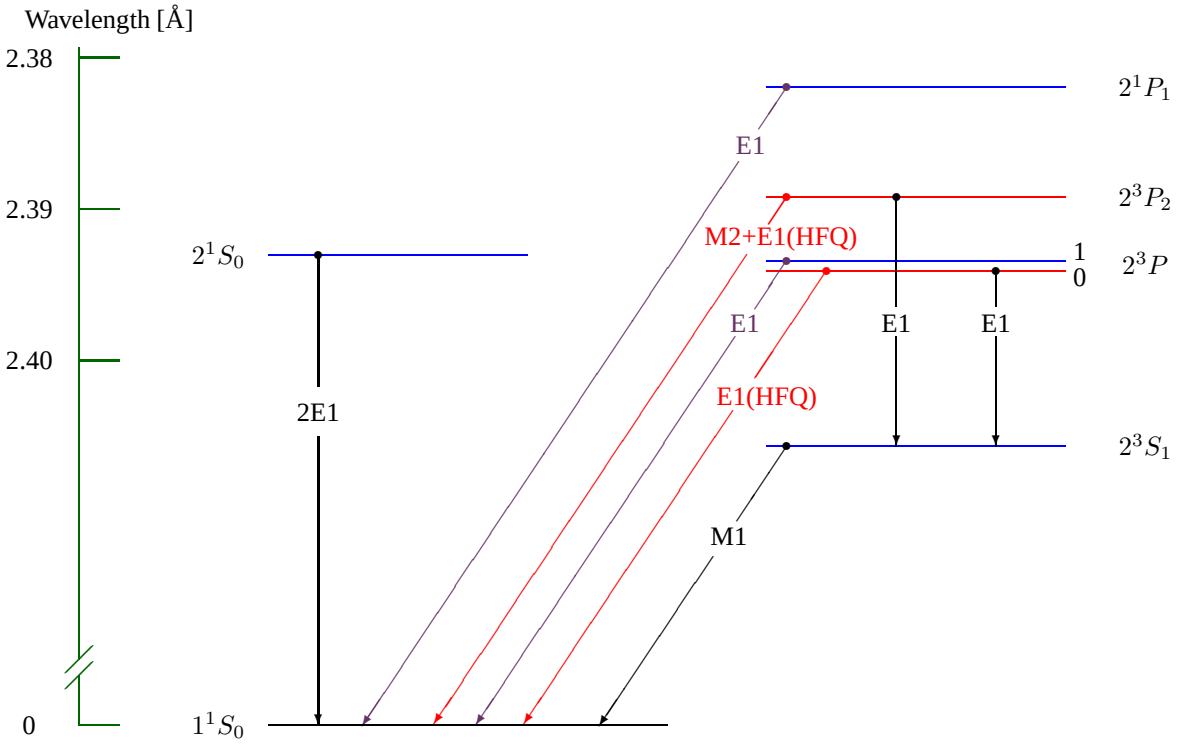

where $h_{\rm D}$ is the one-particle Dirac operator given by Eq. (3.1), and the index in the round brackets enumerates the electrons. Since we consider fully relativistic calculation, it is natural to take the jj-coupling states as the basis functions. The LS-coupling states 2^3P_2 and 2^3P_0 coincide with the jj-coupling states $(1s2p_{\frac{3}{2}})_2$ and $(1s2p_{\frac{1}{2}})_0$, respectively. The connection between LS- and jj-coupling schemes for the another states under consideration is given by

$$\begin{pmatrix} |2^3P_1\rangle \\ |2^1P_1\rangle \end{pmatrix}_{LS} = R \begin{pmatrix} |(1s2p_{\frac{1}{2}})_1\rangle \\ |(1s2p_{\frac{3}{2}})_1\rangle \end{pmatrix}_{jj} , \tag{6.3}$$

with

$$R = \frac{1}{\sqrt{3}} \begin{pmatrix} \sqrt{2} & -1 \\ 1 & \sqrt{2} \end{pmatrix} . \tag{6.4}$$

Following the method suggested in Ref. [102], we consider the Hamiltonian matrix

$$H_{\rm eff} = (H_0 + V_{\rm int})_{jj} + R^{-1}(H_{\rm NR} + B_P)_{LS}R - R^{-1}\Delta R \tag{6.5}$$

in the basis of the states $(1s2p_{\frac{1}{2}})_1$ and $(1s2p_{\frac{3}{2}})_1$. Here $H_{\rm NR}$ is the two-electron Schrödinger Hamiltonian, B_P is the Pauli form of the Breit interaction, $V_{\rm int} = V_{\rm C}+V_{\rm B}$, where $V_{\rm C}$ and $V_{\rm B}$ are the Coulomb and Breit interelectronic-interaction operators, respectively, and Δ subtracts the terms which are counted twice. The subscript LS means that the matrix elements are calculated in the LS-coupling with accurate nonrelativistic eigenfunctions of $H_{\rm NR}$, while the jj-matrix The expansions in powers of $1/Z$ were obtained for $H_{\rm NR}$ in Refs. [180, 181] through 19th order and for B_P in Ref. [182] through fifth order. For our consideration, it is sufficient to take these matrix elements up to third order. The jj-matrix elements are calculated numerically. Diagonalizing the matrix $H_{\rm eff}$, we determine the coefficients a and b in Eq. (6.1).

To obtain the coefficients of the mixing we consider the ordinary eigenvalue problem,

$$(H_{\rm eff} + H_\mu)|\xi IFM_F\rangle = E_{\xi F}|\xi IFM_F\rangle \tag{6.6}$$

in the subspace of four unperturbed atomic states $|2^3P_2 IFM_F\rangle$, $|2^3P_0 IFM_F\rangle$, $|(1s2p_{\frac{1}{2}})^*_1 IFM_F\rangle$, and $|(1s2p_{\frac{3}{2}})^*_1 IFM_F\rangle$ with a given total angular momentum F and its projection M_F. Here $H_{\rm eff}$ is a direct extension of the Hamiltonian (6.5) on the subspace of four unperturbed states under consideration. The hyperfine operator H_μ describes the interaction of the electrons with the magnetic field induced by a non-zero nuclear magnetic moment. Within the point-dipole approximation, this interaction is given by the sum of one-electron Fermi-Breit operators defined by Eq. (2.1),

$$H_\mu = \sum_i \frac{|e|}{4\pi}\frac{(\boldsymbol{\mu}_I \cdot [\mathbf{r}_i \times \boldsymbol{\alpha}_i])}{r_i^3}\,, \tag{6.7}$$

where the index i refers to the ith electron of the ion. The magnetic-dipole hyperfine interaction is diagonal in F and has non-zero matrix elements between states with $\Delta J = 0, \pm 1$. In particular, it implies that the matrix element $\langle 2^3P_2 IFM_F|H_\mu|2^3P_0 IFM_F\rangle$ vanishes. Employing the fact that the hyperfine interaction operator H_μ is a scalar product of two operators, one of which acts only on nuclear coordinates while the other one acts only on electronic coordinates, we obtain by means of Wigner-Eckart theorem [143]

$$\begin{aligned}\langle (n_1\kappa_1 n_2\kappa_2)_J IFM_F|H_\mu|(n_1'\kappa_1' n_2'\kappa_2')_{J'} IFM_F\rangle = (-1)^{J'+I+F}\left\{\begin{array}{ccc} J & I & F \\ I & J' & 1 \end{array}\right\} \\ \times\langle I \parallel \boldsymbol{\mu}_I \parallel I\rangle\langle (n_1\kappa_1 n_2\kappa_2)_J \parallel \sum_i \mathbf{t}_i \parallel (n_1'\kappa_1' n_2'\kappa_2')_{J'}\rangle\,,\end{aligned} \tag{6.8}$$

where

$$\mathbf{t}_i = \frac{|e|}{4\pi}\frac{[\mathbf{r}_i \times \boldsymbol{\alpha}_i]}{r_i^3} \tag{6.9}$$

is the one-electron operator, which acts on the coordinates of the ith electron. The nuclear reduced matrix element is given by

$$\langle I \parallel \boldsymbol{\mu}_I \parallel I\rangle = \sqrt{\frac{(2I+1)(I+1)}{I}}\mu_I\,, \tag{6.10}$$

where μ_I is the nuclear magnetic moment. The electronic reduced matrix element in Eq. (6.8) is expressed in terms of the one-electron reduced matrix elements by

$$\begin{aligned}\langle (n_1\kappa_1 n_2\kappa_2)_J \parallel \sum\nolimits_i \mathbf{t}_i \parallel (n_1'\kappa_1' n_2'\kappa_2')_{J'}\rangle = \sqrt{(2J+1)(2J'+1)}\;\Xi_{n_1\kappa_1,n_2\kappa_2}\Xi_{n_1'\kappa_1',n_2'\kappa_2'} \\ \times\left\{(-1)^{j_1+j_2+J'+1}\left\{\begin{array}{ccc} 1 & J & J' \\ j_2 & j_1' & j_1 \end{array}\right\}\langle n_1\kappa_1 \parallel \mathbf{t} \parallel n_1'\kappa_1'\rangle\delta_{n_2 n_2'}\delta_{\kappa_2\kappa_2'}\right. \\ +(-1)^{j_1+j_2'+J+1}\left\{\begin{array}{ccc} 1 & J & J' \\ j_1 & j_2' & j_2 \end{array}\right\}\langle n_2\kappa_2 \parallel \mathbf{t} \parallel n_2'\kappa_2'\rangle\delta_{n_1 n_1'}\delta_{\kappa_1\kappa_1'} \\ +(-1)^{j_1+j_2'+1}\left\{\begin{array}{ccc} 1 & J & J' \\ j_2 & j_2' & j_1 \end{array}\right\}\langle n_1\kappa_1 \parallel \mathbf{t} \parallel n_2'\kappa_2'\rangle\delta_{n_2 n_1'}\delta_{\kappa_2\kappa_1'} \\ \left.+(-1)^{J+J'}\left\{\begin{array}{ccc} 1 & J & J' \\ j_1 & j_1' & j_2 \end{array}\right\}\langle n_2\kappa_2 \parallel \mathbf{t} \parallel n_1'\kappa_1'\rangle\delta_{n_1 n_2'}\delta_{\kappa_1\kappa_2'}\right\},\end{aligned} \tag{6.11}$$

where $\Xi_{nn',\kappa\kappa'}$ is a normalization factor,

$$\Xi_{nn',\kappa\kappa'} = \left\{\begin{array}{ll} 1, & n \neq n' \;\text{ or }\; \kappa \neq \kappa' \\ 1/\sqrt{2}\,, & n = n' \;\text{ and }\; \kappa = \kappa' \end{array}\right. . \tag{6.12}$$

The one-electron reduced matrix elements appearing in formula (6.11) have been calculated numerically. Whereas the diagonal matrix elements can be found analytically by employing the virial relations for the Dirac equation [183, 184]. In the calculation of the off-diagonal reduced matrix elements the one-electron wave functions of the $2p_{1/2}$ and $2p_{3/2}$ states have to be chosen with the same overall sign in the nonrelativistic limit, since these functions are used in the transition employing the LS-coupling according to Eq. (6.3).
In the range of Z under consideration the interelectronic interaction as well as the relativistic effects contribute significantly to the transition amplitudes. Starting with the fully relativistic transition amplitude, we account for the interelectronic-interaction corrections within perturbation theory up to the order $(\alpha Z)^2/Z$. In particular, the contributions from the negative-continuum states are incorporated in this way, which yield up to about 10% of the total amplitude for the electric dipole transition evaluated within the velocity gauge. The transition amplitudes are evaluated both in the length and velocity gauges.

6.3 Numerical results

In Table 6.1 we present the results for the hyperfine-induced decay probabilities $W_\mu^{\rm l,v}$ and the lifetimes $\tau^{\rm l,v}$ of the 2^3P_0 state evaluated in both length and velocity gauges. The results for the transition rate of the line $2^3P_2 - 1^1S_0$, which is the sum of the M2-transition $W_{\rm M2}$ and the hyperfine-induced $W_\mu^{\rm l,v}$ rates, and the lifetimes $\tau^{\rm l,v}$ of the 2^3P_2 state are given in Table 6.2. The superscripts l and v correspond to the length and velocity gauge, respectively. For comparison, the values of the hyperfine-induced rates and the lifetimes obtained in works [163, 175, 177] are presented. Both Tables contain also the experimental lifetimes for those ions where the hyperfine quenching effect has definitely to be taken into account to achieve an agreement between theory and experiment. Analyzing the negative-continuum contribution in both gauges, we find that in the length gauge in contrast to the velocity gauge it is suppressed by the factor $(\alpha Z)^2$, and can be neglected. This confirms by a good agreement between our values and others theoretical results (see Tables 6.1 and 6.2), which were calculated in the length gauge without inclusion of the negative-continuum contribution [163, 175, 177]. However, in the velocity gauge the negative-continuum states should be taken into account. The small difference between the hyperfine-induced rates and therefore between the lifetimes calculated in the length and velocity gauges originates from the next order interelectronic-interaction corrections, $1/Z^2$. The decrease of the deviation for larger values of Z gives evidence for this. It becomes clear from Tables 6.1 and 6.2, that our results agree well with the previous theoretical calculations [163, 175, 177] and contradict with the experimental value for the vanadium $^{51}\mathrm{V}^{21+}$, obtained in work [178].

Table 6.1: The lifetimes of the 2^3P_0 state in He-like ions with non-zero nuclear spins in the range of $Z = 15 - 30$. The transition probabilities $W_{\rm E1}$ corresponding to the line $2^3P_0 - 2^3S_1$ are taken from Ref. [177]. In columns 5-8, the transition probabilities of the hyperfine-induced decay are presented. $W_\mu^{\rm l,v}$ and $\tau^{\rm l,v}$ are the results for the decay rates and lifetimes obtained within length and velocity gauge in the present work. For comparison, the hyperfine-induced decay rates W_μ and lifetimes τ obtained in works [175, 177] and experimental values $\tau_{\rm exp}$ are presented as well. The transition probabilities and the lifetimes are given in units $\rm ns^{-1}$ and in units ns, respectively. μ_I is the nuclear magnetic moment expressed in units of the nuclear magneton.

Ions	μ_I	I	$W_{\rm E1}$ [177]	$W_\mu^{\rm l}$	$W_\mu^{\rm v}$	W_μ [177]	W_μ [175]	$\tau^{\rm l}$	$\tau^{\rm v}$	τ [177]	$\tau_{\rm exp}$ & Ref.
$^{31}P^{13+}$	1.1316	1/2	0.1659	0.0415	0.0411	0.0409	0.041	4.821	4.830	4.836	4.88(9) [185]
$^{33}S^{14+}$	0.64382	3/2	0.1799	0.0117	0.0116	0.0116		5.218	5.221	5.223	
$^{35}Cl^{15+}$	0.82187	3/2	0.1944	0.0302	0.0299	0.0297	0.030	4.453	4.458	4.462	
$^{36}Cl^{15+}$	1.28547	2	0.1944	0.0665	0.0660	0.0655		3.833	3.841	3.848	
$^{37}Cl^{15+}$	0.68412	3/2	0.1944	0.0209	0.0207	0.0206		4.645	4.648	4.652	
$^{39}K^{17+}$	0.39149	3/2	0.2250	0.0163	0.0162	0.0160	0.016	4.144	4.146	4.149	
$^{40}K^{17+}$	−1.2981	4	0.2250	0.1337	0.1328	0.1317		2.788	2.795	2.804	
$^{41}K^{17+}$	0.21488	3/2	0.2250	0.0049	0.0049	0.0048		4.350	4.350	4.351	
$^{41}Ca^{18+}$	−1.5948	7/2	0.2412	0.3144	0.3124	0.3095		1.800	1.806	1.816	
$^{43}Ca^{18+}$	−1.3176	7/2	0.2412	0.2148	0.2133	0.2114		2.193	2.200	2.209	
$^{45}Sc^{19+}$	4.7565	7/2	0.2581	4.2498	4.2235	4.181	4.15	0.2218	0.2231	0.2253	
$^{47}Ti^{20+}$	−0.78848	5/2	0.2758	0.1868	0.1857	0.1836		2.162	2.167	2.177	
$^{49}Ti^{20+}$	−1.1042	7/2	0.2758	0.3364	0.3345	0.3307		1.633	1.639	1.649	
$^{50}V^{21+}$	3.3457	6	0.2941	4.1568	4.1344	4.084		0.2247	0.2258	0.2284	
$^{51}V^{21+}$	5.1487	7/2	0.2941	10.918	10.859	10.73	10.5	0.0892	0.0897	0.09075	
$^{53}Cr^{22+}$	−0.47454	3/2	0.3134	0.1737	0.1728	0.1705		2.053	2.057	2.066	
$^{51}Mn^{23+}$	3.5683	5/2	0.3335	12.166	12.109	11.93		0.0800	0.0804	0.08154	
$^{55}Mn^{23+}$	3.4687	5/2	0.3335	11.493	11.439	11.27	10.7	0.0846	0.0849	0.08618	
$^{57}Fe^{24+}$	0.09062	1/2	0.3545	0.0241	0.0240	0.0236		2.641	2.642	2.645	
$^{59}Co^{25+}$	4.627	7/2	0.3765	39.182	39.028	38.32	36.0	0.0253	0.0254	0.02584	
$^{61}Ni^{26+}$	−0.75002	3/2	0.3996	1.8887	1.8819	1.845		0.4370	0.4383	0.4455	0.470(50) [98]
$^{63}Cu^{27+}$	2.2273	3/2	0.4239	24.425	24.345	23.80	21.7	0.0402	0.0404	0.04128	
$^{65}Cu^{27+}$	2.3816	3/2	0.4239	27.955	27.864	27.24		0.0352	0.0354	0.03615	
$^{67}Zn^{28+}$	0.8752	5/2	0.4493	4.4983	4.4851	4.373		0.2021	0.2027	0.2074	

Table 6.2: The lifetimes of the 2^3P_2 state of He-like ions with non-zero nuclear spins in the range of $Z = 15 - 30$. The transition probabilities $W_{\rm E1}$ corresponding to the line $2^3P_2 - 2^3S_1$ are taken from Ref. [92]. $W_{\rm M2}$ is the transition rate of the magnetic-quadrupole decay $2^3P_2 - 1^1S_0$ evaluated in this work. In columns 4-6, the transition probabilities of the hyperfine-induced decay are presented. $W_\mu^{\rm l,v}$ and $\tau^{\rm l,v}$ are the results for the decay rates and lifetimes obtained within length and velocity gauge in the present work. For comparison, the hyperfine-induced decay rates W_μ and lifetimes τ obtained in Refs. [163, 177] and experimental values $\tau_{\rm exp}$, where the hyperfine quenching effect contributes on the level of the current experimental accuracy, are presented. The transition probabilities and the lifetimes are given in $\rm ns^{-1}$ and in ns, respectively. The values of the nuclear magnetic moments μ_I and the nuclear spins I are the same as in Table 6.1 for the corresponding ions.

Ions	$W_{\rm M2}$	$W_{\rm E1}$ [92]	$W_\mu^{\rm l}$	$W_\mu^{\rm v}$	W_μ [177]	$\tau^{\rm l}$	$\tau^{\rm v}$	τ [177]	τ [163]	$\tau_{\rm exp}$ & Ref.
$^{31}P^{13+}$	0.0691	0.2214	0.0038	0.0037		3.398	3.399			
$^{33}S^{14+}$	0.1183	0.2562	0.0011	0.0011		2.662	2.662		2.66	
$^{35}Cl^{15+}$	0.1958	0.2978	0.0029	0.0029		2.014	2.014		2.01	
$^{36}Cl^{15+}$	0.1958	0.2978	0.0065	0.0064		2.000	2.000			
$^{37}Cl^{15+}$	0.1958	0.2978	0.0020	0.0020		2.018	2.018			
$^{39}K^{17+}$	0.4921	0.4079	0.0016	0.0016		1.109	1.109			
$^{40}K^{17+}$	0.4921	0.4079	0.0131	0.0130		1.095	1.095			
$^{41}K^{17+}$	0.4921	0.4079	0.0005	0.0005		1.111	1.111			
$^{41}Ca^{18+}$	0.7518	0.4809	0.0305	0.0303		0.7916	0.7918			
$^{43}Ca^{18+}$	0.7518	0.4809	0.0208	0.0207		0.7977	0.7978			
$^{45}Sc^{19+}$	1.1246	0.5697	0.3990	0.3960	0.3928	0.4777	0.4784	0.4795		
$^{47}Ti^{20+}$	1.6501	0.6782	0.0173	0.0171		0.4263	0.4264			
$^{49}Ti^{20+}$	1.6501	0.6782	0.0311	0.0308		0.4238	0.4239			
$^{50}V^{21+}$	2.3792	0.8109	0.3682	0.3656	0.3622	0.2810	0.2812	0.2817		
$^{51}V^{21+}$	2.3792	0.8109	0.9608	0.9541	0.9453	0.2409	0.2413	0.2420	0.253	
$^{53}Cr^{22+}$	3.3762	0.9735	0.0148	0.0147		0.2291	0.2291			
$^{51}Mn^{23+}$	4.7215	1.173	0.9753	0.9692	0.9584	0.1456	0.1457	0.1460		
$^{55}Mn^{23+}$	4.7215	1.173	0.9217	0.9158	0.9056	0.1467	0.1468	0.1471		
$^{57}Fe^{24+}$	6.5149	1.419	0.0018	0.0018		0.1260	0.1260		0.126	
$^{59}Co^{25+}$	8.8788	1.721	2.7853	2.7693	2.733	0.0747	0.0748	0.07504		
$^{61}Ni^{26+}$	11.962	2.092	0.1271	0.1264		0.0705	0.0705			
$^{63}Cu^{27+}$	15.946	2.549	1.4843	1.4765	1.453	0.0501	0.0501	0.05014		0.047(5) [186]
$^{65}Cu^{27+}$	15.946	2.549	1.6970	1.6881	1.662	0.0495	0.0495	0.04963		
$^{67}Zn^{28+}$	21.048	3.112	0.2531	0.2519		0.0410	0.0410			

7 Summary and concluding remarks

In conclusion, the most important and new results obtained within this thesis can be stated as follows:

Spectroscopic measurements in atomic physics provides a very powerful tool for the most accurate and independent extraction of informations about the fundamental constants and nuclear parameters. In this thesis, we have determined the proton structure parameters from the theoretical and experimental values of the hyperfine structure in hydrogen and in muonium. Improved calculations of corrections to the hyperfine splitting of the ground state in hydrogen have been provided by taking into account the most recent value for the proton charge radius. An iterative procedure for the extraction of the Zemach and magnetic radii of the proton has been proposed by comparison between theoretical and experimental values of the hyperfine splitting. As a result, the Zemach and magnetic radii are found to be $1.045(16)$ fm and $0.778(29)$ fm, respectively. We have also confirmed these values by reconsidering and correcting an another theoretical analysis performed in Ref. [120] employing the rescaled difference between the hyperfine structure in hydrogen and in muonium. Besides, a relativistic model independent formula for the nuclear-size correction to the hyperfine splitting has been derived in terms of moments of the nuclear charge and magnetization distributions. Although the magnetization distribution correction has been obtained employing the homogeneous sphere model for the nuclear charge distribution, to a good accuracy, the formulas may also apply for similar models with spherical symmetry. Comparing the Zemach and magnetic radii with the results obtained from the experiments in elastic electron-proton scattering, we find some disagreement. One may expect that a further reanalysis of empirical fits of the elastic form factors by taking into account the constraints (Zemach, electric and magnetic radii of the proton) obtained from the independent atomic physics measurements, could elucidate the situation. Since the muonic hydrogen is more sensitive to the proton structure effects than hydrogen, experiments on measurements of the Lamb shift and hyperfine splitting in this system are also highly desirable and anticipated.

Best-to-date measurements of the decay rates allow to achieve an accuracy of the order of 0.1%. This has opened new possibilities for probing the influences of QED and relativistic-correlation effects on atomic transition probabilities. In this thesis, a rigorous QED approach to the transition probabilities within the framework of the two-time Green's function method has been provided. The transition rates are obtained in terms of contour integrals in the complex plane involving Green's functions, which can be systematically derived within QED perturbation theory. The formulas obtained apply for both single and degenerate or quasidegenerate electron states. The detailed derivation of renormalized expressions for the radiative and interelectronic-interaction corrections in first order of perturbation theory in α has been presented for one-, two-electron ions and for ions with one electron over closed shells. Simple analytical formulas for the so called reducible part of the interelectronic-interaction correction have been obtained. Although the formulas have been derived for the single-determinant functions, they allow for an easy generalization for the case of multi-determinant functions. The interelectronic-interaction corrections of first order in $1/Z$ to the magnetic transition probabilities $2^3S_1 - 1^1S_0$, $2^3P_2 - 1^1S_0$, and $3^3S_1 - 2^3S_1$ in heliumlike ions have been investigated in details. Rigorous QED treatment of the interelectronic interaction via the photon propagator leads to the so-called frequency-dependent contribution to the transition amplitudes, which have been evaluated for the first time. The additional contribution originating from the summation over the negative-continuum states in the electron propagator and being dependent on the choice of the one-electron basis,

can become significant for matrix elements of odd operators, which mix large and small components of the wave functions. Only the systematic QED approach to the transition rates allows for restoring the gauge invariance. For demonstrating the gauge invariance of the approach all contributions under consideration have been calculated in Feynman and Coulomb gauge.

In the nonrelativistic limit the QED corrections to the transitions between fine-structure levels can be found by including the anomalous magnetic moment of a free electron in the M1-operator, as it has been shown in this work. The calculation of QED corrections to the transition rates to all orders in αZ is already rather challenging. Due to occurring cancellations it requires excellent numerical accuracy. In this thesis, the one-loop QED correction to the magnetic-dipole transition amplitude $2p_{3/2} - 2p_{1/2}$ has been calculated to all orders in αZ for the first time. The vacuum-polarization contribution has been evaluated within the Uehling approximation, since Wichmann-Kroll contributions turn out to be negligible. For the exact evaluation of self-energy correction a scheme, which allows for a considerable improvement of the accuracy of the numerical calculations, has been developed. In this way the one-potential term is treated separately in the momentum space.

In this thesis, we have systematically evaluated the relativistic, interelectronic-interaction, and QED corrections to the M1-transitions $(1s^2 2s^2 2p)\,^2P_{3/2} - {}^2P_{1/2}$ in B-like ions and $(1s^2 2s 2p)\,^3P_2 - {}^3P_1$ in Be-like ions. As a result, one of the most accurate theoretical values for these transition probabilities have been obtained. For example, in the case of $^{40}Ar^{13+}$ ion the theoretical accuracy of the level of 0.003% has been achieved. In comparison most experimental results have error bars larger than 1.5% and, within these error bars, most of them are in fair agreement with our theoretical predictions. However, in case of the recent precise lifetime measurement in $^{40}Ar^{13+}$ ion [76, 77] with an accuracy level on the order of 0.1%, the disagreement between our prediction and the experimental value amounts to about 0.37% of the total transition probability. This is less than the value of the corresponding QED correction. At present we have no explanation for this discrepancy.

In order to clarify the present disagreement between theory and experiment in the case of the lifetime of the $(1s^2 2s^2 2p)\,^2P_{3/2}$ state in $^{40}Ar^{13+}$ ion, further investigations of the transition probabilities in more complex systems with several electrons could be very interesting. The precise experiment on the determination of the lifetime of the $(1s^2 2s^2 2p^6 3s^2 3p)\,^2P_{3/2}$ state in $^{56}Fe^{13+}$ [85] gives an additional impetus for this. In this case the correlation correction can be accurately calculated perturbatively up to first order in $1/Z$, and the higher-order terms can be obtained within configuration-interaction method. Potential difficulties associated with the large screened QED effects can be overcome by introducing an effective local potential.

For He-like ions with nonzero nuclear spin the hyperfine-quenched lifetimes of the states $2^3P_{0,2}$ have been calculated and the obtained results are in fair agreement with the previous calculations. The evaluation has been performed in length and velocity gauges for the emitted photon wave function. The necessity of accounting for the negative-continuum spectrum contribution in the velocity gauge has been demonstrated.

Appendix A: Nuclear-size correction

The nuclear-size correction to the hyperfine splitting in the nonrelativistic limit is determined by the Zemach formula (2.16). This formula can be used to calculate the nuclear-size correction for any given model of the nuclear charge and magnetization distributions. It would be desirable, however, to have a formula at hand which expresses the nuclear-size correction directly in terms of moments of the nuclear charge and magnetization distributions. In this Appendix we derive a formula which achieves this goal. In the external field approximation the corresponding relativistic formula is also derived.

The another implementation of the correction under consideration is the contribution to the difference D_{21}, where the nuclear-size correction cancels in the nonrelativistic limit. At present, one of the major sources for the theoretical uncertainty of D_{21} is due to the relativistic correction to the Zemach formula. In Refs. [33, 109] this correction has been evaluated to lowest order in αZ. A dominant nuclear contribution to D_{21} results from the $(\alpha Z)^2$ correction, which has been evaluated in Refs. [33, 109] by taking into account the relativistic correction to the Schrödinger wave function at the nucleus. In this Appendix we also rederive this correction in a more systematic way. The results reported here can be found in work [121].

The nuclear-size correction $\Delta E_{\rm nucl.size}$ to the hyperfine splitting can be decomposed into two terms $\Delta E_{\rm ext.ch.}$ and $\Delta E_{\rm ext.mag.}$ corresponding to the extended charge and magnetization distributions, respectively,

$$\Delta E_{\rm nucl.size} = \Delta E_{\rm ext.ch.} + \Delta E_{\rm ext.mag.}\,. \tag{7.1}$$

For low-Z hydrogen-like ions, the nuclear charge distribution correction to the hyperfine splitting can be evaluated by perturbation theory,

$$\Delta E_{\rm ext.ch.} = 2\sum_{N}^{\varepsilon_N\neq\varepsilon_A}\frac{\langle A|\delta V_{\rm ch}|N\rangle\langle N|H_\mu|A\rangle}{\varepsilon_A-\varepsilon_N}\,, \tag{7.2}$$

where A and N are the states of the total atomic system (electron plus nucleus), H_μ is the Fermi-Breit operator defined by Eq. (2.1), $\delta V_{\rm ch}$ denotes the difference between the potentials of an extended and a point-charge nucleus, respectively, ε_A and ε_N denote the Dirac-Coulomb energies. Taking into account that $\delta V_{\rm ch}$ is a spherically symmetric potential, we can easily integrate over the angles. As a result of this integration, we have

$$\begin{aligned}\Delta E_{\rm ext.ch.} &= \frac{|e|}{4\pi}\frac{\mu_I}{I}[F(F+1)-I(I+1)-j(j+1)]\frac{\kappa}{j(j+1)}\\ &\times\sum_{n'}^{n'\neq n}\frac{\langle\Phi_{n\kappa}|\delta V_{\rm ch}|\Phi_{n'\kappa}\rangle\langle\Phi_{n'\kappa}|\dfrac{\sigma_x}{r^2}|\Phi_{n\kappa}\rangle}{\varepsilon_{n\kappa}-\varepsilon_{n'\kappa}}\,,\end{aligned} \tag{7.3}$$

where the two-component vector $\Phi_{n\kappa}(r)$ is defined by Eq. (5.8). The sum

$$|\xi\rangle = \sum_{n'}^{n'\neq n}\frac{|\Phi_{n'\kappa}\rangle\langle\Phi_{n'\kappa}|\dfrac{\sigma_x}{r^2}|\Phi_{n\kappa}\rangle}{\varepsilon_{n\kappa}-\varepsilon_{n'\kappa}} \tag{7.4}$$

can be calculated by employing the generalized virial relations for the Dirac equation [183]. Such a calculation yields [139]

$$|\xi\rangle = \frac{1}{4(\alpha Z)^2+(1-4\kappa^2)}\Big\{2\alpha Z\frac{\sigma_x}{r}+4\alpha Z\kappa i\frac{\sigma_y}{r}+(1-4\kappa^2)\frac{\sigma_z}{r}-\frac{2(\alpha Z)^3\kappa m_{\rm e}}{N^3\gamma} -\frac{1-4\kappa^2}{\kappa}(\varepsilon_{n\kappa}i\sigma_y+m_{\rm e}\sigma_x)\Big\}|\Phi_{n\kappa}\rangle-\frac{2\alpha Z(2\varepsilon_{n\kappa}-m_{\rm e}/\kappa)}{4(\alpha Z)^2+(1-4\kappa^2)}\frac{\rm d}{{\rm d}\kappa}|\Phi_{n\kappa}\rangle\,. \tag{7.5}$$

When evaluating matrix elements involving $\delta V_{\rm ch}(r)$, which contributes only inside the nucleus, the radial function $|\xi\rangle$ as well as $|\Phi_{n\kappa}\rangle$ can be approximated by the lowest order term of the series expansion in powers of r. (In particular, it implies that the last term in Eq. (7.5) can be omitted.) Accordingly, we have to evaluate the integral

$$I=\int {\rm d}\mathbf{r}\; r^\beta\delta V_{\rm ch}\,. \tag{7.6}$$

Employing the identity

$$r^\beta=\frac{1}{(\beta+2)(\beta+3)}\Delta r^{\beta+2}\,, \tag{7.7}$$

where Δ is the Laplacian, and integrating by parts, we obtain

$$I=\int {\rm d}\mathbf{r}\;\frac{\Delta r^{\beta+2}}{(\beta+2)(\beta+3)}\delta V_{\rm ch}=\int {\rm d}\mathbf{r}\;\frac{r^{\beta+2}}{(\beta+2)(\beta+3)}\Delta(\delta V_{\rm ch})\,. \tag{7.8}$$

By means of the Poisson equation

$$\Delta(\delta V_{\rm ch}(r))=4\pi\alpha Z[\rho_{\rm E}(r)-\delta(\mathbf{r})]\,, \tag{7.9}$$

we derive

$$I=4\pi\alpha Z\frac{\langle r^{\beta+2}\rangle_{\rm E}}{(\beta+2)(\beta+3)}\,. \tag{7.10}$$

Thus the nuclear charge distribution correction (7.3) takes the form

$$\begin{aligned}\Delta E_{\rm ext.ch.} &= \frac{|e|}{4\pi}\frac{\mu_I}{I}[F(F+1)-I(I+1)-j(j+1)]\frac{\kappa}{j(j+1)}\frac{\Gamma(2\gamma+n_r+1)}{\Gamma^2(2\gamma+1)n_r!}\\ &\quad\times\Big\{2\alpha Z\sqrt{m_{\rm e}^2-\varepsilon_{n\kappa}^2}(n_r^2-(N-\kappa)^2)\\ &\quad+(1-4\kappa^2)[\varepsilon_{n\kappa}(n_r^2+(N-\kappa)^2)-2n_rm_{\rm e}(N-\kappa)]\Big\}\\ &\quad\times\left(\frac{2\alpha Z}{N}\right)^{2\gamma+1}\frac{\alpha Z m_{\rm e}^{2\gamma}}{(4(\alpha Z)^2+(1-4\kappa^2))4N(N-\kappa)}\frac{\langle r^{2\gamma-1}\rangle_{\rm E}}{\gamma(2\gamma-1)}\,,\end{aligned} \tag{7.11}$$

where $\Gamma(x)$ is the gamma function. For low-Z ions it is convenient to express this correction in terms of $\delta_{\rm E}$ defined by

$$\Delta E_{\rm ext.ch.}=-\Delta E_0\delta_{\rm E}\,, \tag{7.12}$$

where ΔE_0 denotes the nonrelativistic hyperfine splitting energy, which is the nonrelativistic limit of Eq. (2.2). Keeping the two lowest-order terms in αZ, Eq. (7.11) yields for the s states

$$\begin{aligned}\delta_{\rm E}^{(s)} &= 2\alpha Z m_{\rm e}\langle r\rangle_{\rm E}\Bigg\{1+(\alpha Z)^2\Big[2\psi(3)-\psi(n+1)-\ln\Big(\frac{2\alpha Z}{n}\Big)\\ &\quad-\frac{\langle r\ln(m_{\rm e}r)\rangle_{\rm E}}{\langle r\rangle_{\rm E}}+\frac{8n-9}{4n^2}+\frac{11}{4}\Big]\Bigg\}\,,\end{aligned} \tag{7.13}$$

Table 7.1: The nuclear charge distribution correction $\delta_{\rm E}$, in %, for the $1s$ state, calculated by means of formulas (7.11), (7.13), (7.14), and (7.16). For comparison, the results of a more accurate numerical calculation [187] are given in the seventh column. The values for $\langle r^2\rangle_{\rm E}^{1/2}$ are taken from Refs. [3, 152].

Z	$\langle r^2\rangle_{\rm E}^{1/2}$ [fm]	Eq. (7.14)	Eq. (7.13)	Eq. (7.11)	Eq. (7.16)	Ref. [187]
1	0.875	0.00320	0.00320	0.00320	0.00320	0.00320
5	2.452	0.0449	0.0456	0.0456	0.0455	0.0455
10	2.967	0.109	0.115	0.115	0.114	0.114
15	3.190	0.175	0.197	0.198	0.193	0.194
20	3.495	0.256	0.309	0.316	0.301	0.306

Table 7.2: The nuclear charge distribution correction $\delta_{\rm E}$, in %, for the $2s$ state, calculated by means of formulas (7.11), (7.13), (7.14), and (7.16). For comparison, the results of a more accurate numerical calculation [187] are given in the sixth column. The values for $\langle r^2\rangle_{\rm E}^{1/2}$ are the same as in Table 7.1.

Z	Eq. (7.14)	Eq. (7.13)	Eq. (7.11)	Eq. (7.16)	Ref. [187]
1	0.00320	0.00320	0.00320	0.00320	0.00320
5	0.0449	0.0456	0.0456	0.0455	0.0455
10	0.109	0.115	0.116	0.114	0.114
15	0.175	0.198	0.200	0.195	0.197
20	0.256	0.314	0.322	0.305	0.311

where $\psi(x) = \dfrac{\rm d}{{\rm d}x}\ln\Gamma(x)$. The nonrelativistic limit is given by

$$\delta_{\rm E}^{(s){\rm nr}} = 2\alpha Z m_{\rm e}\langle r\rangle_{\rm E}\,. \tag{7.14}$$

For the $p_{1/2}$ states, one easily finds in the nonrelativistic limit

$$\delta_{\rm E}^{(p_{1/2}){\rm nr}} = \frac{3}{2}(\alpha Z)^3 m_{\rm e}\langle r\rangle_{\rm E}\frac{n^2-1}{n^2}\,. \tag{7.15}$$

Formulas (7.14) and (7.15) coincide with the related expressions derived in Ref. [187] for the case of a homogeneously charged sphere, while the relativistic n-independent term in formula (7.13) differs from the corresponding term that can be derived from the formulas presented in work [187]. Since, for the sphere model, the approach developed in Ref. [187] provides a more accurate evaluation of the nuclear-size correction than the perturbation theory employed here, formula (7.13) can be improved by replacing the relativistic n-independent term with the corresponding term derived from Ref. [187]. As a result, we obtain

$$\begin{aligned}\delta_{\rm E}^{(s)} &= 2\alpha Z m_{\rm e}\langle r\rangle_{\rm E}\Bigg\{1+(\alpha Z)^2\Big[2\psi(3)-\psi(n+1)-\ln\Big(\frac{2\alpha Z}{n}\Big)\\ &\quad -\frac{\langle r\ln(m_{\rm e}r)\rangle_{\rm E}}{\langle r\rangle_{\rm E}}+\frac{8n-9}{4n^2}+\frac{839}{750}\Big]\Bigg\}\,,\end{aligned} \tag{7.16}$$

which differs from Eq. (7.13) only by the last constant term.

In Tables 7.1, 7.2, and 7.3 we present numerical values for $\delta_{\rm E}$ as calculated according to Eqs. (7.11) – (7.16) and compare them with the results of a more accurate numerical evaluation [187]. All the calculations are performed for the homogeneously charged sphere model of the nuclear charge distribution.

Table 7.3: The nuclear charge distribution correction $\delta_{\rm E}$, in %, for the $2p_{1/2}$ state, calculated by means of formulas (7.11) and (7.15). For comparison, the results of a more accurate numerical calculation [187] are given in the fourth column. The values for $\langle r^2\rangle_{\rm E}^{1/2}$ are the same as in Table 7.1. The symbol $[-n]$ means $\times 10^{-n}$.

Z	Eq. (7.15)	Eq. (7.11)	Ref. [187]
1	0.959[-7]	0.959[-7]	0.959[-7]
5	0.336[-4]	0.342[-4]	0.342[-4]
10	0.325[-3]	0.347[-3]	0.344[-3]
15	0.118[-2]	0.136[-2]	0.133[-2]
20	0.306[-2]	0.390[-2]	0.377[-2]

For low-Z ions the nuclear magnetization distribution correction can be written as

$$\Delta E_{\rm ext.mag.} = -\Delta E \int {\rm d}\mathbf{r}\; K(r)\rho_{\rm M}(r)\,, \tag{7.17}$$

where ΔE is given by Eq. (2.2), $\rho_{\rm M}(r)$ is the nuclear magnetization distribution density, and $K(r)$ is defined by

$$K(r) = \frac{\displaystyle\int_0^r {\rm d}r'\;\frac{1}{r'^2}\,F_{n\kappa}(r')G_{n\kappa}(r')}{\displaystyle\int_0^\infty {\rm d}r'\;\frac{1}{r'^2}\,F_{n\kappa}(r')G_{n\kappa}(r')}\,. \tag{7.18}$$

In order to derive an analytical expression for this correction, we will employ the sphere model for the nuclear charge distribution, with a radius $R_0 = \sqrt{5/3}\langle r^2\rangle_{\rm E}^{1/2}$, keeping the lowest-order term in $m_{\rm e}R_0$ and the two lowest-order terms in αZ. For s states, the function $K(r)$ is given by [187]

$$\begin{aligned} K^{(s)}(r) &= \alpha Z m_{\rm e}R_0\left(\frac{r^2}{R_0^2}-\frac{r^4}{10R_0^4}\right) + (\alpha Z)^3 m_{\rm e}R_0\left\{\left[2\Psi(3)-\Psi(n+1)\right.\right. \\ &\quad \left.-\ln\left(\frac{2\alpha Z m_{\rm e}R_0}{n}\right)-\frac{112n^2-30n+25}{60n^2}\right]\left(\frac{r^2}{R_0^2}-\frac{r^4}{10R_0^4}\right) \\ &\quad \left.-\frac{1}{5}\left(\frac{3r^4}{2R_0^4}-\frac{19r^6}{42R_0^6}+\frac{19r^8}{360R_0^8}-\frac{2}{825}\frac{r^{10}}{R_0^{10}}\right)\right\}. \end{aligned} \tag{7.19}$$

Although Eq. (7.19) holds strictly only for $r \le R_0$, it yields a reasonably good approximation for $K^{(s)}(r)$ in the region $R_0 < r < 2R_0$ as well. Introducing $\delta_{\rm M}$ via

$$\Delta E_{\rm ext.mag.} = -\Delta E_0 \delta_{\rm M}\,, \tag{7.20}$$

one easily finds

$$\delta_{\rm M} = \frac{\Delta E}{\Delta E_0}\int {\rm d}\mathbf{r}\; K(r)\rho_{\rm M}(r)\,. \tag{7.21}$$

Table 7.4: The nuclear magnetization distribution correction $\delta_{\rm M}$, in %, for the $1s$ and $2s$ states, as calculated via formulas (7.22) and (7.23). The sphere model is employed for the nuclear charge and magnetization distributions. For comparison, the results of a more accurate numerical calculation [187] are given in the fifth and eighth columns. The values for $\langle r^2\rangle_{\rm E}^{1/2}$ are taken from Refs. [3, 152].

Z	$\langle r^2\rangle_{\rm E/M}^{1/2}$ [fm]	$1s$, Eq. (7.23)	$1s$, Eq. (7.22)	$1s$, Ref. [187]	$2s$, Eq. (7.23)	$2s$, Eq. (7.22)	$2s$, Ref. [187]
1	0.875	0.00119	0.00119	0.00119	0.00119	0.00119	0.00119
5	2.452	0.0167	0.0169	0.0169	0.0167	0.0169	0.0169
10	2.967	0.0403	0.0419	0.0420	0.0403	0.0421	0.0422
15	3.190	0.0650	0.0705	0.0709	0.0650	0.0712	0.0716
20	3.495	0.0950	0.108	0.110	0.0950	0.110	0.112

Substituting (7.19) into (7.21) yields to first order in $m_{\rm e}R_0$ and to two lowest orders in αZ

$$\begin{aligned}\delta_{\rm M}^{(s)} &= \alpha Z m_{\rm e}R_0\left(\frac{\langle r^2\rangle_{\rm M}}{R_0^2}-\frac{\langle r^4\rangle_{\rm M}}{10R_0^4}\right)+(\alpha Z)^3 m_{\rm e}R_0\Bigg\{\Bigg[2\Psi(3)-\Psi(n+1)\\ &\quad -\ln\left(\frac{2\alpha Z m_{\rm e}R_0}{n}\right)+\frac{8n-9}{4n^2}-\frac{1}{30}\Bigg]\left(\frac{\langle r^2\rangle_{\rm M}}{R_0^2}-\frac{\langle r^4\rangle_{\rm M}}{10R_0^4}\right)\\ &\quad -\frac{1}{5}\left(\frac{3\langle r^4\rangle_{\rm M}}{2R_0^4}-\frac{19\langle r^6\rangle_{\rm M}}{42R_0^6}+\frac{19\langle r^8\rangle_{\rm M}}{360R_0^8}-\frac{2}{825}\frac{\langle r^{10}\rangle_{\rm M}}{R_0^{10}}\right)\Bigg\}. \end{aligned} \tag{7.22}$$

The leading terms in the nonrelativistic approximation are given by

$$\delta_{\rm M}^{(s)\rm nr}=\alpha Z m_{\rm e}R_0\left(\frac{\langle r^2\rangle_{\rm M}}{R_0^2}-\frac{1}{10}\frac{\langle r^4\rangle_{\rm M}}{R_0^4}\right). \tag{7.23}$$

Table 7.4 compiles numerical results for $\delta_{\rm M}$ in comparison with the more accurate numerical results obtained in Ref. [187]. As one can see from the Table, formula (7.22) properly accounts for the relativistic effects.

Formulas (7.22) and (7.23) are derived for the homogeneously charged sphere model of the nuclear charge distribution. However, they also yield sufficiently accurate results for other models of the nuclear charge distribution (with $R_0=\sqrt{5/3}\langle r^2\rangle_{\rm E}^{1/2}$), which are close enough to the homogeneously charged sphere model.

According to the formulas derived above, the total finite nuclear-size correction to the hyperfine splitting of an ns state in a low-Z hydrogen-like ion is given by

$$\Delta E_{\rm nucl.size}=-\Delta E_0(\delta_{\rm E}+\delta_{\rm M}), \tag{7.24}$$

where

$$\begin{aligned}\delta_{\rm E}^{(s)}+\delta_{\rm M}^{(s)} &= (\delta_{\rm E}^{(s)\rm nr}+\delta_{\rm M}^{(s)\rm nr})\left\{1+(\alpha Z)^2\left[2\Psi(3)-\Psi(n+1)-\ln\left(\frac{2\alpha Z}{n}\right)+\frac{8n-9}{4n^2}\right]\right\}\\ &\quad -\delta_{\rm M}^{(s)\rm nr}(\alpha Z)^2\left(\ln(m_{\rm e}R_0)+\frac{1}{30}\right)-\delta_{\rm E}^{(s)\rm nr}(\alpha Z)^2\left(\frac{\langle r\ln(m_{\rm e}r)\rangle_{\rm E}}{\langle r\rangle_{\rm E}}-\frac{839}{750}\right)\\ &\quad -\frac{(\alpha Z)^3 m_{\rm e}R_0}{5}\left(\frac{3\langle r^4\rangle_{\rm M}}{2R_0^4}-\frac{19\langle r^6\rangle_{\rm M}}{42R_0^6}+\frac{19\langle r^8\rangle_{\rm M}}{360R_0^8}-\frac{2}{825}\frac{\langle r^{10}\rangle_{\rm M}}{R_0^{10}}\right). \end{aligned} \tag{7.25}$$

The corresponding nonrelativistic approximation is given by

$$\delta_{\rm E}^{(s)\rm nr}+\delta_{\rm M}^{(s)\rm nr}=2\alpha Z m_{\rm e}\langle r\rangle_{\rm E}+\alpha Z m_{\rm e}R_0\left(\frac{\langle r^2\rangle_{\rm M}}{R_0^2}-\frac{1}{10}\frac{\langle r^4\rangle_{\rm M}}{R_0^4}\right). \tag{7.26}$$

Table 7.5: The total nuclear-size correction $\delta_{\rm E} + \delta_{\rm M}$, expressed in %, for the s states, calculated by means of formula (30). The sphere model is used for the nuclear charge distribution together with four different models for the nuclear magnetization distribution as described in the text. For comparison, the corresponding results derived from the Zemach formula (2.16) obtained in Ref. [116] are presented as well. The values for $\langle r^2\rangle_{\rm E}^{1/2}$ are taken from Refs. [3, 152]. The values for $\langle r^2\rangle_{\rm M}^{1/2}$ are assumed to be equal to the corresponding values for $\langle r^2\rangle_{\rm E}^{1/2}$.

Z	$\langle r^2\rangle_{\rm e/m}^{1/2}$ [fm]	S	S [116]	SS	SS [116]	E	E [116]	G	G [116]
1	0.875	0.00439	0.00439	0.00441	0.00441	0.00429	0.00431	0.00436	0.00436
2	1.844	0.0185	0.0185	0.0186	0.0186	0.0181	0.0182	0.0184	0.0184
3	2.39	0.0360	0.0360	0.0361	0.0361	0.0352	0.0353	0.0357	0.0357
5	2.452	0.0615	0.0615	0.0617	0.0617	0.0601	0.0604	0.0610	0.0610
10	2.967	0.149	0.149	0.149	0.149	0.145	0.146	0.148	0.148

To compare this nonrelativistic formula with the Zemach expression, let us consider the following models for the nuclear magnetization distribution:
1) the sphere model (S model)

$$\rho_{\rm M}(r) = \frac{\theta(R_0 - r)}{\frac{4}{3}\pi R_0^3}\,, \tag{7.27}$$

2) the spherical shell model (SS model)

$$\rho_{\rm M}(r) = \frac{\delta(R_0 - r)}{4\pi R_0^2}\,, \tag{7.28}$$

3) an exponential distribution (E model)

$$\rho_{\rm M}(r) = \frac{\Lambda^3}{8\pi} e^{-\Lambda r}\,, \tag{7.29}$$

4) a Gaussian distribution (G model)

$$\rho_{\rm M}(r) = \frac{\Lambda^{\frac{3}{2}}}{2\pi\Gamma(\frac{3}{2})} e^{-\Lambda r^2}\,. \tag{7.30}$$

In Table 7.5 we present the nonrelativistic values for the total nuclear-size correction employing the sphere model of the nuclear charge distribution together with various models of the nuclear magnetization distributions as calculated by means of Eq. (7.26). For comparison, the results obtained by the Zemach formula are also presented in the table. As one can see from the table, the results derived by formula (7.26) are in very good agreement with the Zemach values. It can be shown that a slight difference between the Zemach results and our nonrelativistic results, as it appears, e.g., for the E model, is determined by the integral

$$\Delta\delta_{\rm M}^{(s){\rm nr}} = 8\pi\frac{\alpha Z}{R_0^3}\int_{R_0}^{\infty} {\rm d}r\,\rho_{\rm M}(r) r\Big(\frac{1}{5}R_0^5 - \frac{3}{4}rR_0^4 + r^2R_0^3 - \frac{1}{2}r^3R_0^2 + \frac{1}{20}r^5\Big)\,. \tag{7.31}$$

Performing similar calculations employing other models for the nuclear charge distribution (with $R_0 = \sqrt{5/3}\langle r^2\rangle_{\rm E}^{1/2}$) and comparing the corresponding results with the Zemach ones, again a good agreement is obtained for models of the nuclear charge distribution that are close to the sphere model. In particular, it follows that for all these models the relativistic correction to the Zemach formula can be determined by Eq. (7.25) with a good accuracy.
To compare the n-dependent terms in formula (7.25) with those in Refs. [33, 109], we consider the difference

$$D_{n1}^{\rm nucl.size} = n^3\Delta E_{\rm nucl.size}^{(ns)} - \Delta E_{\rm nucl.size}^{(1s)}\,. \tag{7.32}$$

From Eq. (7.25), we derive

$$D_{n1}^{\rm nucl.size} \;=\; (\alpha Z)^2\Big(\Psi(n+1)-\Psi(2)-\ln n-\frac{(n-1)(n+9)}{4n^2}\Big)\Delta E_0^{(1s)}(\delta_{\rm E}^{(s)\rm nr}+\delta_{\rm M}^{(s)\rm nr})\,. \quad (7.33)$$

Here $\Delta E_0^{(1s)}$ is the ground-state hyperfine splitting obtained from the nonrelativistic theory. This expression exactly coincides with the corresponding formula derived in Refs. [33, 109].

Appendix B: Zero-potential vertex term

This Appendix provides some details of the derivation of the explicit formulas for the zero-potential vertex contribution in the momentum representation as employed in the numerical evaluation. Integrating by parts and performing the integration over $\mathbf{p}'$ in Eq. (4.48) yields

$$\begin{aligned}\Delta A^{\mathrm{ver}(0)} &= -\sqrt{\frac{\omega^3}{6\pi}}\, ie \left\{ \int \frac{\mathrm{d}\mathbf{p}}{(2\pi)^3}\, \overline{\phi}_b(\mathbf{p})\, \Xi(\varepsilon_b, \varepsilon_a, \mathbf{p})\, \phi_a(\mathbf{p}) \right. \\ &\quad \left. - \int \frac{\mathrm{d}\mathbf{p}}{(2\pi)^3}\, \overline{\phi}_b(\mathbf{p})\, [\mathbf{\Gamma}_{\mathrm{R}}(\varepsilon_b, \mathbf{p}; \varepsilon_a, \mathbf{p}) \times \boldsymbol{\nabla}_{\mathbf{p}}]_z\, \phi_a(\mathbf{p}) \right\}, \end{aligned} \tag{7.34}$$

where

$$\Xi(\varepsilon_b, \varepsilon_a, \mathbf{p}) = [\boldsymbol{\nabla}_{\mathbf{p}'} \times \mathbf{\Gamma}_{\mathrm{R}}(\varepsilon_b, \mathbf{p}; \varepsilon_a, \mathbf{p}')]_z \,|_{\mathbf{p}'=\mathbf{p}}\,. \tag{7.35}$$

The right side of Eq. (7.34) is naturally divided into two parts $\Delta A^{\mathrm{ver}(0),1}$ and $\Delta A^{\mathrm{ver}(0),2}$. Starting with the first one, we present the function $\Xi(\varepsilon_b, \varepsilon_a, \mathbf{p})$ in the form

$$\begin{aligned}\Xi(\varepsilon_b, \varepsilon_a, \mathbf{p}) &= 4\pi i\, \alpha \int \frac{\mathrm{d}^4 k}{(2\pi)^4} \frac{1}{k^2} \gamma_\sigma \frac{\not{p} - \not{k} + m}{(p-k)^2 - m^2} \\ &\quad \times [\boldsymbol{\gamma} \times \boldsymbol{\nabla}_{\mathbf{p}}]_z \frac{\not{p}' - \not{k} + m}{(p'-k)^2 - m^2} \gamma^\sigma \end{aligned} \tag{7.36}$$

with $p = (\varepsilon_b, \mathbf{p})$ and $p' = (\varepsilon_a, \mathbf{p})$. Using the anticommutation relations for the γ matrices yields

$$\begin{aligned}\Xi(\varepsilon_b, \varepsilon_a, \mathbf{p}) = \frac{\alpha}{4i\pi^3} \int \frac{\mathrm{d}^4 k}{k^2} \frac{1}{[(p-k)^2 - m^2]\,[(p'-k)^2 - m^2]} \Bigg\{ \gamma_\sigma (\not{p} - \not{k} + m) \\ \times [\boldsymbol{\gamma} \times \boldsymbol{\gamma}]_z \gamma^\sigma + 2\, \gamma_\sigma \frac{(\not{p} - \not{k} + m)(\not{p}' - \not{k} - m)}{(p'-k)^2 - m^2} [\boldsymbol{\gamma} \times (\mathbf{p} - \mathbf{k})]_z \gamma^\sigma \Bigg\}. \end{aligned} \tag{7.37}$$

Expressing the integration over the loop momenta k in terms of the integrals over the Feynman parameters, one can derive the formula

$$\begin{aligned}\Xi(\varepsilon_b, \varepsilon_a, \mathbf{p}) = \frac{\alpha}{\pi} \Bigg\{ i\gamma_0\gamma_5\gamma_z (C_0 + C_{11} + C_{12})\ \not{p} - \Big[\not{p}'(A_0 - A_1)\ \not{p} - (A_0 + 3A_1) \\ + 2p^2 (A_{11} - A_{21}) + 2p'^2 (A_{12} - A_{22}) - 4pp' A_{23} \Big] [\boldsymbol{\gamma} \times \mathbf{p}]_z \Bigg\}, \end{aligned} \tag{7.38}$$

which coincides with the corresponding equation in calculations of the g factor [27], if one considers $\varepsilon_a = \varepsilon_b$. Here the Feynman integrals are determined by Eqs. (4.42), (4.43), and

$$A_0 = \int_0^1 \mathrm{d}x \mathrm{d}y\, \frac{(1-x)(1-y)}{Z^2}\,, \tag{7.39}$$

$$A_1 = \int_0^1 \mathrm{d}x\mathrm{d}y\, \frac{x(1-x)(1-y)}{Z^2}\,, \tag{7.40}$$

$$\begin{pmatrix} A_{11} \\ A_{12} \end{pmatrix} = \int_0^1 \mathrm{d}x\mathrm{d}y\, \frac{x(1-x)(1-y)}{Z^2} \begin{pmatrix} y \\ 1-y \end{pmatrix}\,, \tag{7.41}$$

$$\begin{pmatrix} A_{21} \\ A_{22} \\ A_{23} \end{pmatrix} = \int_0^1 \mathrm{d}x\mathrm{d}y\, \frac{x^2(1-x)(1-y)}{Z^2} \begin{pmatrix} y^2 \\ (1-y)^2 \\ y(1-y) \end{pmatrix}\,, \tag{7.42}$$

$Z = x[yp + (1-y)p']^2 + 1 - yp^2 - (1-y)p'^2$.

To carry out the angular integration for the transition $2p_{3/2} - 2p_{1/2}$ under consideration we employ the following formulas ($m = 1/2$)

$$\int \mathrm{d}\Omega_{\mathbf{p}} \chi^\dagger_{\kappa_1 m}(\hat{\mathbf{p}}) \sigma_z \chi_{\kappa_2 m}(\hat{\mathbf{p}}) = \begin{cases} -\dfrac{2\sqrt{2}}{3} & \text{for} \quad \kappa_1 = 1, \quad \kappa_2 = -2 \\ 0 & \text{for} \quad \kappa_1 = -1, \quad \kappa_2 = 2 \end{cases}\,, \tag{7.43}$$

$$\int \mathrm{d}\Omega_{\mathbf{p}} \chi^\dagger_{\kappa_1 m}(\hat{\mathbf{p}}) [\boldsymbol{\sigma} \times \hat{\mathbf{p}}]_z \chi_{\kappa_2 m}(\hat{\mathbf{p}}) = \begin{cases} -\dfrac{\sqrt{2}i}{3} & \text{for} \quad \kappa_1 = -1, \quad \kappa_2 = -2 \\ \dfrac{\sqrt{2}i}{3} & \text{for} \quad \kappa_1 = 1, \quad \kappa_2 = 2 \end{cases}\,, \tag{7.44}$$

where $\mathbf{p} = \mathbf{p}/|\mathbf{p}|$ and $\boldsymbol{\sigma}$ denotes the vector of Pauli matrices. Finally, for the first part $\Delta A^{\mathrm{ver}(0),1}$ we obtain

$$\begin{aligned} \Delta A^{\mathrm{ver}(0),1} \;=\; & -\sqrt{\frac{\omega^3}{3\pi}} \frac{\alpha e}{24\pi^4} \int_0^\infty \mathrm{d}p_r\, p_r^2 \Big\{ -2(C_0 + C_{11} + C_{12})(\varepsilon_b g_b g_a + p_r g_b f_a) \\ & + p_r \Big[(\varepsilon_a \varepsilon_b - p_r^2)(A_0 - A_1 - 4A_{23}) - (A_0 + 3A_1) + 2(\varepsilon_b^2 - p_r^2) \\ & \times (A_{11} - A_{21}) + 2(\varepsilon_a^2 - p_r^2)(A_{12} - A_{22}) \Big] (g_b f_a - f_b g_a) \\ & - p_r^2 (\varepsilon_a - \varepsilon_b)(A_0 - A_1)(g_b g_a - f_b f_a) \Big\}\,, \end{aligned} \tag{7.45}$$

where $p_r = |\mathbf{p}|$, $g_a(p_r)$ and $f_a(p_r)$ are the upper and lower radial components of the wave function in the momentum representation, respectively.

The second term $\Delta A^{\mathrm{ver}(0),2}$ can be calculated similarly. Using the expression for the free-electron vertex function and employing in addition to Eq. (7.44) the following formulas

$$\int \mathrm{d}\Omega_{\mathbf{p}} \chi^\dagger_{\kappa_1 m}(\hat{\mathbf{p}}) [\hat{\mathbf{p}} \times \boldsymbol{\nabla}_{\Omega_{\mathbf{p}}}]_z \chi_{\kappa_2 m}(\hat{\mathbf{p}}) = \begin{cases} \dfrac{\sqrt{2}i}{3} & \text{for} \quad \kappa_1 = 1, \quad \kappa_2 = -2 \\ 0 & \text{for} \quad \kappa_1 = -1, \quad \kappa_2 = 2 \end{cases}\,, \tag{7.46}$$

$$\int \mathrm{d}\Omega_{\mathbf{p}} \chi^\dagger_{\kappa_1 m}(\hat{\mathbf{p}}) [\boldsymbol{\sigma} \times \boldsymbol{\nabla}_{\Omega_{\mathbf{p}}}]_z \chi_{\kappa_2 m}(\hat{\mathbf{p}}) = \begin{cases} -\dfrac{2\sqrt{2}i}{3} & \text{for} \quad \kappa_1 = -1, \quad \kappa_2 = -2 \\ \sqrt{2}\, i & \text{for} \quad \kappa_1 = 1, \quad \kappa_2 = 2 \end{cases}\,, \tag{7.47}$$

where $\boldsymbol{\nabla}_{\Omega_{\mathbf{p}}}$ is the angular part of the gradient, we have

$$\begin{aligned} \Delta A^{\mathrm{ver}(0),2} \;=\; & -\sqrt{\frac{\omega^3}{3\pi}} \frac{\alpha e}{96\pi^4} \int_0^\infty \mathrm{d}p_r\, p_r^2 \Big\{ (A - \varepsilon_a \varepsilon_b D + p_r^2 D)(g_b f_a' - f_b g_a' \\ & + \frac{3}{p_r} g_b f_a - \frac{2}{p_r} f_b g_a) - p_r D(\varepsilon_a - \varepsilon_b)(f_b f_a' - g_b g_a' + \frac{3}{p_r} f_b f_a - \frac{2}{p_r} g_b g_a) \\ & + (\varepsilon_b B + 2\varepsilon_b D + \varepsilon_a C + 4D) g_b g_a + p_r (B + 2D + C) f_b g_a \Big\}\,, \end{aligned} \tag{7.48}$$

where $g'_a(p_r) = \mathrm{d}g_a(p_r)/\mathrm{d}p_r$, $f'_a(p_r) = \mathrm{d}f_a(p_r)/\mathrm{d}p_r$. Here the coefficients A, $B = B_1 + B_2$, $C = C_1 + C_2$, and D are defined by Eqs. (4.34)-(4.39).

The total result for the zero-potential vertex contribution is the sum of the corresponding terms from Eqs. (7.45) and (7.48).

Appendix C: Configuration-interaction Dirac-Fock-Sturm method

The method of the configuration-interaction in the basis of Dirac-Fock-Sturm orbitals has been developed by I. I. Tupitsyn and partially presented in Refs. [61, 140, 188]. To evaluate the interelectronic-interaction contributions, one usually starts with the relativistic Hamiltonian within the no-pair approximation [189, 190]

$$H_{\rm np} = \Lambda_+ H \Lambda_+ \,, \qquad H = \sum_i h_{\rm D}(i) + \sum_{i<j} V(i,j) \,, \tag{7.49}$$

where $h_{\rm D}(i)$ is the one-particle Dirac Hamiltonian, the index $i = 1, \ldots, N$ labels the electrons, and $V(i,j) = V_{\rm C}(i,j) + V_{\rm B}(i,j)$ denotes the two-electron Coulomb-Breit interaction operator. Λ_+ is the projector on the positive-energy states, which can be represented as the product of the one-electron projectors $\lambda_+(i)$ as

$$\Lambda_+ \,=\, \lambda_+(1) \cdots \lambda_+(N), \tag{7.50}$$

and

$$\lambda_+(i) \,=\, \sum_n \mid u_n(i)\rangle \, \langle u_n(i) \mid . \tag{7.51}$$

Here u_n are the positive-energy eigenstates of an effective one-particle Hamiltonian h_u, which can be taken to be the Dirac Hamiltonian $h_{\rm D}$, the Dirac Hamiltonian in an external field or the Dirac-Fock Hamiltonian in an external field [61, 62, 189, 190].

In order to determine the space of one-electron orbitals $\{\varphi_n\}_{n=1}^{M}$, we employed the combined Dirac-Fock (DF) and Dirac-Fock-Sturm (DFS) basis set. Here the index n enumerates different occupied and vacant one-electron states. For occupied atomic shells, the orbitals φ_n with $n = 1, \ldots, M_0$ were obtained by means of the standard restricted Dirac-Fock method (RDF), based on a numerical solution of the radial RDF equations [188]

$$\left\{ \begin{array}{rcl} \left(-\dfrac{\mathrm{d}}{\mathrm{d}r} + \dfrac{\kappa}{r}\right) F_n(r) \,-\, \alpha\, \dfrac{Z - Y_n(r)}{r}\, G_n(r) & = & E_n\, G_n(r) \,-\, \dfrac{\alpha}{r}\, X_n^F(r) \\ \left(\dfrac{\mathrm{d}}{\mathrm{d}r} + \dfrac{\kappa}{r}\right) G_n(r) \,-\, \alpha\, \dfrac{Z - Y_n(r)}{r}\, F_n(r) \,-\, 2\, F_n(r) & = & E_n\, F_n(r) \,-\, \dfrac{\alpha}{r}\, X_n^G(r) \end{array} \right. , \tag{7.52}$$

where $G_n(r)$ and $F_n(r)$ are the radial components of the wave function φ_n determined according to Eq. (5.5). $Y_n(r)/r$ denotes the screened Coulomb potential, while $X_n^G(r)$ and $X_n^F(r)$ incorporate the exchange terms corresponding to the G_n and F_n components, respectively, and contribution from the nondiagonal Lagrangian coefficients.

The vacant orbitals were obtained by solving the Dirac-Fock-Sturm equations

$$[h_{\rm DF} \,-\, E_{n_0}]\, \varphi_n \,=\, \xi_n\, W(r)\, \varphi_n, \qquad n = M_0 + 1, \ldots, M, \tag{7.53}$$

which can be considered as a generalization of the method proposed in Ref. [191] to the relativistic Hamiltonian and to an arbitrary constant-sign weight function $W(r)$. For each relativistic quantum number κ we choose an

occupied DF function φ_{n_0}, which we call as reference DF orbital together with E_{n_0} in Eq. (7.53) being the energy of this orbital. The parameter ξ_n in Eq. (7.53) can be considered as an eigenvalue of the Sturmian operator. It should be noted that the DFS orbitals are orthogonal with respect to the weight function $W(r)$,

$$\int \mathrm{d}\mathbf{r}\, W(r)\, \varphi_n(\mathbf{r})\, \varphi_{n'}(\mathbf{r}) = \delta_{nn'}\,, \tag{7.54}$$

and, therefore, form a linear independent basis set. In calculations we employed the following weight function

$$W(r) \;=\; \frac{1 \,-\, \exp[-(\alpha\, r)^2]}{(\alpha\, r)^2}\,. \tag{7.55}$$

To generate the one-electron wave functions u_n, we used the unrestricted DF method in the joined DF and DFS basis,

$$u_n \;=\; \sum_m C_{mn}\, \varphi_m\,. \tag{7.56}$$

The coefficients C_{mn} were obtained by solving the matrix equations

$$\mathbf{F}\, \mathbf{C}_n \;=\; \varepsilon_n\, \mathbf{S}\, \mathbf{C}_n, \tag{7.57}$$

where $F_{mn} = \langle \varphi_m \mid h_u \mid \varphi_n \rangle$ is the DF matrix in the joined basis of DF and DFS orbitals of a free ion. The matrix $S_{mn} = \langle \varphi_m \mid \varphi_n \rangle$ is nonorthogonal, since the DFS orbitals are not orthogonal in the usual sense. The negative-energy DFS functions were included in the total basis set as well. Eq. (7.57) was used to generate the whole set of orthogonal one-electron wave functions u_n $(n = 1, \ldots, M)$.

The many-electron wave function $\Psi_+(\gamma J M_J)$ with quantum numbers γ, J, and M_J is expanded in terms of a large set of configuration state functions (CSFs) $\Phi_\alpha(J M_J)$

$$\Psi_+(\gamma J M_J) \;=\; \Lambda_+ \Psi(\gamma J M_J) \;=\; \sum_\alpha c_\alpha\, \Phi_\alpha(J M_J). \tag{7.58}$$

The CSFs are constructed as a linear combination of Slater determinants. The set of the CSFs is generated including all single, double, and triple excitations into one-electron states of the positive spectrum.

Due to some freedom in the choice of the set of wave functions $\{u_n\}_{n=1}^M$, the positive-energy subspace and the corresponding projector λ_+ Eq. (7.51) can be determined in different ways. This freedom can be used to find the optimum many-electron wave function Ψ_{opt} within the variational method.

The energy determined by the Hamiltonian (7.49) can be written as

$$E \;=\; \langle \Psi \mid H_{\mathrm{np}} \mid \Psi \rangle \;=\; \langle \Psi_+ \mid H \mid \Psi_+ \rangle\,. \tag{7.59}$$

The real orthogonal transformation (rotation) of the one-electron function space $\{u_n\}_{n=1}^M$ modifies the wave function Ψ_+ [192]

$$\tilde{\Psi} \;=\; \exp(T)\, \Psi_+\,, \tag{7.60}$$

where the operator T is antihermitian ($T^\dagger = -T$),

$$T \;=\; \sum_{n<m} E_{nm}\, t_{nm}\,, \qquad E_{nm} \;=\; a_n^\dagger\, a_m - a_m^\dagger\, a_n\,, \tag{7.61}$$

where $a_n^\dagger$ and a_n are the creation and annihilation operators of electron in the u_n state. The matrix elements t_{nm} can be obtained from the variational principle. Then the optimum wave function Ψ_{opt} satisfies the generalized Brillouin theorem

$$\langle \Psi_{\mathrm{opt}} \mid [a_n^\dagger\, a_m, H] \mid \Psi_{\mathrm{opt}} \rangle \;=\; 0\,. \tag{7.62}$$

This means that the optimum wave function $\Psi_{\rm opt}$ is invariable under the single-particle excitations including excitations from the negative-energy spectrum. However, this does not hold for the wave function Ψ_+. Therefore, one should revise the calculation of the matrix element $\langle\Psi_+ \mid A \mid \Psi_+\rangle$ of any one-electron operator A by admixing the negative-energy spectrum excitations to Ψ_+.

We consider two equivalent methods for evaluating the negative-continuum contribution to the matrix elements of a hermitian one-electron operator A with the wave functions Ψ_+. The first one is based on the Hellman-Feynman theorem whereas the second one employs perturbation theory.

The space of the wave functions used to determine $\Psi_{\rm opt}$ is invariant under the transformation $U = \exp(iA)$, if A is a one-particle operator. Therefore, one can employ the Hellman-Feynman theorem [193] to obtain the expectation value of A

$$\overline{A} \,=\, \frac{\partial}{\partial\mu}\,\langle\Psi_{\rm opt}(\mu) \mid H(\mu) \mid \Psi_{\rm opt}(\mu)\rangle\Big|_{\mu=0}\,, \qquad H(\mu) \,=\, H + \mu A\,. \tag{7.63}$$

where it is implied that μA is included into the one-particle Hamiltonian, $h_u(\mu) = h_u + \mu A$. Since the wave function correction $\delta\Psi \,=\, \Psi_{\rm opt} - \Psi_+$ accounts for single-particle excitations only, the generalized Brillouin theorem yields

$$\langle\delta\Psi(\mu) \mid H(\mu) \mid \Psi_{\rm opt}(\mu)\rangle + \langle\Psi_{\rm opt}(\mu) \mid H(\mu) \mid \delta\Psi(\mu)\rangle = 0\,, \tag{7.64}$$

and, therefore,

$$\overline{A} \,=\, \frac{\partial}{\partial\mu}\,\left[\langle\Psi_+(\mu) \mid H(\mu) \mid \Psi_+(\mu)\rangle - \langle\delta\Psi(\mu) \mid H(\mu) \mid \delta\Psi(\mu)\rangle\right]_{\mu=0}\,. \tag{7.65}$$

Neglecting the second quadratic term in the equation above yields

$$\overline{A} \,\simeq\, \frac{\partial}{\partial\mu}\,\left[\langle\Psi_+(\mu) \mid H(\mu) \mid \Psi_+(\mu)\rangle\right]_{\mu=0}\,. \tag{7.66}$$

Thus, the negative-continuum contribution can be evaluated by means of the formula

$$\Delta\overline{A}_{\rm neg} \,=\, \frac{\partial}{\partial\mu}\,\left[\langle\Psi_+(\mu) \mid H(\mu) \mid \Psi_+(\mu)\rangle\right]_{\mu=0} \,-\, \langle\Psi_+ \mid A \mid \Psi_+\rangle\,. \tag{7.67}$$

Alternative expression for this contribution can be obtained employing perturbation theory. Using the equation for the derivative of $u_n(\mu)$

$$\frac{\partial}{\partial\mu}u_n(\mu)\Big|_{\mu=0} \,=\, \sum_{m\neq n}\,\frac{\langle u_m(0) \mid A \mid u_n(0)\rangle}{\varepsilon_n \,-\, \varepsilon_m}\,u_m(0)\,, \tag{7.68}$$

we obtain

$$\Delta\overline{A}_{\rm neg} \,=\, 2\sum_n^{\rm (pos)}\,\sum_m^{\rm (neg)}\,\frac{\langle u_m \mid A \mid u_n\rangle}{\varepsilon_n \,-\, \varepsilon_m}\,\langle a_m^\dagger\, a_n\,\Psi_+ \mid H \mid \Psi_+\rangle\,. \tag{7.69}$$

Here the indices $({\rm pos})$ and $({\rm neg})$ indicate that the summation is carried out over the positive- and negative-energy spectrum, respectively.

For the nondiagonal matrix elements, one can derive

$$\Delta A_{\rm neg} \,=\, \frac{\partial}{\partial\mu}\,\left[\langle\Psi_+(\mu) \mid H(\mu) \mid \Psi'_+(\mu)\rangle\right]_{\mu=0} \,-\, \langle\Psi_+ \mid A \mid \Psi'_+\rangle \tag{7.70}$$

and

$$\begin{aligned}\Delta A_{\rm neg} \;&=\; \sum_n^{\rm (pos)}\,\sum_m^{\rm (neg)}\,\frac{\langle u_m \mid A \mid u_n\rangle}{\varepsilon_n \,-\, \varepsilon_m} \\ &\quad\times\left[\langle a_m^\dagger\, a_n\,\Psi_+ \mid H \mid \Psi'_+\rangle \,+\, \langle\Psi_+ \mid H \mid a_m^\dagger\, a_n\,\Psi'_+\rangle\right]\,.\end{aligned} \tag{7.71}$$

These formulas were employed for evaluating the negative-continuum contribution to the M1-transition amplitude. It was found that the results obtained by means of Eqs. (7.70) and (7.71) are in perfect agreement with each other.

Bibliography

[1] Conceptual Design Report for the GSI Future Project, 2002, http://www.gsi.de/GSI-Future/cdr/

[2] M. Niering, R. Holzwarth, J. Reichert, P. Pokasov, Th. Udem, M. Weitz, T.W. Hänsch, P. Lemonde, G. Santarelli, M. Abgrall, P. Laurent, C. Salomon, and A. Clairon, Phys. Rev. Lett. **84**, 5496 (2000).

[3] P. J. Mohr and B. N. Taylor, Rev. Mod. Phys. **77**, 1 (2005).

[4] C. Schwob, L. Jozefowski, B. de Beauvoir, L. Hilico, F. Nez, L. Julien, F. Biraben, O. Acef, J.-J. Zondy, and A. Clairon, Phys. Rev. Lett. **82**, 4960 (1999); **86**, 4193 (2001).

[5] B. de Beauvoir, C. Schwob, O. Acef, L. Jozefowski, L. Hilico, F. Nez, L. Julien, A. Clairon, and F. Biraben, Eur. Phys. J. D **12**, 61 (2000).

[6] K. Pachucki, Phys. Rev. A **63**, 042503 (2001).

[7] K. Pachucki and U. D. Jentschura, Phys. Rev. Lett. **91**, 113005 (2003).

[8] V. A. Yerokhin, P. Indelicato, and V. M. Shabaev, Phys. Rev. A **71**, 040101 (2005).

[9] I. Sick, Phys. Lett. B **576**, 62 (2003).

[10] R. Pohl, F. Biraben, C. A. N. Conde, C. Donche-Gay, T. W. Hänsch, F. J. Hartmann, P. Hauser, V. W. Hughes, O. Huot, P. Indelicato, P. Knowles, F. Kottmann, Y.-W. Liu, V. E. Markushin, F. Mulhauser, F. Nez, C. Petitjean, P. Rabinowitz, J. M. F. don Santos, L. A. Schaller, H. Schneuwly, W. Schott, D. Taqqu, and J. F. C. A. Veloso, in : S. G. Karshenboim, *et al.* (Eds.), Hydrogen atom: Precision physics of simple atomic systems, Springer, Berlin, Heidelberg, p. 454, 2001.

[11] M. C. George, L. D. Lombardi, and E. A. Hessels, Phys. Rev. Lett. **87**, 173002 (2001).

[12] K. Pachucki and J. Sapirstein, J. Phys. B **35**, 1783 (2002); **35**, 3087 (2002).

[13] G. W. F. Drake, Can. J. Phys. **80**, 1195 (2002).

[14] D. C. Morton, Q. Wu, and G. W. F. Drake, Phys. Rev. A **73**, 034502 (2006).

[15] L.-B. Wang, P. Mueller, K. Bailey, G. W. F. Drake, J. P. Greene, D. Henderson, R. J. Holt, R. V. F. Janssens, C. L. Jiang, Z.-T. Lu, T. P. O'Connor, R. C. Pardo, K. E. Rehm, J. P. Schiffer, and X. D. Tang, Phys. Rev. Lett. **93**, 142501 (2004).

[16] G. Ewald, W. Nörtershäuser, A. Dax, S. Götte, R. Kirchner, H.-J. Kluge, Th. Kühl, R. Sanchez, A. Wojtaszek, B. A. Bushaw, G. W. F. Drake, Z.-C. Yan, and C. Zimmermann, Phys. Rev. Lett. **93**, 113002 (2004).

[17] R. Sánchez, W. Nörtershäuser, G. Ewald, D. Albers, J. Behr, P. Bricault, B. A. Bushaw, A. Dax, J. Dilling, M. Dombsky, G. W. F. Drake, S. Götte, R. Kirchner, H.-J. Kluge, Th. Kühl, J. Lassen, C. D. P. Levy, M. R. Pearson, E. J. Prime, V. Ryjkov, A. Wojtaszek, Z.-C. Yan, and C. Zimmermann, Phys. Rev. Lett. **96**, 033002 (2006).

[18] N. Hermanspahn, H. Häffner, H.-J. Kluge, W. Quint, S. Stahl, J. Verdú, and G. Werth, Phys. Rev. Lett. **84**, 427 (2000).

[19] H. Häffner, T. Beier, N. Hermanspahn, H.-J. Kluge, W. Quint, S. Stahl, J. Verdú, and G. Werth, Phys. Rev. Lett. **85**, 5308 (2000).

[20] J. Verdú, S. Djekić, S. Stahl, T. Valenzuela, M. Vogel, G. Werth, T. Beier, H.-J. Kluge, and W. Quint, Phys. Rev. Lett. **92**, 093002 (2004).

[21] S. A. Blundell, K. T. Cheng, and J. Sapirstein, Phys. Rev. A **55**, 1857 (1997).

[22] H. Persson, S. Salomonson, P. Sunnergren, and I. Lindgren, Phys. Rev. A **56**, R2499 (1997).

[23] T. Beier, I. Lindgren, H. Persson, S. Salomonson, P. Sunnergren, H. Häffner, and N. Hermanspahn, Phys. Rev. A **62**, 032510 (2000).

[24] A. V. Nefiodov, G. Plunien, and G. Soff, Phys. Rev. Lett. **89**, 081802 (2002).

[25] V. M. Shabaev and V. A. Yerokhin, Phys. Rev. Lett. **88**, 091801 (2002).

[26] V. A. Yerokhin, P. Indelicato, and V. M. Shabaev, Phys. Rev. Lett. **89**, 143001 (2002).

[27] V. A. Yerokhin, P. Indelicato, and V. M. Shabaev, Phys. Rev. A **69**, 052503 (2004).

[28] K. Pachucki, A. Czarnecki, U. D. Jentschura, and V. A. Yerokhin, Phys. Rev. A **72**, 022108 (2005).

[29] H. Hellwig, R. F. C. Vessot, M. W. Levine, P. W. Zitzewitz, D. W. Allan, and D. J. Glaze, IEEE Trans. Instr. Meas. **19**, 200 (1970).

[30] K. Pachucki, Phys. Rev. A **54**, 1994 (1996).

[31] T. Kinoshita, e-print arXiv:hep-ph/9808351 (1998).

[32] V. A. Yerokhin and V. M. Shabaev, Phys. Rev. A **64**, 012506 (2001).

[33] S. G. Karshenboim and V. G. Ivanov, Eur. Phys. J. D **19**, 13 (2002).

[34] R. N. Faustov and A. P. Martynenko, Phys. At. Nucl. **65**, 265 (2002); Yad. Fiz. **65**, 291 (2002).

[35] V. A. Yerokhin, A. N. Artemyev, V. M. Shabaev, and G. Plunien, Phys. Rev. A **72**, 052510 (2005).

[36] D. E. Zwanziger, Phys. Rev. **121**, 1128 (1961).

[37] M. Sternheim, Phys. Rev. **130**, 211 (1963).

[38] W. Liu, M. G. Boshier, S. Dhawan, O. van Dyck, P. Egan, X. Fei, M. Grosse Perdekamp, *et al.*, Phys. Rev. Lett. **82**, 711 (1999).

[39] M. W. Ritter, P. O. Egan, V. W. Hughes, and K. A. Woodle, Phys. Rev. A **30**, 1331 (1984).

[40] P. J. Mohr, G. Plunien, and G. Soff, Phys. Rep. **293**, 227 (1998).

[41] A. Gumberidze, Th. Stöhlker, D. Bana, K. Beckert, P. Beller, H. F. Beyer, F. Bosch, S. Hagmann, C. Kozhuharov, D. Liesen, F. Nolden, X. Ma, P. H. Mokler, M. Steck, D. Sierpowski, and S. Tashenov, Phys. Rev. Lett. **94**, 223001 (2005).

[42] V. M. Shabaev, O. V. Andreev, A. N. Artemyev, S. S. Baturin, A. A. Elizarov, Y. S. Kozhedub, N. S. Oreshkina, I. I. Tupitsyn, V. A. Yerokhin, and O. M. Zherebtsov, Int. J. Mass Spectr. **251**, 109 (2006).

[43] R. E. Marrs, S. R. Elliott, and T. Stöhlker, Phys. Rev. A **52**, 3577 (1995).

[44] A. Gumberidze, Th. Stöhlker, D. Bana, K. Beckert, P. Beller, H. F. Beyer, F. Bosch, X. Cai, S. Hagmann, C. Kozhuharov, D. Liesen, F. Nolden, X. Ma, P. H. Mokler, A. Orsic-Muthig, M. Steck, D. Sierpowski, S. Tashenov, A. Warczak, and Y. Zou, Phys. Rev. Lett. **92**, 203004 (2004).

[45] A. N. Artemyev, V. M. Shabaev, V. A. Yerokhin, G. Plunien, and G. Soff, Phys. Rev. A **71**, 062104 (2005).

[46] C. Brandau, C. Kozhuharov, A. Müller, W. Shi, S. Shippers, T. Bartsch, S. Böhm, C. Böhme, A. Hoffknecht, H. Knopp, N. Grün, W. Sheid, T. Steih, F. Bosch, B. Franzke, P. H. Mokler, F. Nolden, M. Steck, T. Stöhlker, and Z. Stachura, Phys. Rev. Lett. **91**, 073202 (2003).

[47] P. Beiersdorfer, H. Chen, D. B. Thorn, and E. Träbert, Phys. Rev. Lett. **95**, 233003 (2005).

[48] I. Draganić, J. R. Crespo López-Urrutia, R. DuBois, S. Fritzsche, V. M. Shabaev, R. Soria Orts, I. I. Tupitsyn, Y. Zou, and J. Ullrich, Phys. Rev. Lett. **91**, 183001 (2003).

[49] V. A. Yerokhin, A. N. Artemyev, V. M. Shabaev, M. M. Sysak, O. M. Zherebtsov, and G. Soff, Phys. Rev. Lett. **85**, 4699 (2000).

[50] O. Y. Andreev, L. N. Labzowsky, G. Plunien, and G. Soff, Phys. Rev. A **64**, 042513 (2001).

[51] J. Sapirstein and K. T. Cheng, Phys. Rev. A **64**, 022502 (2001).

[52] V. A. Yerokhin and V. M. Shabaev, Phys. Rev. A **64**, 062507 (2001).

[53] I. I. Tupitsyn, V. M. Shabaev, J. R. Crespo López-Urrutia, I. Draganić, R. Soria Orts, and J. Ullrich, Phys. Rev. A **68**, 022511 (2003).

[54] V. A. Yerokhin, P. Indelicato, and V. M. Shabaev, Phys. Rev. Lett. **91**, 073001 (2003).

[55] P. Seelig, S. Borneis, A. Dax, T. Engel, S. Faber, M. Gerlach, C. Holbrow, G. Huber, T. Kühl1, D. Marx, K. Meier, P. Merz, W. Quint, F. Schmitt, M. Tomaselli, L. Völker, H. Winter, M. Würtz, K. Beckert, B. Franzke, F. Nolden, H. Reich, M. Steck, and T. Winkler, Phys. Rev. Lett. **81**, 4824 (1998).

[56] J. R. Crespo López-Urrutia, P. Beiersdorfer, K. Widmann, B. B. Birkett, A.-M. Mårtensson-Pendrill, and M. G. H. Gustavsson, Phys. Rev. A **57**, 879 (1998).

[57] P. Beiersdorfer, S. B. Utter, K. L. Wong, J. R. Crespo López-Urrutia, J. A. Britten, H. Chen, C. L. Harris, R. S. Thoe, D. B. Thorn, and E. Träbert, Phys. Rev. A **64**, 032506 (2001).

[58] V. M. Shabaev, A. N. Artemyev, V. A. Yerokhin, O. M. Zherebtsov, and G. Soff, Phys. Rev. Lett. **86**, 3959 (2001).

[59] A. A. Elizarov, V. M. Shabaev, N. S. Oreshkina, and I. I. Tupitsyn, Nucl. Instr. Meth. Phys. Res. B **235**, 65 (2005).

[60] V. M. Shabaev, D. A. Glazov, M. B. Shabaeva, V. A. Yerokhin, G. Plunien, and G. Soff, Phys. Rev. A **65**, 062104 (2002).

[61] D. A. Glazov, V. M. Shabaev, I. I. Tupitsyn, A. V. Volotka, V. A. Yerokhin, G. Plunien, and G. Soff, Phys. Rev. A **70**, 062104 (2004).

[62] D. A. Glazov, V. M. Shabaev, I. I. Tupitsyn, A. V. Volotka, V. A. Yerokhin, P. Indelicato, G. Plunien, and G. Soff, Nucl. Instr. Meth. Phys. Res. B **235**, 55 (2005).

[63] D. A. Glazov, A. V. Volotka, V. M. Shabaev, I. I. Tupitsyn, and G. Plunien, Phys. Lett. A, doi:10.1016/j.physleta.2006.04.056.

[64] V. M. Shabaev, D. A. Gazov, N. S. Oreshkina, A. V. Volotka, G. Plunien, H.-J. Kluge, and W. Quint, accepted for publication in Phys. Rev. Lett.

[65] I. B. Khriplovich, Parity non-Conservation in Atomic Phenomena, Gordon and Breach, New York, 1991.

[66] M. G. Kozlov, S. G. Porsev, and I. I. Tupitsyn, Phys. Rev. Lett. **86**, 3260 (2001).

[67] W. R. Johnson, I. Bednyakov, and G. Soff, Phys. Rev. Lett. **87**, 233001 (2001).

[68] V. A. Dzuba, V. V. Flambaum, and J. S. M. Ginges, Phys. Rev. D **66**, 076013 (2002).

[69] V. M. Shabaev, K. Pachucki, I. I. Tupitsyn, and V. A. Yerokhin, Phys. Rev. Lett. **94**, 213002 (2005).

[70] V. M. Shabaev, I. I. Tupitsyn, K. Pachucki, G. Plunien, and V. A. Yerokhin, Phys. Rev. A. **72**, 062105 (2005).

[71] C. S. Wood, S. C. Bennet, D. Cho, B. P. Masterson, J. L. Roberts, C. E. Tanner, C. E. Wieman, Science **275**, 1759 (1997).

[72] L. N. Labzowsky, A. V. Nefiodov, G. Plunien, G. Soff, R. Marrus, and D. Liesen, Phys. Rev. A **63**, 054105 (2001).

[73] E. Träbert, Phys. Scr. **T100**, 88 (2002).

[74] E. Träbert, Can. J. Phys. **80**, 1481 (2002).

[75] A. Simionovici, B. B. Birkett, R. Marrus, P. Charles, P. Indelicato, D. D. Dietrich, and K. Finlayson, Phys. Rev. A **49**, 3553 (1994).

[76] A. Lapierre, U. D. Jentschura, J. R. Crespo López-Urrutia, J. Braun, G. Brenner, H. Bruhns, D. Fischer, A. J. González Martínez, Z. Harman, W. R. Johnson, C. H. Keitel, V. Mironov, C. J. Osborne, G. Sikler, R. Soria Orts, V. M. Shabaev, H. Tawara, I. I. Tupitsyn, J. Ullrich, and A. V. Volotka, Phys. Rev. Lett. **95**, 183001 (2005).

[77] A. Lapierre, J. R. Crespo López-Urrutia, J. Braun, G. Brenner, H. Bruhns, D. Fischer, A. J. González Martínez, V. Mironov, C. Osborne, G. Sikler, R. Soria Orts, H. Tawara, J. Ullrich, V. M. Shabaev, I. I. Tupitsyn, and A. V. Volotka, Phys. Rev. A **73**, 052507 (2006).

[78] T. V. Back, H. S. Margolis, P. K. Oxley, J. D. Silver, and E. G. Myers, Hyperfine Int. **114**, 203 (1998).

[79] D. P. Moehs and D. A. Church, Phys. Rev. A **58**, 1111 (1998).

[80] F. G. Serpa, J. D. Gillaspy, and E. Träbert, J. Phys. B **31**, 3345 (1998).

[81] E. Träbert, G. Gwinner, A. Wolf, X. Tordoir, and A. G. Calamai, Phys. Lett. A **264**, 311 (1999).

[82] E. Träbert, P. Beiersdorfer, S. B. Utter, G. V. Brown, H. Chen, C. L. Harris, P. A. Neill, D. W. Savin, and A. J. Smith, Astrophys. J. **541**, 506 (2000).

[83] E. Träbert, P. Beiersdorfer, G. V. Brown, H. Chen, E. H. Pinnington, and D. B. Thorn, Phys. Rev. A **64**, 034501 (2001).

[84] E. Träbert, P. Beiersdorfer, G. Gwinner, E. H. Pinnington, and A. Wolf, Phys. Rev. A **66**, 052507 (2002).

[85] G. Brenner, *et al.*, in proceeding of 27th Workshop on Atomic Collisions (EAS 27), Riezlern, Austria, 2006.

[86] C. F. Fischer, J. Phys. B **16**, 157 (1983).

[87] A. V. Borovskiy, S. A. Zapryagaev, O. I. Zatsarinny, and N. L. Manakov, Plasma of Multicharged Ions, Khimiya, St. Petersburg, 1995.

[88] K. T. Cheng, Y.-K. Kim, and J. P. Desclaux, At. Data Nucl. Data Tables **24**, 111 (1979).

[89] T. R. Verhey, B. P. Das, and W. F. Perger, J. Phys. B **20**, 3639 (1987).

[90] P. Indelicato, Phys. Rev. Lett. **77**, 3323 (1996).

[91] C. Z. Dong, S. Fritzsche, B. Fricke, and W.-D. Sepp, Phys. Scr. **T92**, 294 (2001).

[92] W. R. Johnson, D. R. Plante, and J. Sapirstein, Adv. At., Mol., Opt. Phys. **35**, 255 (1995).

[93] A. Derevianko, I. M. Savukov, W. R. Johnson, and D. R. Plante, Phys. Rev. A **58**, 4453 (1998).

[94] U. I. Safronova, W. R. Johnson, and A. Derevianko, Phys. Scr. **60**, 46 (1999).

[95] J. Sapirstein, K. Pachucki, and K. T. Cheng, Phys. Rev. A **69**, 022113 (2004).

[96] B. B. Birkett, J. P. Briand, P. Charles, D. D. Dietrich, K. Finlayson, P. Indelicato, D. Liesen, R. Marrus, and A. Simionovici, Phys. Rev. A **47**, R2454 (1993).

[97] R. Marrus, A. Simionovici, P. Indelicato, D. D. Dietrich, P. Charles, J. P. Briand, K. Finlayson, F. Bosch, D. Liesen, and F. Parente, Phys. Rev. Lett. **63**, 502 (1989).

[98] R. W. Dunford, C. J. Liu, J. Last, N. Berrah-Mansour, R. Vondrasek, D. A. Church, and L. J. Curtis, Phys. Rev. A **44**, 764 (1991).

[99] P. Indelicato, B. B. Birkett, J. P. Briand, P. Charles, D. D. Dietrich, R. Marrus, and A. Simionovici, Phys. Rev. Lett. **68**, 1307 (1992).

[100] V. M. Shabaev, Phys. Rep. **356**, 119 (2002).

[101] V. M. Shabaev, I. I. Tupitsyn, V. A. Yerokhin, G. Plunien, and G. Soff, Phys. Rev. Lett. **93**, 130405 (2004).

[102] G. W. F. Drake, Phys. Rev. A **19**, 1387 (1979).

[103] P. Pyykkö, E. Pajanne, and M. Inokuti, Int. J. Quantum Chem. **7**, 785 (1973).

[104] E. Fermi, Z. Phys. **60**, 320 (1930).

[105] T. Kinoshita and M. Nio, Phys. Rev. D **53**, 4909 (1996).

[106] S. G. Karshenboim, V. G. Ivanov, and V. M. Shabaev, JETP **90**, 59 (2000); Can. J. Phys. **76**, 503 (1998).

[107] R. N. Faustov, A. Karimkhodzhaev, and A. P. Martynenko, Phys. Rev. A **59**, 2498 (1999); Phys. At. Nucl. **62**, 2103 (1999); Yad. Fiz. **62**, 2284 (1999).

[108] A. P. Martynenko and R. N. Faustov, JETP **98**, 39 (2004).

[109] S. G. Karshenboim, Phys. Lett. A **225**, 97 (1997).

[110] M. A. B. Bég and G. Feinberg, Phys. Rev. Lett. **33**, 606 (1974); **35**, 130 (1975).

[111] M. I. Eides, Phys. Rev. A **53**, 2953 (1996).

[112] G. T. Bodwin and D. R. Yennie, Phys. Rev. D **37**, 498 (1988).

[113] G. T. Bodwin, D. R. Yennie, and M. A. Gregorio, Rev. Mod. Phys. **57**, 723 (1985).

[114] A. V. Volotka, V. M. Shabaev, G. Plunien, and G. Soff, Eur. Phys. J. D **33**, 23 (2005).

[115] A. Pineda, Phys. Rev. C **67**, 025201 (2003).

[116] A. C. Zemach, Phys. Rev. **104**, 1771 (1956).

[117] O. Gayou, K. Wijesooriya, A. Afanasev, M. Amarian, K. Aniol, S. Becher, K. Benslama, *et al.*, Phys. Rev. C **64**, 038202 (2001).

[118] O. Gayou, K. A. Aniol, T. Averett, F. Benmokhtar, W. Bertozzi, L. Bimbot, E. J. Brash, *et al.*, Phys. Rev. Lett. **88**, 092301 (2002).

[119] P. A. M. Guichon and M. Vanderhaeghen, Phys. Rev. Lett. **91**, 142303 (2003).

[120] S. J. Brodsky, C. E. Carlson, J. R. Hiller, and D. S. Hwang, Phys. Rev. Lett. **94**, 022001 (2005); **94**, 169902 (2005).

[121] A. V. Volotka, V. M. Shabaev, G. Plunien, and G. Soff, Eur. Phys. J. D **23**, 51 (2003).

[122] A. Dupays, A. Beswick, B. Lepetit, C. Rizzo, and D. Bakalov, Phys. Rev. A **68**, 052503 (2003).

[123] S. G. Karshenboim, JETP **76**, 541 (1993).

[124] K. Melnikov and A. Yelkhovsky, Phys. Rev. Lett. **86**, 1498 (2001).

[125] R. J. Hill, Phys. Rev. Lett. **86**, 3280 (2001).

[126] M. I. Eides, H. Grotch, and V. A. Shelyuto, Can. J. Phys. **83**, 363 (2005).

[127] J. L. Friar and I. Sick, Phys. Lett. B **579**, 285 (2004).

[128] H.-W. Hammer and U.-G. Meißner, Eur. Phys. J. A **20**, 469 (2004).

[129] W. H. Furry, Phys. Rev. **81**, 115 (1951).

[130] C. Itzykson and J.-B. Zuber, Quantum Field Theory, McGraw-Hill, New York, 1980.

[131] V. M. Shabaev, in : U. I. Safronova (Ed.), Many-Particles Effects in Atoms, AN SSSR, Moscow, p. 15, 1988.

[132] V. M. Shabaev, in : U. I. Safronova (Ed.), Many-Particles Effects in Atoms, AN SSSR, Moscow, p. 24, 1988.

[133] V. M. Shabaev, Izv. Vuz. Fiz. **33**, 43 (1990) [Sov. Phys. J. **33**, 660 (1990)].

[134] V. M. Shabaev, Teor. Mat. Fiz. **82**, 83 (1990) [Theor. Math. Phys. **82**, 57 (1990)].

[135] V. M. Shabaev, J. Phys. A **24**, 5665 (1991).

[136] V. B. Berestetsky, E. M. Lifshitz, and L. P. Pitaevsky, Quantum Electrodynamics, Pergamon Press, Oxford, 1982.

[137] J. D. Bjorken and D. Drell, Relativistic Quantum Fields, McGraw-Hill, New York, 1965.

[138] P. Indelicato, V. M. Shabaev, and A. V. Volotka, Phys. Rev. A **69**, 062506 (2004).

[139] M. B. Shabaeva and V. M. Shabaev, Phys. Rev. A **52**, 2811 (1995).

[140] I. I. Tupitsyn, A. V. Volotka, D. A. Glazov, V. M. Shabaev, G. Plunien, J. R. Crespo López-Urrutia, A. Lapierre, and J. Ullrich, Phys. Rev. A **72**, 062503 (2005).

[141] A. V. Volotka, D. A. Glazov, G. Plunien, V. M. Shabaev, and I. I. Tupitsyn, Eur. Phys. J. D **38**, 293 (2006).

[142] L. N. Labzowsky, Atomic Theory: Quantum Electrodynamics of Electron Shells and Emission Processes, Nauka, Fizmatlit, Moscow, 1996.

[143] I. I. Sobelman, Atomic Spectra and Radiative Transitions, Springer, New York, 1979.

[144] A. I. Akhiezer and V. B. Berestetsky, Quantum Electrodynamics, Nauka, Moscow, 1969.

[145] W. Greiner and J. Reinhardt, Quantum Electrodynamics, Springer, Berlin, 1994.

[146] G. Soff and P. J. Mohr, Phys. Rev. A **38**, 5066 (1988).

[147] N. L. Manakov, A. A. Nekipelov, and A. G. Fainshtein, Zh. Eksp. Teor. Fiz. **95**, 1167 (1989) [Sov. Phys. JETP **68**, 673 (1989)].

[148] A. G. Fainshtein, N. L. Manakov, and A. A. Nekipelov, J. Phys. B **23**, 559 (1990).

[149] N. J. Snyderman, Ann. Phys. (N.Y.) **211**, 43 (1991).

[150] S. A. Blundell and N. J. Snyderman, Phys. Rev. A **44**, R1427 (1991).

[151] V. A. Yerokhin and V. M. Shabaev, Phys. Rev. A **60**, 800 (1999).

[152] G. Fricke, C. Bernhardt, K. Heilig, L. A. Schaller, L. Schellenberg, E. B. Shera, and C. W. de Jager, At. Data Nucl. Data Tabl. **60**, 177 (1995).

[153] S. A. Zapryagaev, N. L. Manakov, and V. G. Pal'chikov, Theory of Multicharged Ions with one and two electrons, Enegoatomizdat, Moscow, 1985.

[154] P. J. Mohr and G. Soff, Phys. Rev. Lett. **70**, 158 (1993).

[155] A. N. Artemyev, V. M. Shabaev, and V. A. Yerokhin, Phys. Rev. A **56**, 3529 (1997).

[156] V. A. Yerokhin, A. N. Artemyev, and V. M. Shabaev, Phys. Lett. A **234**, 361 (1997).

[157] J. Sapirstein and K. T. Cheng, Phys. Rev. A **66**, 042501 (2002).

[158] S. Salomonson and P. Öster, Phys. Rev. A **40**, 5548 (1989).

[159] P. Sunnergren, H. Persson, S. Salomonson, S. M. Schneider, I. Lindgren, and G. Soff, Phys. Rev. A **58**, 1055 (1998).

[160] W. R. Johnson and J. Sapirstein, Phys. Rev. Lett. **57**, 1126 (1986).

[161] W. R. Johnson, S. A. Blundell, and J. Sapirstein, Phys. Rev. A **37**, 307 (1988).

[162] O. Yu. Andreev, L. N. Labzowsky, G. Plunien, and G. Soff, in proceeding of 26th Workshop on Atomic Collisions (EAS 26), Riezlern, Austria, 2005.

[163] H. Gould, R. Marrus, and P. J. Mohr, Phys. Rev. Lett. **33**, 676 (1974).

[164] R. W. Dunford, D. A. Church, C. J. Liu, H. G. Berry, M. L. Raphaelian, M. Haas, and L. J. Curtis, Phys. Rev. A **41**, 4109 (1990).

[165] S. Cheng, R. W. Dunford, C. J. Liu, B. J. Zabransky, A. E. Livingston, and L. J. Curtis, Phys. Rev. A **49**, 2347 (1994).

[166] R. Marrus, P. Charles, P. Indelicato, L. de Billy, C. Tazi, J. P. Briand, A. Simionovici, D. D. Dietrich, F. Bosch, and D. Liesen, Phys. Rev. A **39**, 3725 (1989).

[167] B. Edlén, Phys. Scr. **28**, 483 (1983).

[168] B. Edlén, Phys. Scr. **28**, 51 (1983).

[169] W. R. Johnson, unpublished.

[170] M. E. Galavís, C. Mendoza, and C. J. Zeippen, Astron. Astrophys. Suppl. Ser. **131**, 499 (1998).

[171] K. Koc, J. Phys. B **36**, L93 (2003).

[172] E. Charro, S. López-Ferrero, and I. Martín, J. Phys. B **34**, 4243 (2001).

[173] V. Kaufman and J. Sugar, J. Phys. Chem. Ref. Data **15**, 321 (1986).

[174] R. Glass, Astrophys. Space Sci. **91**, 417 (1983).

[175] P. J. Mohr, in : I. Sellin and D. J. Pegg (Eds.), Beam-Foil Spectroscopy, Atomic Structure, and Lifetimes, Plenum, New York, v. 1, p. 97, 1976.

[176] P. Indelicato, F. Parente, and R. Marrus, Phys. Rev. A **40**, 3505 (1989).

[177] W. R. Johnson, K. T. Cheng, and D. R. Plante, Phys. Rev. A **55**, 2728 (1997).

[178] T. Nandi, P. Marketos, P. Joshi, R. P. Singh, C. P. Safvan, P. Verma, A. Mandal, A. Roy, and R. K. Bhowmik, Phys. Rev. A 66, 052510 (2002).

[179] A. V. Volotka, V. M. Shabaev, G. Plunien, G. Soff, and V. A. Yerokhin, Can. J. Phys. **80**, 1263 (2002).

[180] R. E. Knight and C. W. Scherr, Rev. Mod. Phys. **35**, 431 (1963).

[181] F. C. Sanders and C. W. Scherr, Phys. Rev. **181**, 84 (1969).

[182] G. W. Drake, Can. J. Phys. **66**, 586 (1988).

[183] V. M. Shabaev, J. Phys. B **24**, 4479 (1991).

[184] J. Epstein and S. Epstein, Am. J. Phys. **30**, 266 (1962).

[185] A. E. Livingston and S. J. Hinterlong, Nucl. Instr. Meth. Phys. Res. **202**, 103 (1982).

[186] J. P. Buchet, M. C. Buchet-Poulizac, A. Denis, J. Désesquelles, M. Dreutta, J. P. Grandin, X. Husson, D. Lecler, and H. F. Beyer, Nucl. Instr. Meth. Phys. Res. B **9**, 645 (1985).

[187] V. M. Shabaev, J. Phys. B **27**, 5825 (1994).

[188] V. F. Bratzev, G. B. Deyneka, and I. I. Tupitsyn, Izv. Akad. Nauk SSSR **41**, 2655 (1977) [Bull. Acad. Sci. USSR, Phys. Ser. **41**, 173 (1977)].

[189] J. Sucher, Phys. Rev. A **22**, 348 (1980).

[190] M. H. Mittleman, Phys. Rev. A **24**, 1167 (1981).

[191] P. F. Gruzdev, G. S. Soloveva, and A. I. Sherstyuk, Opt. Spektrosk. **42**, 1198 (1977) [Opt. Spectrosc. **42**, 690 (1977)].

[192] E. Dalgaard and P. Jørgensen, J. Chem. Phys. **69**, 3833 (1978).

[193] S. T. Epstein, Variation Method in Quantum Chemistry, Academic Press, New York, 1974.

Acknowledgements

It is my pleasure to thank at first Prof. Dr. Rüdiger Schmidt for his willingness to become my supervisor.

Prof. Dr. Gerhard Soff was the person, who strongly supported and encouraged me during my visits in 2002 and 2003 at the Institut for Theoretical Physics as a student, where some parts of this thesis were initiated.

I would like to express my gratitude to Priv. Doz. Dr. Günter Plunien for offering me the opportunity to perform this dissertation thesis under his continuous friendly guidance. I also would like to acknowledge his very valuable comments and suggestions and to thank for his continuous interest in the forthgoing of this thesis.

I am very grateful to Prof. Dr. Vladimir M. Shabaev, who sparked my interest in theoretical physics and taught me the fascinating field of physics, namely quantum electrodynamics. His help and inspiring suggestions and ideas were crucial for the development of my thesis.

I am deeply indebted to my colleagues and collaborators Dr. Dmitry A. Glazov and Dr. Ilya I. Tupitsyn for many fruitful and encouraging discussions.

I would like to express my gratitude to my collaborators on the experimental side Dr. Alain Lapierre, Priv. Doz. Dr. José R. Crespo López-Urrutia, and Prof. Dr. Joachim Ullrich from the Max-Planck Institut for Nuclear Physics in Heidelberg.

For the valuable conversations I am grateful to my colleagues Dr. Oleg Yu. Andreev, Dr. Anton N. Artemyev, Dr. Andrei V. Nefiodov, Dr. Dmitry A. Solovyev, and Dr. Vladimir A. Yerokhin. I also would like to thank the members of the group “Theory of hadrons and nuclei” and the whole Institute for Theoretical Physics for providing the very friendly environment.

Financial support by DAAD (Deutscher Akademischer Austausch Dienst) and GSI (Gesellschaft für Schwerionenforschung, Darmstadt) is gratefully acknowledged.

Lebenslauf

Persönliche Angaben:

Name:	Andrey Viktorovich Volotka
Geburtstag:	23. September 1979
Geburtsort:	Murmansk, USSR
Heimatanschrift:	Hochschulstraße 46, 01069 Dresden
Arbeitsanschrift:	Institut für Theoretische Physik, Technische Universität Dresden, Zellescher Weg 17, 01069 Dresden Tel.: +49(0)351 463 35539 Fax: +49(0)351 463 37297
E-mail:	volotka@theory.phy.tu-dresden.de

Schulausbildung:

Sep. 1994 – Juni 1996	Mittelschulbildung am Akademischen Gymnasium an der St. Petersburg Staatlichen Universität, St. Petersburg, Rußland
Juni 1996	Abitur bestanden

Diplomstudium:

Sep. 1996 – Feb. 2003	Physikstudium an der St. Petersburg Staatlichen Universität, St. Petersburg, Rußland
Juni 2000	Sponsion cum laude zum Bac. rer. nat.
Feb. 2003	Sponsion cum laude zum Mag. rer. nat.

Wissenschaftlicher Werdegang:

Juni 2003 – Mai 2006	Rechnungen zur Promotionarbeit mit dem Titel: “High-precision QED calculations of the hyperfine structure in hydrogen and transition rates in multicharged ions”
Okt. 2003 – Sep. 2004	Stipendium des Präsidenten der Russischen Föderation
Aug. 2004 – Juli 2005	DAAD Stipendium zur wissenschaftlichen Aus- und Fortbildung an der Technischen Universität Dresden
Juli 2005 –	Wiss. Mitarbeiter am Institut für Theoretische Physik an der Technischen Universität Dresden

Publikationen

1. *Hyperfine quenching of the $2^3P_{0,2}$ states in He-like ions*,
   A. V. Volotka, V. M. Shabaev, G. Plunien, G. Soff, and V. A. Yerokhin,
   Can. J. Phys. **80**, 1263 (2002).

2. *Nuclear size correction to the hyperfine splitting in low-Z hydrogen-like atoms*,
   A. V. Volotka, V. M. Shabaev, G. Plunien, and G. Soff,
   Eur. Phys. J. D **23**, 51 (2003).

3. *Interelectronic-interaction effect on the transition probability in high-Z He-like ions*,
   P. Indelicato, V. M. Shabaev, and A. V. Volotka,
   Phys. Rev. A **69**, 062506 (2004).

4. *Relativistic and QED corrections to the g factor of Li-like ions*,
   D. A. Glazov, V. M. Shabaev, I. I. Tupitsyn, A. V. Volotka, V. A. Yerokhin, G. Plunien, and G. Soff,
   Phys. Rev. A **70**, 062104 (2004).

5. *Zemach and magnetic radius of the proton from the hyperfine splitting in hydrogen*,
   A. V. Volotka, V. M. Shabaev, G. Plunien, and G. Soff,
   Eur. Phys. J. D **33**, 23 (2005).

6. *g factor of lithiumlike ions*,
   D. A. Glazov, V. M. Shabaev, I. I. Tupitsyn, A. V. Volotka, V. A. Yerokhin,
   P. Indelicato, G. Plunien, and G. Soff,
   Nucl. Instr. Meth. Phys. Res. B **235**, 55 (2005).

7. *Relativistic electron correlation, quantum electrodynamics, and the lifetime of the $1s^22s^22p\ ^2P_{3/2}$ level in boronlike argon*,
   A. Lapierre, U. D. Jentschura, J. R. Crespo López-Urrutia, J. Braun, G. Brenner, H. Bruhns, D. Fischer,
   A. J. González Martínez, Z. Harman, W. R. Johnson, C. H. Keitel, V. Mironov, C. J. Osborne, G. Sikler,
   R. Soria Orts, V. M. Shabaev, H. Tawara, I. I. Tupitsyn, J. Ullrich, and A. V. Volotka,
   Phys. Rev. Lett. **95**, 183001 (2005).

8. *Magnetic-dipole transition probabilities in B-like and Be-like ions*,
   I. I. Tupitsyn, A. V. Volotka, D. A. Glazov, V. M. Shabaev, G. Plunien, J. R. Crespo López-Urrutia,
   A. Lapierre, and J. Ullrich,
   Phys. Rev. A **72**, 062503 (2005).

9. *Radiative corrections to the magnetic-dipole transition amplitude in B-like ions*,
   A. V. Volotka, D. A. Glazov, G. Plunien, V. M. Shabaev, and I. I. Tupitsyn,
   Eur. Phys. J. D **38**, 293 (2006).

10. *Lifetime measurement of the Ar XIV $1s^2 2s^2 2p\ ^2P_{3/2}$ metastable level at the Heidelberg electron-beam ion trap*,
A. Lapierre, J. R. Crespo López-Urrutia, J. Braun, G. Brenner, H. Bruhns, D. Fischer, A. J. González Martínez, V. Mironov, C. Osborne, G. Sikler, R. Soria Orts, H. Tawara, J. Ullrich, V. M. Shabaev, I. I. Tupitsyn, and A. V. Volotka,
Phys. Rev. A **73**, 052507 (2006).

11. *Screened QED corrections to the g factor of Li-like ions*,
D. A. Glazov, A. V. Volotka, V. M. Shabaev, I. I. Tupitsyn, and G. Plunien,
Phys. Lett. A, doi:10.1016/j.physleta.2006.04.056.

12. *g factor of heavy ions: A new access to the fine structure constant*,
V. M. Shabaev, D. A. Gazov, N. S. Oreshkina, A. V. Volotka, G. Plunien, H.-J. Kluge, and W. Quint,
accepted for publication in Phys. Rev. Lett.

Versicherung

Hiermit versichere ich, daß ich die vorliegende Arbeit ohne unzulässige Hilfe Dritter und ohne Benutzung anderer als der angegebenen Hilfsmittel angefertigt habe; die aus fremden Quellen direkt oder indirekt übernommenen Gedanken sind als solche kenntlich gemacht. Die Arbeit wurde bisher weder in Inland noch im Ausland in gleicher oder ähnlicher Form einer anderen Prüfungsbehörde vorgelegt.

Ich versichere, daß ich bisher keine erfolglosen Promotionsverfahren unternommen habe. Ich erkenne die Promotionsordnung der Fakultät Mathematik und Naturwissenschaften der Technischen Universität Dresden an.

Dresden, den 14.06.2006,